POLITECNICO DI TORINO

Corso di Laurea Magistrale
in
Ingegneria Civile

Tesi di laurea Magistrale

Use of gauged and remote sensing data to improve the implementation of the hydraulic flood forecasting model of the Fitzroy River (Western Australia)

Relatore:
Prof. Francesco Laio
Correlatore:
Ing. Stefania Grimaldi

Candidato:
Silvio Pastorino

Anno Accademico 2018/2019

Alla mia famiglia

Abstract

The extreme flooding event of the Fitzroy River occurred in Kimberley region (Western Australia) at the turn of 2016 and 2017 caused high economic and social damages. The aim of this thesis was the understanding of the floodplain inundation dynamics in the Fitzroy catchment by using a two dimensional hydraulic model. The model was set-up using data available at the continental scale and its predictive performances were evaluated using a multi-objective approach. Specifically, the results of the model were compared with gauged data and remote sensing-derived observations of flood extent. This analysis allowed the diagnosis of the quality of the implementation of the model revealing the low accuracy of the digital elevation model. To solve this issue and improve the accuracy of the hydraulic model, a pragmatic methodology based on the comparison with gauged data and remote sensing derived flood extent was used. The methodology enabled correcting the digital elevation model and thus achieving higher performances of the hydraulic model. The low accuracy of the digital elevation model is a common and well known problem in data scarce areas. The pragmatic method used in this thesis has the potential to be applied to other catchments.

Contents

List of Tables IV

List of Figures VIII

1 Introduction 1

2 Flood inundation modelling 3
- 2.1 Models types overview . . . 3
  - 2.1.1 Empirical methods . . . 3
  - 2.1.2 Hydrodynamic models . . . 4
  - 2.1.3 Numerical approximations of the shallow water equations . . . 6
  - 2.1.4 LISFLOOD-FP model . . . 10
- 2.2 Data used for models calibration and validation . . . 12
  - 2.2.1 Gauge station data . . . 13
  - 2.2.2 Remote sensing data . . . 15
  - 2.2.3 Crowd-sourced data . . . 20

3 Methods 21
- 3.1 Model implementation . . . 21
  - 3.1.1 Topography . . . 21
  - 3.1.2 Boundary conditions . . . 22
  - 3.1.3 Surface roughness . . . 23
  - 3.1.4 Model solver typology . . . 24
- 3.2 Simulation and outputs . . . 24
  - 3.2.1 Comparison with hydrometric measurements . . . 25
  - 3.2.2 Comparison with RS - derived flood extent . . . 26

4 Case study: Fitzroy River (Western Australia) 31
- 4.1 Study area . . . 32
  - 4.1.1 Geomorphology and land use . . . 32
  - 4.1.2 Climate and hydrology . . . 33
- 4.2 Study event . . . 35
  - 4.2.1 Synoptic analyses . . . 35
  - 4.2.2 Temperature . . . 37
  - 4.2.3 Rainfall . . . 38
- 4.3 Economic and social damages . . . 39

5 Results 41
5.1 Input and comparison data . . . 41
5.1.1 DEM selection . . . 41
5.1.2 Gauged and remote sensing data selection . . . 43
5.2 Initial simulations Dem0 . . . 44
5.3 Dem correction . . . 54
5.4 Simulations Dem1 . . . 58
5.4.1 Case Dem1_n0.025 . . . 61
5.4.2 Case Dem1_n0.018 . . . 62
5.4.3 Case Dem1_extended_n0.018 . . . 63
5.5 Simulations Dem3 . . . 65
5.5.1 Case Dem3_n0.025 . . . 68
5.5.2 Case Dem3_extended_n0.025 . . . 69
5.5.3 Case Dem3_n0.018 . . . 70
5.5.4 Case Dem3_extended_n0.018 . . . 72
5.5.5 Case Dem3_n0.0075 . . . 73
5.6 Simulations Dem9 . . . 74
5.6.1 Case Dem9_n0.025 . . . 77
5.6.2 Case Dem9_extended_n0.025 . . . 78
5.7 Flood event 2016-2017: summary of the results . . . 79

6 Historical data analysis 87
6.1 Data research . . . 87
6.2 Model of the 2009 historical event . . . 91
6.2.1 Hydrometric measurements comparisons . . . 92
6.2.2 Remote sensing comparisons . . . 96

7 Conclusions and future developments 99

A MATLAB Codes 101
A.1 Script to modify DEM pixels values . . . 101
A.2 Script to create the roughness input file . . . 103
A.3 Script to compute discharge values . . . 105
A.4 Script to compute water depth values . . . 108
A.5 Script to apply the HAND index to the DEM . . . 110
A.6 Script to plot simulated water depth results . . . 112
A.7 Script to count wet cells in simulated data . . . 114
A.8 Script to count wet cells in observed data . . . 116
A.9 Script to calculate performance metrics indexes . . . 117
A.10 Script to write the envelope raster file of simulated data . . . 119

Bibliography 121

List of Tables

2.1 Landsat acquisitions characteristics. 17
2.2 Contingency table 19
5.1 Measurement stations included in the study area. 43
5.2 Case Dem0_n0.025: performance metrics of gauged and simulated discharge comparison at Fitzroy Crossing station. 46
5.3 Case Dem0_n0.025: performance metrics of gauged and simulated water depth comparison at Fitzroy Crossing station. 46
5.4 Case Dem0_n0.025: performance metrics of gauged and simulated discharge comparison at Noonkanbah station. 47
5.5 Case Dem0_n0.025: performance metrics of gauged and simulated water depth comparison at Noonkanbah station. 47
5.6 Case Dem0_n0.025: quantitative comparison (contingency table and performance metrics) between daily WOfS image and correspondent water depth plot. 48
5.7 Case Dem0_n0.025: quantitative comparison (contingency table and performance metrics) between summary filtered WOfS image and maximum modelled flood extent plot. 49
5.8 Cases Dem0: performance metrics of gauged and simulated discharge comparisons at Fitzroy Crossing station. 50
5.9 Cases Dem0: performance metrics of gauged and simulated water depth comparisons at Fitzroy Crossing station. 50
5.10 Cases Dem0: performance metrics of gauged and simulated discharge comparisons at Noonkanbah station. 51
5.11 Cases Dem0: performance metrics of gauged and simulated water depth comparisons at Noonkanbah station. 51
5.12 Case Dem0_n0.018: quantitative comparison (contingency table and performance metrics) between daily WOfS image and correspondent water depth plot. 51
5.13 Case Dem0_n0.018: quantitative comparison (contingency table and performance metrics) between summary filtered WOfS image and maximum modelled flood extent plot. 52
5.14 Case Dem0_n0.0075: quantitative comparison (contingency table and performance metrics) between daily WOfS image and correspondent water depth plot. 53

5.15 Case Dem0_n0.0075: quantitative comparison (contingency table and performance metrics) between summary filtered WOfS image and maximum modelled flood extent plot. 53
5.16 Cases Dem1: performance metrics of gauged and simulated discharge comparisons at Fitzroy Crossing station. 59
5.17 Cases Dem1: performance metrics of gauged and simulated water depth comparisons at Fitzroy Crossing station. 59
5.18 Cases Dem1: performance metrics of gauged and simulated discharge comparisons at Noonkanbah station. 60
5.19 Cases Dem1: performance metrics of gauged and simulated water depth comparisons at Noonkanbah station. 60
5.20 Case Dem1_n0.025: quantitative comparison (contingency table and performance metrics) between daily WOfS image and correspondent water depth plot. 61
5.21 Case Dem1_n0.025: quantitative comparison (contingency table and performance metrics) between summary filtered WOfS image and maximum modelled flood extent plot. 62
5.22 Case Dem1_n0.018: quantitative comparison (contingency table and performance metrics) between daily WOfS image and correspondent water depth plot. 62
5.23 Case Dem1_n0.018: quantitative comparison (contingency table and performance metrics) between summary filtered WOfS image and maximum modelled flood extent plot. 63
5.24 Case Dem1_extended_n0.018: quantitative comparison (contingency table and performance metrics) between daily WOfS image and correspondent water depth plot. 64
5.25 Case Dem1_extended_n0.018: quantitative comparison (contingency table and performance metrics) between summary filtered WOfS image and maximum modelled flood extent plot. 64
5.26 Cases Dem3: performance metrics of gauged and simulated discharge comparisons at Fitzroy Crossing station. 66
5.27 Cases Dem3: performance metrics of gauged and simulated water depth comparisons at Fitzroy Crossing station. 66
5.28 Cases Dem3: performance metrics of gauged and simulated discharge comparisons at Noonkanbah station. 67
5.29 Cases Dem3: performance metrics of gauged and simulated water depth comparisons at Noonkanbah station. 67
5.30 Case Dem3_n0.025: quantitative comparison (contingency table and performance metrics) between daily WOfS image and correspondent water depth plot. 68
5.31 Case Dem3_n0.025: quantitative comparison (contingency table and performance metrics) between summary filtered WOfS image and maximum modelled flood extent plot. 69
5.32 Case Dem3_extended_n0.025: quantitative comparison (contingency table and performance metrics) between daily WOfS image and correspondent water depth plot. 69

5.33 Case Dem3_extended_n0.025: quantitative comparison (contingency table and performance metrics) between summary filtered WOfS image and maximum modelled flood extent plot. 70
5.34 Case Dem3_n0.018: quantitative comparison (contingency table and performance metrics) between daily WOfS image and correspondent water depth plot. 71
5.35 Case Dem3_n0.018: quantitative comparison (contingency table and performance metrics) between summary filtered WOfS image and maximum modelled flood extent plot. 71
5.36 Case Dem3_extended_n0.018: quantitative comparison (contingency table and performance metrics) between daily WOfS image and correspondent water depth plot. 72
5.37 Case Dem3_extended_n0.018: quantitative comparison (contingency table and performance metrics) between summary filtered WOfS image and maximum modelled flood extent plot. 73
5.38 Case Dem3_n0.0075: quantitative comparison (contingency table and performance metrics) between daily WOfS image and correspondent water depth plot. 73
5.39 Case Dem3_n0.0075: quantitative comparison (contingency table and performance metrics) between summary filtered WOfS image and maximum modelled flood extent plot. 74
5.40 Cases Dem9: performance metrics of gauged and simulated discharge comparisons at Fitzroy Crossing station. 76
5.41 Cases Dem9: performance metrics of gauged and simulated water depth comparisons at Fitzroy Crossing station. 76
5.42 Cases Dem9: performance metrics of gauged and simulated discharge comparisons at Noonkanbah station. 76
5.43 Cases Dem9: performance metrics of gauged and simulated water depth comparisons at Noonkanbah station. 76
5.44 Case Dem9_n0.025: quantitative comparison (contingency table and performance metrics) between daily WOfS image and correspondent water depth plot. 77
5.45 Case Dem9_n0.025: quantitative comparison (contingency table and performance metrics) between summary filtered WOfS image and maximum modelled flood extent plot. 78
5.46 Case Dem9_extended_n0.025: quantitative comparison (contingency table and performance metrics) between daily WOfS image and correspondent water depth plot. 78
5.47 Case Dem9_extended_n0.025: quantitative comparison (contingency table and performance metrics) between summary filtered WOfS image and maximum modelled flood extent plot. 79
5.48 Performance metrics of gauged and simulated discharge comparisons for all cases at Fitzroy Crossing station. 81
5.49 Performance metrics of gauged and simulated water depth comparisons for all cases at Fitzroy Crossing station. 81

5.50 Performance metrics of gauged and simulated discharge comparisons for all cases at Noonkanbah station. 83
5.51 Performance metrics of gauged and simulated water depth comparisons for all cases at Noonkanbah station. 83
5.52 Values of peak time, discharge peak and water depth peak for Fitzroy Crossing station. 84
5.53 Values of peak time, discharge peak and water depth peak for Noonkanbah station. 84
5.54 Performance metrics summary for comparison with daily WOfS. 85
5.55 Performance metrics summary for comparison with summary filtered WOfS. 85
5.56 Values of total wet area for Daily and Summary filtered WOfS footprints. . 86
6.1 Performance metrics of comparisons between gauged and simulated discharge at Fitzroy Crossing station for the 2009 event. 95
6.2 Performance metrics of comparisons between gauged and simulated water depth at Fitzroy Crossing station for the 2009 event. 95
6.3 Performance metrics of comparisons between gauged and simulated discharge at Noonkanbah station for the 2009 event. 95
6.4 Performance metrics of comparisons between gauged and simulated water depth at Noonkanbah station for the 2009 event. 95
6.5 Case Dem0_n0.025: quantitative comparison (contingency table and performance metrics) between 2009 daily WOfS image and correspondent water depth plot. 96
6.6 Case Dem0_n0.018: quantitative comparison (contingency table and performance metrics) between 2009 daily WOfS image and correspondent water depth plot. 97
6.7 Case Dem3_extended_n0.025: quantitative comparison (contingency table and performance metrics) between 2009 daily WOfS image and correspondent water depth plot. 98
6.8 Case Dem3_extended_n0.018: quantitative comparison (contingency table and performance metrics) between 2009 daily WOfS image and correspondent water depth plot. 98

List of Figures

2.1 The one-dimensional representation of flow using a series of cross-sections [10]. 5
2.2 Spatial mesh types [10]. 6
2.3 Examples of a direct observation gauge and a gauge station with multiple devices. 13
2.4 Examples of current meters. 14
2.5 Satellite Landsat 7 [23]. 17
2.6 WOfS grid: each cell contains a time-series of observations [22]. 18
2.7 WOfS filtered summary [22]. 19
3.1 An example of a DEM and labels of a raster file. 23
3.2 Examples of Manning's values [27]. 24
3.3 The interactive map of the Bureau of Meteorology data archive showing the number of measurement station across Australia [28]. 25
3.4 Example of daily WOfS image and its legend. For example, a value of 192 indicates water (128) and cloud (64) were observed for the pixel. 27
3.5 Example of HAND index application to post-process the WOfS image. . . 28
3.6 Example of WOfS filtered summary image. 29
4.1 Flooding condition at Fitzroy Crossing Bridge on 20th December 2016 (a), on 24th December 2016 (b) and on 25th December 2016 [31], [32]. 31
4.2 The Fitzroy River catchment [33]. 32
4.3 Surface geology of the Fitzroy catchment [34]. 33
4.4 Historical monthly rainfall (range is the 10th to 90th percentile monthly rainfall) (a) and historical annual rainfall (b) at Fitzroy Crossing [7]. . . . 34
4.5 Historical mean annual rainfall across the Fitzroy catchment [33]. 34
4.6 Streamflow observation in the Fitzroy catchment [33]. 35
4.7 Mean Sea Level Pressure (MSLP) Analysis for early December 2016 [36]. . 36
4.8 MSLP Analysis for the end of December 2016 [36]. 36
4.9 Anomalies of mean daily max (a) and min (b) temperatures for December 2016 [36]. 37
4.10 Anomalies of mean daily max (a) and min (b) temperatures for January 2017 [36]. 37
4.11 Total rainfall in December 2016 (a) and January 2017 (b) [36]. 38
4.12 Rainfall totals for the period from 20 to 31 December 2016 [37]. 38
4.13 Floodplains around the town of Fitzroy Crossing isolated the area that requested the intervention of emergency services [9]. 39

5.1 Dem chosen as input for the model and its headers. Gauge stations used as inflow points (blue) and as comparison points (black) are marked. 42
5.2 Plot of gauged discharges. 43
5.3 Plot of gauged water depth. 44
5.4 The figure shows the WOfS image captured on 28/12/2016 laid on top of the DEM. The WOfS image covers the area around Noonkanbah station. . 45
5.5 The WOfS filtered summary image cut on the footprint of the DEM. . . . 45
5.6 Case Dem0_n0.025: gauged and simulated data comparisons at Fizroy Crossing station. 46
5.7 Case Dem0_n0.025: gauged and simulated data comparisons at Noonkanbah station. 47
5.8 Case Dem0_n0.025: visual comparison between daily WOfS image and correspondent water depth plot. 48
5.9 Case Dem0_n0.025: visual comparison between summary filtered WOfS image and maximum modelled flood extent plot. 49
5.10 Cases Dem0: observed and simulated data comparisons at Fizroy Crossing station. 50
5.11 Cases Dem0: observed and simulated data comparisons at Noonkanbah station. 50
5.12 Case Dem0_n0.018: visual comparison between daily WOfS image and correspondent water depth plot. 51
5.13 Case Dem0_n0.018: visual comparison between summary filtered WOfS image and maximum modelled flood extent plot. 52
5.14 Case Dem0_n0.0075: visual comparison between daily WOfS image and correspondent water depth plot. 52
5.15 Case Dem0_n0.0075: visual comparison between summary filtered WOfS image and maximum modelled flood extent plot. 53
5.16 Reach interested by the increase of the bottom slope and its terrain profile. 54
5.17 Water depth plots of the first eight days of simulation Dem0_n0.025. . . . 56
5.18 Detail of water depth plots. The area marked with red indicates the zone where the water flow stops. 57
5.20 Local DEM modifications and related terrain profiles of the stretch interested for case one pixels width digging. 58
5.21 Cases Dem1: gauged and simulated data comparisons at Fizroy Crossing station. 59
5.22 Cases Dem1: gauged and simulated data comparisons at Noonkanbah station. 60
5.23 Case Dem1_n0.025: visual comparison between daily WOfS image and correspondent water depth plot. 61
5.24 Case Dem1_n0.025: visual comparison between summary filtered WOfS image and maximum modelled flood extent plot. 61
5.25 Case Dem1_n0.018: visual comparison between daily WOfS image and correspondent water depth plot. 62
5.26 Case Dem1_n0.018: visual comparison between summary filtered WOfS image and maximum modelled flood extent plot. 63
5.27 Case Dem1_extended_n0.018: visual comparison between daily WOfS image and correspondent water depth plot. 63

5.28 Case Dem1_extended_n0.018: visual comparison between summary filtered WOfS image and maximum modelled flood extent plot. 64
5.30 Local DEM modifications and related terrain profiles of the stretch interested for case three pixels width digging. 65
5.31 Comparisons between observed and simulated data for Dem3 cases at Fizroy Crossing station. 66
5.32 Comparisons between observed and simulated data for Dem3 cases at Noonkanbah station. 67
5.33 Case Dem3_n0.025: visual comparison between daily WOfS image and correspondent water depth plot. 68
5.34 Case Dem3_n0.025: visual comparison between summary filtered WOfS image and maximum modelled flood extent plot. 68
5.35 Case Dem3_extended_n0.025: visual comparison between daily WOfS image and correspondent water depth plot. 69
5.36 Case Dem3_extended_n0.025: visual comparison between summary filtered WOfS image and maximum modelled flood extent plot. 70
5.37 Case Dem3_n0.018: visual comparison between daily WOfS image and correspondent water depth plot. 70
5.38 Case Dem3_n0.018: visual comparison between summary filtered WOfS image and maximum modelled flood extent plot. 71
5.39 Case Dem3_extended_n0.018: visual comparison between daily WOfS image and correspondent water depth plot. 72
5.40 Case Dem3_extended_n0.018: visual comparison between summary filtered WOfS image and maximum modelled flood extent plot. 72
5.41 Case Dem3_n0.0075: visual comparison between daily WOfS image and correspondent water depth plot. 73
5.42 Case Dem3_n0.0075: visual comparison between summary filtered WOfS image and maximum modelled flood extent plot. 74
5.44 Local DEM modifications and related terrain profiles of the stretch interested for case nine pixels width digging. 75
5.45 Comparisons between observed and simulated data for Dem9 cases at Fizroy Crossing station. 75
5.46 Comparisons between observed and simulated data for Dem9 cases at Noonkanbah station. 76
5.47 Case Dem9_n0.025: visual comparison between daily WOfS image and correspondent water depth plot. 77
5.48 Case Dem9_n0.025: visual comparison between summary filtered WOfS image and maximum modelled flood extent plot. 77
5.49 Case Dem9_extended_n0.025: visual comparison between daily WOfS image and correspondent water depth plot. 78
5.50 Case Dem9_extended_n0.025: visual comparison between summary filtered WOfS image and maximum modelled flood extent plot. 79
5.51 Comparisons between gauged and simulated data for all cases at Fizroy Crossing station. 80
5.52 Comparisons between gauged and simulated data for all cases at Noonkanbah station. 82

6.1 Detail of flooded area between Dimond Gorge and Fitzroy Crossing stations. 88
6.2 Five hystorical events (green marked) with discharge peak greater than 2000 m^3/s have been selected due to related availability of daily WOfS images capturing the interested area. 88
6.3 1991 event: hydrograph and available daily WOfS image. 89
6.4 1995 event: hydrograph and available daily WOfS image. 89
6.5 1997 event: hydrograph and available daily WOfS image. 90
6.6 2001 event: hydrograph and available daily WOfS image. 90
6.7 2009 event: hydrograph and available daily WOfS image. 91
6.8 Plot of gauged discharges of the 2009 event. 92
6.9 Plot of gauged water depths of the 2009 event. 92
6.10 2009 event: comparisons between observed and simulated data for all cases at Fizroy Crossing station. 93
6.11 2009 event: comparisons between observed and simulated data for all cases at Noonkanbah station. 94
6.12 Case Dem0_n0.025: visual comparison between 2009 daily WOfS image and correspondent water depth plot. 96
6.13 Case Dem0_n0.018: visual comparison between 2009 daily WOfS image and correspondent water depth plot. 97
6.14 Case Dem3_extended_n0.025: visual comparison between 2009 daily WOfS image and correspondent water depth plot. 97
6.15 Case Dem3_extended_n0.018: visual comparison between 2009 daily WOfS image and correspondent water depth plot. 98

Chapter 1

Introduction

Flooding is one of the most common, widespread and destructive natural disaster worldwide, affecting approximately 250 million people with an average number on an annual basis of about 5250 deaths and causing 40 billion dollars in losses [1]. Even in Australia, commonly credited to be the driest inhabited continent, it causes fatalities and costly damages. Flood losses in Australia are estimated at an average of approximately three cases of death per year [2] and over $400 million of costs [3]. Regard to economic issues, since Australia is a major agricultural producer and exporter, flooding can particularly be catastrophic in terms of loss of stock, fodder and topsoil and damage to crops and infrastructure. Indeed, in 2016 over than 200 thousand people, representing 2.2 per cent of all employed people in Australia, were directly employed in the agriculture industry and the gross value of Australian farm production was $60 billion, 3 percent to Australia's total gross domestic product [4][5][6]. On the other hand, despite the disastrous effects, floods provide many environmental and ecological benefits contributing to species diversity, groundwater recharge and soil fertility. During floods, in fact, there is an exchange of water, sediments, chemicals, organic matter and biota between the main river channels and floodplains [7]. For these reasons, a significant and increasing government policy attention is being focussed on quantifying the inundation dynamics in terms of extent, frequency and duration. The aim of all of this is to find ways to, on one side effectively protect human lives and the historical, cultural and economic values of wetlands ecosystems, and on the other manage the financial impacts of flood risk, both in terms of economical losses and impact of water resource for agricultural development.

The purpose of this thesis is to study the behaviour of an extreme flooding event occurred in Kimberley region (Western Australia) at the turn of 2016 and 2017. The main character is the Fitzroy River, the largest watercourse in Western Australia in terms of discharge [7]. This significant event caused four deaths [8] and high economic and social damages: tens people have been evacuated and rescued, some towns remained isolated for days requiring aerial emergency services [9] and main economic activities interrupted for months. This last fact provoked a price increase of many products sold in markets throughout Australia, with consequent inconveniences for the poorest families. Moreover, a vast area of the Fitzroy catchment is covered by nature conservation and Indigenous Protected Areas. These ecosystems provide a range of habitats for rare and threatened flora and fauna, considered to have high ecological value, and have historical significance or high cultural and economic value, particularly to Aboriginal people [7]. Hydraulic flood forecasting model was chosen as way to approach the issue. Indeed, making an accurate model and understanding how territory behaviour is, it allows to do simulations of future scenarios, see the consequences of global warming and apply preventive damage measures. First step was to implement the hydraulic model of the study case, according to the best practice, using as input data a digital elevation model (DEM) with resolution 30 metres and observed discharge values, both available online. These data were implemented in a raster-based simplified numerical method in order to represent the event occurred and try to understand the dynamics of water flow, assessing which areas were actually affected by the floods. A multi-objective analysis was carried out to evaluate the model: the comparison between gauged and simulated data was supported by the use of remote sensing data. Indeed, satellite images were particularly suitable for the Fitzroy river application: they capture information about surface water in areas that are remote, inaccessible, extremely large or dangerous to approach, such as during floods. From the results of the preliminary assessment the presence of an error related to the DEM was clear. Sensitivity analysis approach was used to test several configurations of DEM and roughness input files. Finally, hydraulic models evaluation was made applying the multi objective approach already mentioned, this time processing historical data in order to have a further term of comparison for the analysis.

Chapter 2

Flood inundation modelling

Flood forecasting and warning models have been developed worldwide in order to understand floodplain inundation dynamics and minimize the consequences of a flooding event. These systems permit to predict discharge, flood extent, and water level in rivers and floodplains, precious data in order to intervene with protection measures aimed at safeguarding people and goods. Since the 1970s, systematic efforts within the research community have greatly improved the capability of flood inundation modelling, achieving a large number of different model types, all characterized by advantages and limitations.
This chapter provides an overview of different modelling approaches, their purposes and their limits, and data required for models implementation, calibration, and validation. These concepts will be then useful to better understand how the model analysed for the purposes of this thesis has been built and what types of data have been processed.

2.1 Models types overview

2.1.1 Empirical methods

The empirical methods consist in collecting, processing, integrating and analysing flood data occurred during the years, labelled as "observations". These data, used to give a representation of the reality, include ground measurements, surveys, interviews, aerial photographs and satellite imageries. Empirical methods are the most intuitive and simple approach to achieve useful flood information from observations. Their accuracy depends on the acquisition and processing techniques adopted for each individual method: higher accuracy means higher cost of acquisition and more complex processing of the data. Moreover, disadvantages of their usage are: they are snapshots of the past and cannot directly predict responses to future; they include engineering limitations (such as those associated with the design of sensors), environmental limitations (for example satellite data present common acquisition problems such as vegetation cover and weather conditions) and processing limitations [10]. Since observations are derived with assumptions and uncertainties, empirical methods have a limited capacity to describe a real event. Nevertheless they have received the longest research attention and they are in continuous development as their results are widely used to support decision making and serve as inputs to other types of methods.

2.1.2 Hydrodynamic models

Hydrodynamic models are mathematical models that attempt to simulate water movement solving equations formulated by applying laws of physics. Depending on their spatial representation of the floodplain flow, they can be grouped into different dimensional models: one-dimensional (1D), two-dimensional (2D) and three-dimensional (3D). The governing equations used to solve these models are the shallow water equations, derived by depth-integrating the Navier Stokes equations and given by the mass and momentum conservation equations. Hydrodynamic models are the most widely used tools to simulate detailed flood dynamics in order to provide flood risk mapping, flood forecasting and scenario analysis. Unlike empirical models, the input of hydrodynamic models can be tuned to investigate the impact of changes in initial conditions, boundary conditions, or topographic input.

A one-dimensional model is the simplest representation of floodplain flow that consider the flow along the centre line of the river channel. Despite 1D assumption is a strong hypothesis imposed to solving equations, many hydraulic situations can be replicated with this type of model, particularly when a more detailed solution is unnecessary because the flow is markedly 1D, such as in a confined channel. Furthermore, when floodplain flow can be assumed parallel to the main channel, 1D models are used to estimate both in-channel and floodplain flow routing. Figure 2.1 shows an example of a 1D model and its representation of floodplain flow by a series of cross-sections. The equations 1D models solve to describe the water flow are one-dimensional shallow water equations, also named De Saint Venant equations, derived by ensuring mass (2.1) and momentum (2.2) conservation between two cross sections Δx apart:

$$\frac{\delta Q}{\delta x} + \frac{\delta A}{\delta t} = 0 \tag{2.1}$$

$$\underbrace{\frac{1}{A}\frac{\delta Q}{\delta t}}_{\text{(a)}} + \underbrace{\frac{1}{A}\frac{\delta\left(\frac{Q^2}{A}\right)}{\delta x}}_{\text{(b)}} + \underbrace{g\frac{\delta h}{\delta x}}_{\text{(c)}} - \underbrace{g\left(S_0 - S_f\right)}_{\text{(d)}} = 0 \tag{2.2}$$

where Q [L^3 T^{-1}] is the flow discharge given by product between the cross-sectional averaged velocity u [L T^{-1}] and the flow cross-section area A [L^2], t is the time [T], h [L] is the water depth, g [L T^{-2}] is the gravitational acceleration, S_0 [-] is the channel bed slope and S_f [-] is the friction slope. Moreover, (a) represents the local acceleration term, (b) the convective acceleration term, (c) the pressure force term and (d) the gravity and friction froce terms.
Solving the equations above allows to estimate Q and h for every cross-section at each time step. Depending on the problem submitted it is possible to assume some of the terms of the equation 2.2 negligible: neglecting terms (a), (b) and (c) leads to assume a kinematic model, neglecting terms (a) and (b) gives a diffusive model and neglecting term (a) an inertial one. 1D models are computationally efficient, but they suffer from some limitations: they are unable to simulate lateral diffusion of the flood wave, they do not represent the topography as a continuous surface but as a series of cross sections and the choice of cross sections location and orientation is strongly subjective.

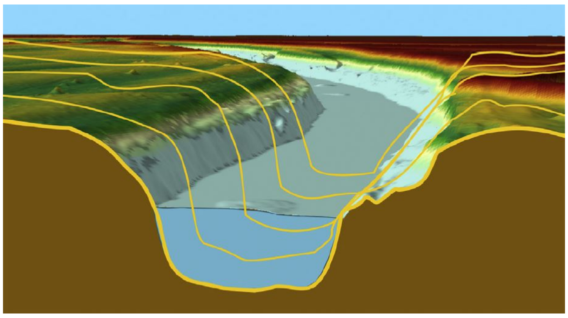

Figure 2.1. *The one-dimensional representation of flow using a series of cross-sections [10].*

2D models models instead represent floodplain flow as a two-dimensional field assuming only the third dimension, the water depth, is shallow compared to the other two dimensions. Now the governing equations are mass (2.3) and momentum (2.4 and 2.5) conservation in a plane:

$$\frac{\delta h}{\delta t} + \frac{\delta (hu)}{\delta x} + \frac{\delta (hv)}{\delta y} = 0 \tag{2.3}$$

$$\frac{\delta (hu)}{\delta t} + \frac{\delta}{\delta x}\left(hu^2 + \frac{1}{2}gh^2\right) + \frac{\delta (huv)}{\delta y} = 0 \tag{2.4}$$

$$\frac{\delta (hv)}{\delta t} + \frac{\delta (huv)}{\delta x} + \frac{\delta}{\delta y}\left(hv^2 + \frac{1}{2}gh^2\right) = 0 \tag{2.5}$$

where x and y are the two spatial dimensions and the vector (u, v) is the horizontal velocity averaged across the vertical column. The solution of these equations leads to estimate the value of u, v, and h over space and time.
2D models can be then classified into subgroups depending on numerical discretisation strategies and time discretisation. The most relevant numerical discretisation strategies are finite element, finite difference, and finite volume methods; relevant time discretisation strategies are implicit (solver cannot proceed to next time step until the whole domain is solved) and explicit (solver of the current unit is independent of the rest of the domain for any given time step). Finally there is the third sub classification of spatial representation: the model can use structured mesh (rectangular grids), unstructured mesh (triangular grids), and flexible mesh (Figure 2.2). For their capacity to be used in several applications two-dimensional hydrodynamic models are perhaps the most widely used typology in flood extent mapping and flood risk estimation studies. Particularly they are generally considered the best approach for studying huge areas with an extension larger than 1000 km^2 [10].

Then the 3D models are the most complete ones based on the three-dimensional Navier-Stokes equations where to the momentum conservation (2.6) the incompressibility condition 2.7 is added.

$$\frac{u}{t} + u \cdot \nabla u + \frac{1}{\varrho}\nabla p = g + \mu \cdot \nabla u \tag{2.6}$$

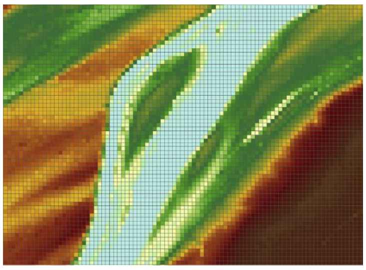

(a) *Rectangular grids*

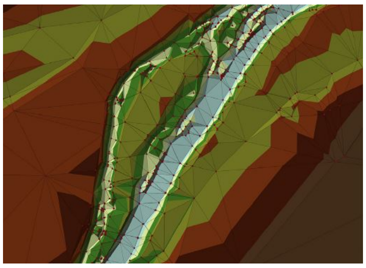

(b) *Triangular grids*

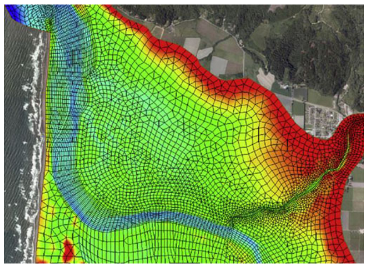

(c) *Flexible mesh*

Figure 2.2. *Spatial mesh types [10].*

$$\nabla \cdot u = 0 \tag{2.7}$$

where u [L T^{-1}] is the velocity, ϱ [M L^{-3}] is the fluid density, p [M L^{-1} T^{-2}] is pressure, g [L T^{-2}] is gravitational acceleration and μ [L^2 T^{-1}] is kinematic viscosity.
3D models emerge as a notable tool to use for specific case of study where is important to understand the behaviour of vertical turbulence, vortices, and spiral flow at bends such as those occurring due to dam breaks or flow through the piers or a bridge. Since the use of 3D models in flood modelling for real topography is pretty recent and still need to be studied and improved [11], this typology is generally considered unnecessary and it can better be replaced by a 2D shallow water approximated model [10].

2.1.3 Numerical approximations of the shallow water equations

During the years simplified numerical methods have been formulated to solve shallow water equations with an acceptable computational time in order to solve practical applications. "Storage cell" methods are an example: their set of equations is derived from 2D shallow water theory where flows in the x and y Cartesian directions are decoupled. This kind of models divide the floodplain into elementary areas and they introduce the water volumes by filling these areas using a filling/spilling process. The advantage of using these models is they can produce a good approximate representation of the flood event with low computational costs compared to hydrodynamic models (indicatively up to 1000 times faster [10]). For this reason, they are becoming increasingly used tools for large-scale applications where is sufficient to calculate the final/maximum flood extent and water levels with a reasonable computational cost, forgetting dynamic effects.
The first method to predict floodplain inundation using storage cell approaches was proposed by Zanobetti et al. in 1970 [12] and it became popular. Initially this method discretized floodplains into irregular polygonal units representing large natural storage compartments, surface areas of 10^0–10^1 km^2 [12]. It calculates the fluxes of water between these areas using some form of the 1D Saint–Venant equations, such as Manning's equations, and when bankfull flow is exceeded, water is routed into and between the floodplain storage units. More recently, thanks to the increased computing power and the availability of detailed descriptions of floodplain topography through remote sensing data, simplified

methods moved away from large, irregular storage units to the discretization of the floodplain using a fine spatial regular grid with a resolution of 10^{-2}–10^{-3} km^2 [12]. Here each cell within the grid is a storage area for which the mass balance is updated at each time step according to the fluxes of water into and out of each cell. Fluxes are calculated analytically using uniform flow formulae but with the advantage of higher resolution predictions and elimination of the need for the modeller to make explicit decisions about the location of storage compartments and the linkages between these. The model therefore solves a continuity equation relating flow into a cell and its change in volume [12]:

$$\frac{\Delta h}{\Delta t} = \frac{\Delta Q}{\Delta x \Delta y} \tag{2.8}$$

and a flux equation for each direction where flow between cells is calculated according to Manning's law:

$$Q_x^{i,j} = \frac{h_{flow}^{5/3}}{n} \left(\frac{h^{i-1,j} - h^{i,j}}{\Delta x} \right)^{1/2} \Delta y \tag{2.9}$$

$$Q_y^{i,j} = \frac{h_{flow}^{5/3}}{n} \left(\frac{h^{i-1,j} - h^{i,j}}{\Delta y} \right)^{1/2} \Delta x \tag{2.10}$$

where Q_x and Q_y [L^3 T^{-1}] are the volumetric flow rates between floodplain cells, h_{flow} [L] is the flow depth that represents the depth through which water can flow between two cells (defined as the difference between the highest water free surface in the two cells and the highest bed elevation), $h^{i,j}$ [L] is the water free surface height at the node (i, j), n [L$^{-1/3}$ T] is the Manning's friction coefficient, Δx and Δy [L] are the cell dimensions and t [T] is the time. Equations 2.9 and 2.10 are solved explicitly using a finite difference discretization of the time derivative term:

$$\frac{{}^{t+\Delta t}h^{i,j} -{}^{t} h^{i,j}}{\Delta t} = \frac{{}^{t}Q_x^{i-1,j} -{}^{t} Q_x^{i,j} +{}^{t} Q_y^{i,j-1} -{}^{t} Q_x^{i,j}}{\Delta x \Delta y} \tag{2.11}$$

where ${}^{t}h$ and ${}^{t}Q$ represent depth and volumetric flow rate at time t and Δt is the model time step which is held constant throughout the simulation.

Therefore in storage cell formulation, fluxes are calculated analytically greatly reducing computational costs per time step compared to equivalent numerical solutions of the full shallow water equations. Moreover, this approach is particularly suitable for studied area with remote sensing data available.

Then, since the utilization of equation 2.11 showed some problem of instabilities (all the water in a particular cell drained into the adjacent ones in a single large time step and at the next time step the direction movement reversed and all the water flowed back), many modellers introduced some kind of 'flow limiter' to avoid too much water leaving a given cell in a single time step. The flow limiter is a function of flow depth, grid cell size and time step that sets the maximum flow that can occur between cells. An example of a flow limiter (the one used by LISFLOOD-FP model) is given by the following formula:

$$Q_x^{i,j} = min\left(Q_x^{i,j}, \frac{\Delta x \Delta y\left(h^{i,j} - h^{i-1,j}\right)}{4\Delta t}\right) \tag{2.12}$$

However the use of flow limiters resulted in an artificially reduced flow sensitivity to floodplain friction. Conversely, in these models, flow predictions were strongly affected by the computational grid size and time step. For these reasons, another way proposed to solve instabilities problems of Manning's equations without invoking the flow limiter was the adaptive time-stepping approach. It consists in finding the optimum time step (large enough for computational efficiency, small enough for stability) at each iteration, obtained using an analysis of the governing equations and their analogy to a diffusion system. In this case the adaptive time step is calculated with equation 2.13 and then used to update the value of h in equation 2.11. Therefore the time step will be adaptive and change during the course of a simulation, but is uniform in space at each time step.

$$\Delta t = \frac{\Delta x^2}{4} min\left(\frac{2n}{h_{flow}^{5/3}}\left|\frac{\delta h}{\delta x}\right|^{1/2}, \frac{2n}{h_{flow}^{5/3}}\left|\frac{\delta h}{\delta y}\right|^{1/2}\right) \tag{2.13}$$

Tests led by Hunter et al. in 2005 and 2006 [12] showed the adaptive time step model is characterised by a better absolute performance than the classical fixed time-step version at low spatial resolution and appears able to simulate floodplain wetting and drying processes more realistically. On the other hand its computational cost increase considerably (approximately six times [12]) and the use of equation 2.13 identifies a fundamental problem: the optimum stable time step reduces quadratically with decreasing grid size. This means that the computational cost will increase as $(1/\Delta x)^2$ with consequent impossibility of use in high resolution applications such as urban flood modelling. Moreover, another problem of the equation 2.13 is the dependence of the time step on the water surface slope that means the time step is reduced for areas with flat water surfaces, where intuitively it would expect the governing equations to be easier to solve.
In order to overcome limits described above and obtain a new hydraulic model formulation able to allow wide area urban flood modelling at fine spatial resolution, Bates et al. proposed in 2010 [12] a new set of flow equations. These equations, suitable for adaptive time step storage cell models, can overcome the quadratic dependency on grid size in equation 2.13 which can be so solved analytically with approximately the same computational cost as equations 2.9 and 2.10. In gradually varying shallow water flows the effect of inertia is to reduce fluxes between cells while in equation 2.13 flux is simply a function of gravity and friction. Therefore this formula overestimates fluxes, particularly in areas of deep water where there is only a small free surface gradient. The solution proposed was to modify explicit storage cell codes to include inertial terms that may allow the use of a larger stable time step and quicker run times. Bates et al. 2010 started from the momentum equation from the one-dimensional shallow water equations 2.2 already seen before, that can be written also in the following way:

$$\frac{\delta Q}{\delta t} + \frac{\delta}{\delta x}\left[\frac{Q^2}{A}\right] + \frac{gA\delta\left(h+z\right)}{\delta x} + \frac{gn^2Q^2}{R^{4/3}A} = 0 \tag{2.14}$$

where Q [L^3 T^{-1}] is the discharge, t [T] is the time, A [L^2] is the flow cross section area, g [L T^{-2}] is the acceleration due to gravity, h [L] is the water free surface height, z [L] is the bed elevation, n [L$^{-1/3}$ T] is the Manning's friction coefficient and R [L] is the hydraulic radius.
Since for many floodplains flows the second term of the equation 2.14, the convective acceleration, is relatively unimportant [12] it can be neglected; then assuming a rectangular channel and dividing through by a constant flow width w [L], an equation in terms of flow per unit width q [L^2 T^{-1}] is obtained:

$$\frac{\delta q}{\delta t} + \frac{gh\delta\left(h+z\right)}{\delta x} + \frac{gn^2q^2}{R^{4/3}h} = 0 \tag{2.15}$$

Then, for wide shallow flows, the hydraulic radius R can be approximated with the flow depth h and introducing the time step discretized Δt the equation become:

$$\left(\frac{q_{t+\Delta t} - q_t}{\Delta t}\right) + \frac{gh_t\delta\left(h_t+z\right)}{\delta x} + \frac{gn^2q_t^2}{h_t^{7/3}} = 0 \tag{2.16}$$

And rearrange to give an explicit equation for q at time $t + \Delta t$:

$$q_{t+\Delta t} = q_t - gh_t\Delta t\left[\frac{\delta\left(h_t+z\right)}{\delta x} + \frac{n^2q_t^2}{h_t^{10/3}}\right] \tag{2.17}$$

This gives an equation for the unit flow at the next time step that can be solved explicitly at a very similar cost to equations 2.9 and 2.10 since it contains only a single additional term. The advantage is that since the acceleration term is now included, the water being modelled has some mass with the consequence of less probability of generating rapid reversals in flow which can lead to a chequerboard oscillation. Moreover shallow water wave propagation is also represented, better than the diffusive behaviour of previous storage cell models.
For a further improvement of the equation 2.17 in order to avoid instabilities due to a rise of the friction term, it is possible to replace the q_t in the friction term by $q_{t+\Delta t}$ obtaining an equation linear in the unknown $q_{t+\Delta t}$ but which has some of the improved convergence properties of an implicit time stepping scheme:

$$q_{t+\Delta t} = q_t - gh_t\Delta t\left[\frac{\delta\left(h_t+z\right)}{\delta x} + \frac{n^2q_tq_{t+\Delta t}}{h_t^{10/3}}\right] \tag{2.18}$$

And finally rearranged into an explicit form for calculation of flows at the new time step in the model:

$$q_{t+\Delta t} = \frac{q_t - gh_t\Delta t\frac{\delta(h_t+z)}{\delta x}}{1 + gh_t\Delta t n^2 q_t/h_t^{10/3}} \tag{2.19}$$

The last equation is now more stable due to the presence in the denominator of the friction term; specifically, when the friction term increases, it forces the flow to zero as it would be

expected for shallow depths.
Differently from equations 2.9 and 2.10, equation 2.19 has to respect the Courant–Freidrichs–Levy condition:

$$C_r = \frac{V \Delta t}{\Delta x} \tag{2.20}$$

where C_r is the non-dimensional Courant number, that needs to be less than 1 for stability, and V [L T^{-1}] is a characteristic velocity of a shallow water flow. When advection is ignored, the celerity can be computed as in:

$$\sqrt{gh} \tag{2.21}$$

The equation of the Courant number is used to estimate a suitable model time step Δt:

$$\Delta t_{max} = \alpha \frac{\Delta x}{\sqrt{g h_t}} \tag{2.22}$$

where α is a coefficient in the range 0.2–0.7 introduced to produce a stable simulation for most floodplain flow situations since equation 2.20 gives a necessary but not sufficient condition for model stability. Therefore choosing an appropriate value of α, equation 2.22 represents a useful approach to choose the best time step for a wide range of flow conditions.
For the purpose of this thesis, the theoretical concepts introduced above are suitable to introduce and understand the working principles of the LISFLOOD-FP model described in the next paragraph and used to simulate the behaviour of the case of study.

2.1.4 LISFLOOD-FP model

LISFLOOD-FP is a raster-based flood inundation model designed for research purposes by the University of Bristol [13]. The model provides a general tool for simulating fluvial flood spreading giving as output raster maps of values of flood water parameters such as depth, water surface elevation and velocity in each grid square at each time step and predicting stage and discharge hydrographs in specified locations. It solves the shallow waters equations to simulate the passage of a flood wave along a channel reach and once bankfull depth is exceeded and the water moves from the channel to adjacent floodplains sections, the two dimensional flood spreading is simulated using a storage cell concept applied over a raster grid.
The LISFLOOD-FP model solvers available for calculating channel flow are [13]:

Kinematic solver
The most simple of the channel flow models which assumes all terms except the friction and bed gradient are negligible. The bed gradient is a simplification of the water slope term which takes into account the effect of changes in bed height with distance, but not changes in the water free surface height.

Diffusive solver
It uses the 1D diffusive wave equation which includes the water slope term that permits

to predict backwater effects. So once channel water depth reaches bankfull height, water is routed onto adjacent floodplain cells to be distributed in accordance with the chosen floodplain solver. Anyway there is no transfer of momentum between the channel and floodplain, but only mass.

The LISFLOOD-FP model solvers available for calculating floodplain flow are [13]:

Routing solver
The simplest method employed to move water between cells. User specified velocity and bed slope direction only, neglecting all the shallow water terms. It is applied only to cells containing either very shallow water or where water slopes are very high. It replaces the shallow water equations in cells with water depths below or water slopes above a user defined threshold. This solver has the effect of reducing model runtime and allowing water to flow over terrain discontinuities without destabilising the solution.

Flow-limited solver
The least complex solver based on the shallow water equations. Friction and water slopes are the shallow water terms included, while local and convective acceleration are neglected. It is an approximation of the diffusion wave equations based on the Manning's equation, calculating flow between cells during a time step as a function of the free surface, bed gradients and the friction slope.

Adaptive solver
A one-dimensional approximation of a diffusion wave based on uniform flow formula, which is decoupled in x and y directions to allow simulation of 2D flows. The difference from the flow limited solver is this one has a time step variable in duration throughout the simulation rather than one with a fixed duration, solving the problem of cells emptying during a time step without the need of a flow limiter. This solver is more suitable for low resolution simulations and rarely used for fine resolution ones.

Acceleration solver
A simplified form of the shallow water equations, where only the convective acceleration term is assumed negligible. Flows between cells are calculated as a function of the friction and water slopes, and local water acceleration. Like the adaptive solver, the time step used by the acceleration solver varies throughout the simulation.

Roe solver
The most complex one, it includes all of the terms in the full shallow water equations.

Finally it is necessary to define assumptions and limitations of LISFLOOD-FP model [13]:

- The code is limited to situations where there is sufficient information to accurately characterise the model boundary conditions, specifically mass flux with time at all inflow points and some basic information on channel geometry.

- The solvers, apart the Routing and the Roe ones, assume flow to be gradually varied.

- The 1D kinematic and diffusive solvers assume the channel geometry simplified to a rectangle.

- The 1D kinematic and diffusive solvers assume the channel geometry simplified to a rectangle and the channel has to be wide and shallow, so the wetted perimeter is approximated by the channel width such that lateral friction is neglected.
- For out-of-bank flow the flow can be treated using a series of storage cells discretised as a raster grid with flow in Cartesian coordinate directions only.
- There is no exchange of momentum between 1D channel solvers and floodplain flows, only mass.
- During floodplain flow lateral friction is assumed negligible and is neglected.
- Due to high computation cost the adaptive solver is rarely suitable for high resolution simulations.
- Using the acceleration solver, low Manning's friction conditions can cause instabilities and a numerical diffusion term must be included.
- The routing solver assumes that flow between cells occurs at a constant speed and that flow direction is controlled purely by DEM elevation. However, it also assumes that water will not flow between cells when the water elevation in the recipient cell is greater than the DEM elevation in the source cell.

2.2 Data used for models calibration and validation

The most common used hydrodynamics models and simplified models as LISFLOOD-FP are parametric models. A parameter can be defined as a measurable factor in the constitutive equations that can assume different values in order to affect the behaviour of simulation results. Since parameters are introduced to adapt the model and optimize its performances in simulating a real world phenomenon, adequate parameter estimation and verification is one of the most important step in modelling. The major sources of uncertainty in flood inundation modelling can be summarized below:

- Roughness coefficients.
- Model input data (boundary and initial conditions, topography and bathymetric data).
- Model structural errors.
- Conceptual model uncertainty.
- Errors in the independent observed data.

All the uncertainties listed above generate errors in the response of the model and need to be compensated introducing effective parameters in order to provide an adequate inundation predictions. The two phases to obtain an effective setting of model parameters are calibration and validation. Calibration is the adjustment of a model's parameters so that the model can reproduce observed data with an acceptable accuracy. Then validation requires that predictions of a model are compared to observed data to demonstrate the accuracy and reliability of the model.

In next paragraphs an overview of data categories used for models calibration and validation and related performance metrics is described. The three major groups of data can be so summarized: gauge station measurements, remote sensing data and crowd sourced data.

2.2.1 Gauge station data

Gauge station data are precise locations selected to take advantage of the best locally available conditions for stage and discharge measurement. Stage is defined as the height in meters of the surface of a stream, measured from the level, named zero gauge, where the graduated rod is stuck in the ground. Zero gauge level is commonly given in meters above an arbitrary chosen gauge datum. Since the river bed level changes (through erosion or redesign of a weir) it is necessary to define a further reference level in order to ensure stage provides a static reference over time for local flood levels: the level at which the river ceases or stops flowing, called cease to flow (CTF). This avoids the confusion of having negative levels when the river bed level changes or the pool level falls below its outlet level.
Discharge, instead, is defined as the volumetric rate of flow of water in an open channel, usually expressed in dimensions of cubic metres per second. A continuous record of stage and discharge is obtained by installing instruments that gauge the water flow condition in the stream and transfer data from gauging stations to hydrological analysis centres, generally in real time, that then publish on internet sites for use by the general public.
Gauge stage records can be obtained by systematic observation with automatic water level sensors and recorders. They are measured in various ways: direct observation of a gauging device, automatic sensing through the use of floats, transducers, gas-bubbler manometers and acoustic methods are just some examples (Figure 2.3).

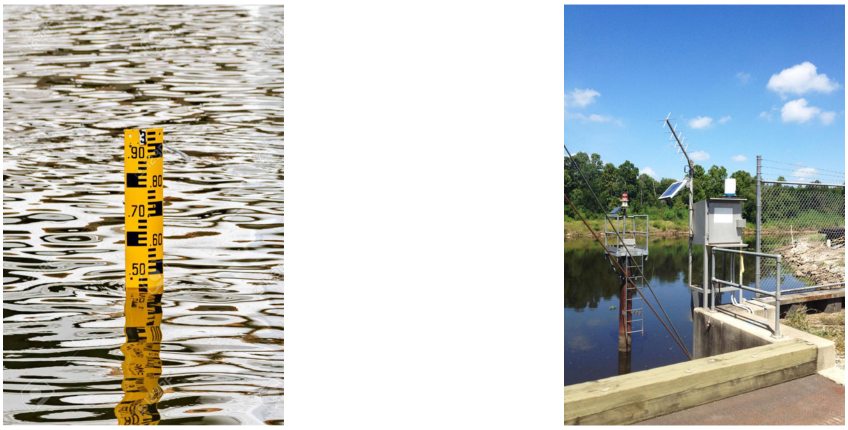

Figure 2.3. *Examples of a direct observation gauge and a gauge station with multiple devices.*

Discharge cannot be measured directly, but must be computed from variables that can be measured directly, such as stream width, stream depth and flow velocity. The basic instrument most commonly used in making the measurement is the current meter, which measures stream velocity whereby to obtain the discharge. This method consists in sub-dividing a stream cross section into segments and measuring the depth and velocity vertically within each segment. Then the total discharge is calculated as sum of the products between partial areas of the stream cross section and their respective average velocities. The most common instrument calibrated to measure the velocity of flowing water and consequently calculate the discharge values, is named current meter [16]. A number of different devices can be used for this purpose; examples include rotating-element mechanical meters (Figure 2.4), electromagnetic meters, acoustic meters and optical meters. Anyway, since direct measurements of discharge in open channels is costly, time consuming, and sometimes impractical during floods, the traditional and simple way to gather information on current discharge is then to measure the water level with gauges and to use a stage-discharge relationship created previously to estimate the flow discharge. The empirical relationship existing between the stage and the simultaneous flow discharge in an open channel is known as "rating curve". The development of a rating curve involves two steps. In the first step the relationship between stage and discharge is established by measuring the stage and corresponding discharge in the river with methods described above. Then, stage of river is measured and discharge is calculated by using the relationship established in the rating curve. Since gauge stage is used as the independent variable in stage-discharge relation to compute discharges, the reliability of the discharge record is dependent on the accuracy and precision of the gauge stage record and the stage-discharge relation.

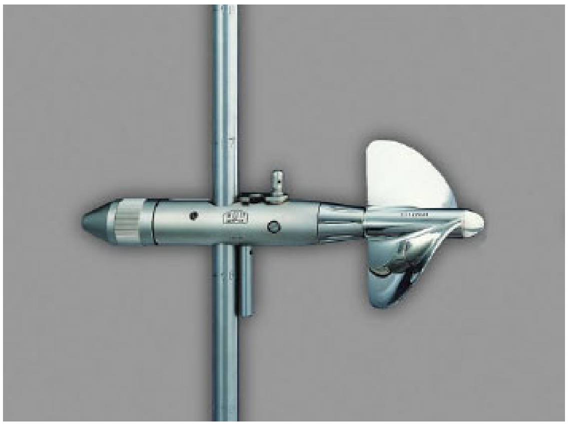

Figure 2.4. *Examples of current meters.*

Continuous time series at discrete locations of gauged water levels and discharge have traditionally been used for model calibration and validation [14][15]. Particularly four quantitative performance measures have been generally recommended: the Nash–Sutcliffe model efficiency coefficient (NSE), the per cent bias (PBIAS), the ratio of the root mean square error (RMSE) and the standard deviation of measured data (RSR).
NSE is used to assess the predictive power of numerical models and it is defined as:

$$NSE = 1 - \frac{\sum_{i=1}^{n} \left(Y_i^{obs} - Y_i^{sim}\right)^2}{\sum_{i=1}^{n} \left(Y_i^{obs} - Y^{mean}\right)^2} \tag{2.23}$$

where Y_i^{obs} is the ith observation for the quantity being evaluated, Y_i^{sim} is the ith simulated

value for the quantity being evaluated, Y^{mean} is the mean of observed data for the quantity being evaluated and n is the total number of observations. An efficiency of 1 corresponds to a perfect match between modelled and observed data, an efficiency of 0 indicates that the model predictions are as accurate as the mean of the observed data, whereas an efficiency less than zero occurs when the observed mean is a better predictor than the model or, in other words, when the residual variance (the numerator in the expression above), is larger than the data variance (the denominator). In practical terms, the closer the model efficiency is to 1, the higher the accuracy of the model is.
PBIAS measures the average tendency of the simulated data to be larger or smaller than their observed counterparts and it is calculated as in:

$$PBIAS = \frac{\sum_{i=1}^{n} \left(Y_i^{obs} - Y_i^{sim}\right) \cdot (100)}{\sum_{i=1}^{n} \left(Y_i^{obs}\right)} \tag{2.24}$$

PBIAS is expressed as a percentage and the optimal value of is 0. Low magnitude values indicate accurate model simulation, positive values indicate model underestimation bias and negative values indicate model overestimation bias.
RMSE is one of the commonly used error index statistics given by the formula:

$$RMSE = \sqrt{\frac{\sum_{i=1}^{n} \left(Y_i^{obs} - Y_i^{sim}\right)^2}{n}} \tag{2.25}$$

From RMSE is obtained the equation of RSR that standardizes RMSE using the observations standard deviation:

$$RSR = \frac{RMSE}{STDEV_{obs}} = \frac{\sqrt{\sum_{i=1}^{n} \left(Y_i^{obs} - Y_i^{sim}\right)^2}}{\sqrt{\sum_{i=1}^{n} \left(Y_i^{obs} - Y^{mean}\right)^2}} \tag{2.26}$$

RSR varies from the optimal value of 0, which indicates zero RMSE that means perfect model simulation, to a large positive value.

2.2.2 Remote sensing data

Remote sensing is defined as the collection and interpretation of information about an object, an area, or an event without being in physical contact with the object. Remotely sensed data offers an inexpensive way to obtain information over large areas. For this reason it has become one of the most effective instrument for flood monitoring, in order to analyze wide areas of a river basin [17].
Aircraft and satellites are the common platforms for remote sensing of the earth and its natural resources. Aerial photography in the visible portion of the electromagnetic wavelength was the original form of remote sensing but technological developments has enabled

the acquisition of information at other not-visible wavelengths including near infrared, thermal infrared and microwave. The measurement of this radiation takes place in what are known as spectral bands. Satellite sensors have been designed to measure responses within particular spectral bands to enable the discrimination of the major Earth surface materials. Actually when radiation reaches the surface of the Earth, some of the energy at specific wavelengths is absorbed and the rest of the energy is reflected by the surface material so measurements can help to distinguish between soil, vegetation or water.
One of the most important features of remote sensing is resolution that can be distinguished in three different categories: spatial resolution, temporal resolution and spectral resolution [17]. Spatial resolution, or ground resolution, may be described as the ground surface area that forms one pixel in the satellite image. For a Landsat Thematic Mapper (NASA) sensor, for example, is 25 m but there are satellites that collect data at less than one meter such as military satellites or very expensive commercial systems. Temporal resolution is a measure of the repeat cycle or frequency with which a sensor revisits the same part of the Earth's surface. Frequency varies from several times per day (geostationary weather satellites) to a few times per months (moderate ground resolution satellite). Generally speaking, the higher the spatial resolution, the lower the frequency of acquisition. Finally the spectral resolution is the number and width of spectral bands in the sensing device. In an optical sensor the simplest form of spectral resolution is with one band only (the image captured would be similar to a black and white photograph) while with three spectral bands would collect similar information to that of the human vision system. Instead a radar sensor is able to collect data in different regions of the spectrum revealing information that cannot be detected by human eyes. Radar are powerful tools since they "see" through clouds and do not require the light of day, so imagery can be recorded through poor atmospheric conditions at any time of day or night.
Use of satellite remote sensing for hydrological and hydraulic applications has advanced greatly over the last 10 years [18], becoming essential particularly in regions where in situ networks are sparse. For the purpose of this research and to understand better the data treated in the following chapters it is useful to provide some further information about Landsat satellite and Water Observations from Space (WOfS) [19][20][21]. Landsat 5 (also called Thematic Mapper or TM) was a low Earth orbit satellite launched on March 1, 1984 to collect imagery of the surface of Earth, afterwards replaced by successors Lansat 7 (also called Enhanced Thematic Mapper or ETM) when it was officially decommissioned on June 5, 2013. The characteristics of the two nominated satellites are summarized in Table 2.1. Particular attention must be paid to the temporal resolution value since it defines the great limitation of remote sensing data: the impossibility of having images available for any time studied, with a consequent lack of information for some period of interest. Landsat-5 and Landsat-7 allowed to collect from 1987 to 2014 a satellite imagery archive of approximately 184,500 images produced from raw data with a pixel size of 0.00025° (about 25 m resolution) [22]. This archive, called WOfS, has become a web service displaying historical surface water observations for all the territory of Australia from 1987 to present day. The WOfS project began in 2011 and its database is continuously updated every three months. The images are ortho-rectified, corrected to measurements of surface and spatially organised into 1×1 degree cells to facilitate processing. The results is a map that describes the presence of water surface across the entire continent from every observation of 27 years of satellite imagery, providing insight into the behaviour of water surface through time,

showing where water is persistent, as in reservoirs, and where it is ephemeral, such as on floodplains during a flood.

Figure 2.5. *Satellite Landsat 7 [23].*

	Spatial resolution [m]	Temporal resolution [days]	Spectral resolution [no. of spectral bands]
Landsat 5	25	16	7
Landsat 7	15÷60	16	8

Table 2.1. *Landsat acquisitions characteristics.*

Particularly WOfS consider the Australian territory divided into a grid (Figure 2.6) where each grid cell within the map provides the following pieces of information:

Wet count
The number of times surface water observed, or rather, how many times water was detected in observations that were clear. As no confidence filtering is applied to this product, it is affected by noise where misclassifications have occurred in the WOfS water classifications.

Clear count
The number of clear observations, or rather, how many times an area could be clearly seen (not affected by clouds, shadows or other satellite observation problems). As above no confidence filtering is applied.

Water Summary
The percentage of clear observations which were detected as wet, or rather, the ratio of wet to clear as a percentage. Also these data are not filtered.

Confidence
The probability that a water observation in a certain location is correct, or rather, the degree of agreement between water shown in the Water Summary and other national datasets.

Filtered Water Summary
A simplified version of the Water Summary, showing the frequency of water observations where the Confidence is above a cutoff level. This layer is a noise-reduced view of surface water across Australia. Even though confidence filtering is applied to the Filtered Water Summary, some cloud and shadow, and sensor noise does persist.

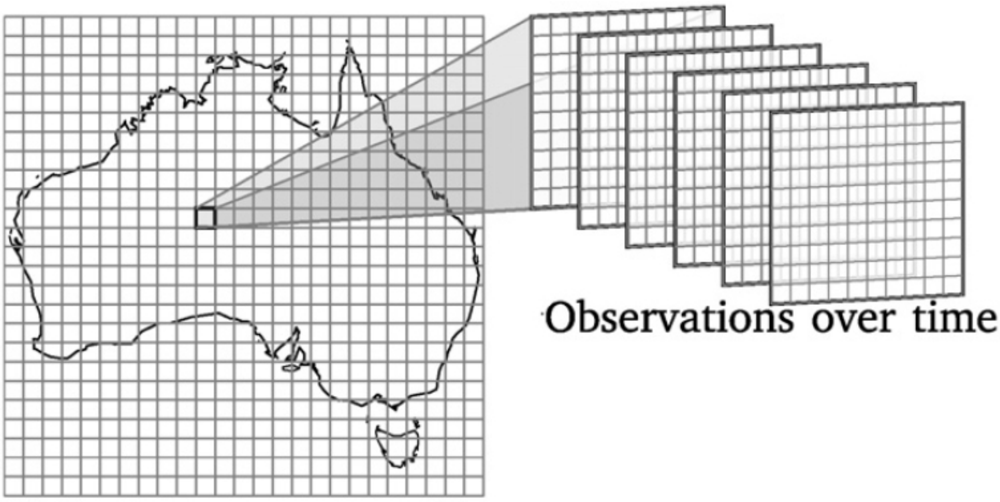

Figure 2.6. *WOfS grid: each cell contains a time-series of observations [22].*

In Figure 2.7 it is reported as example the WOfS filtered summary. It displays the percentage of clear observations for which water was observed across Australia, where the confidence value is at least one percent. White pixels represent areas where water has not been detected. Red pixels where water has been detected in 1% of observations. Yellow and green pixels where water has been detected between 5% and 20% of observations. Blue scale colours indicates areas where water has been detected in more than 50% of observations.

For the purpose of this thesis, it is important to introduce performance metrics based on Remote Sensing-Derived Observations (RS-D Observations): the most widely used are deterministic performance metrics. Observed and modelled data are divided into discrete categories of wet/dry cells separated by deterministic boundaries for the purpose of building a contingency table (Table 2.2) which reports the number of pixels correctly and incorrectly predicted as wet or dry. The model performance is then assessed by the binary measures given below [14].

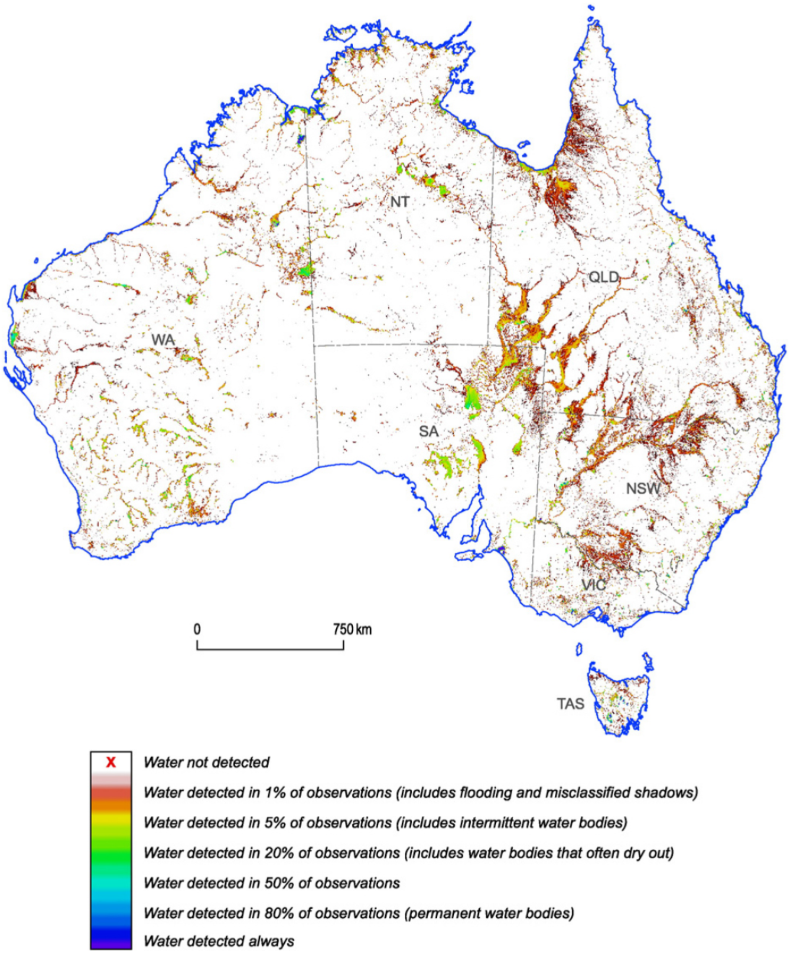

Figure 2.7. *WOfS filtered summary [22].*

	Present in observation	Absent in observation
Present in model	a	b
Absent in model	c	d

Table 2.2. *Contingency table*

$$BIAS = \frac{a+b}{a+c} \tag{2.27}$$

$$PC = \frac{a+b}{a+b+c+d} \tag{2.28}$$

$$CSI = \frac{a}{a+b+c} \tag{2.29}$$

$$F^{<3>} = \frac{a-c}{a+b+c} \tag{2.30}$$

$$F^{<4>} = \frac{a-b}{a+b+c} \tag{2.31}$$

$$H = \frac{a}{a+c} \tag{2.32}$$

$$F = \frac{b}{b+d} \tag{2.33}$$

Bias Index (2.27) gives information on model performance highlighting over-/under prediction; *Proportion Correct Index* (2.28) defines the proportion of cells whose wet/dry state has been correctly predicted over the total extent of the study area; *Critical Success Index* (2.29) is the adjustment of the PC for the quantity being forecast; $F^{<3>}$*Index* (2.30) is designed to penalise underprediction while $F^{<4>}$*Index* (2.31) is designed to penalise overprediction; *Hit Rate Index* (2.32) is the fraction of the observed flood that is correctly predicted and it detects underprediction; *False Alarm Rate Index* (2.33) is the fraction of dry areas that are incorrectly predicted and it detects overprediction.
All the index described are subject to six possible issues related to: the sensitivity to the magnitude of the flood; the bias towards unflooded areas; the bias towards overprediction or underprediction of the flooded areas; the sensitivity to the shape of the valley; the sensitivity to the domain size; the sensitivity to the resolution of the model. Therefore, since the result of a single index can present errors, more than two index are commonly calculated in order to have a more objective evaluation of model performances [24].

2.2.3 Crowd-sourced data

The third group of data usable for building and compare a model increases its relevance in the last few years. Crowd-sourced data collection is a participatory method of building a dataset with the help of a large group of people [25]. Thinking how much the use of smartphones and the exchange of information with networks have grown, it is easy to imagining this kind of data collection will become a primary method in many fields of study and so also for hydraulics applications. Moreover, continued technological advances have stimulated a spread of low cost sensors that can be used not only by technicians, as with observations from traditional physical sensors, but also by regular citizens. Crowd-sourced data collection allows indeed researchers to outsource simple tasks or questionnaires, easily reach people and places, gather data in real time and obtain numerous and widespread observations with costs typically lower than that of traditional data collection methods. However, there are also drawbacks of using these observations, e.g. their relatively limited reliability, varying accuracy in time and space and their irregular and non a-priori defined availability.

In terms of calibration and validation phases, crowd-sourced data can be used as complement for gauge information. The performance metrics of reference are thus the same introduced for gauge station data. Anyway this last category of data is a new frontier of research and their use and the definition of their performance metrics is still work in progress.

Chapter 3

Methods

This chapter presents tools for model implementation and results analysis in order to understand later steps executed for realization and treatment of the case of study. First, practical aspects to execute the model are described, so how to prepare input data and boundary conditions requested. Then, it will give information about hydrometric measurements and how to compare them with the results retrieved from the model and about remote sensing images and how to process them in order to obtain important indication usable as support for the study of the model.

3.1 Model implementation

The model code used to simulate the event of the case of study solves the shallow water equations in their inertial form applying the methodology already used by the well-known code LISFLOOD-FP and described by Bates et al. 2010 studies presented in paragraph 2.1.3. In order to execute the code, several input files need to be completed; the main input requested from the model can be summarized as shown below:

- Topography.
- Channel geometry.
- Boundary conditions.
- Surface roughness.
- Model solver typology.

3.1.1 Topography

The main input for two-dimensional hydrodynamic modelling is the land surface elevation over the entire hydrodynamic model domain, given by a raster digital elevation model (DEM). DEM is a representation of continuous elevation values over a topographic surface, referenced to a common datum, typically derived from satellite photogrammetry and laser altimetry. The DEM is ground only representation and should excludes vegetation such

as trees and shrubs and human constructed features such as sheds and houses. Practically it is represented as a raster file, a 2D raster array of ground elevations in ascii format, that is a grid of quadrangular pixels, or cells, where an elevation value is assigned to each cell. The dimension of cells side defines the resolution of DEM: typical resolution for rural floodplain applications is between 25 and 100 m, although smaller resolutions are preferable in urban areas. The DEM file consists of a six line header followed by the numerical values of each data point on the grid as a 2D array of i rows and j columns. The lines of the header, or labels, give information about the number of colons and rows of the grid, the resolution in metres, the position of the lower left corner of the grid (x and y cartesian coordinate in metres) and the value of null data measurements (generally missing data not measured during the survey). The choice of the DEM to use in the implementation of the model has to be appropriate to include all the area of study interested and particularly the measurement stations available on the territory necessary as input and gauge points. In our case DEM raster file has been downloaded from ELVIS (Elevation and Depth - Foundation Spatial Data) datasets of the Intergovernmental Committee on Surveying and Mapping (ICSM). It is a 1 arc second (about 30 m) gridded digital elevation model derived from the Shuttle Radar Topography Mission (SRTM) in WGS84 datum.
As it will be seen in Chapter 5, the DEM implemented in a hydraulic model may require in specific cases to be calibrated because of the presence of errors that influence the simulated results. The process of the DEM correction consists in:

1. Identify possible errors of the original DEM on the basis of comparisons between observed and simulated data and their location using a geographic information system application, such as Qgis platform.

2. Modify the terrain's elevation values of pixels identified using a MATLAB script (Appendix A.1.)

3. Use the new modified DEM as input file for a new simulation.

4. Repeat steps described above iteratively until observed and simulated data show a good match.

Channel geometry means the river characteristics such as channel slope, channel width and bankfull depth. Can be set individually for each point on the channel vector if necessary or directly taken from the DEM. In our case the DEM will be sufficient to define the geometry of the river modelled.

3.1.2 Boundary conditions

Boundary conditions are the second data input requested to run the model. First it is necessary to specify what kind of boundary condition to use; the model accept different types: uniform flow condition, fixed free surface elevation, time varying free surface elevation, fixed flow into domain and time varying flow into domain. As it will be seen in Chapter 5 our interest will be for the last typology that needs to create a related file of inflow discharge data. Practically, it consists in a series of values of discharge in time representing the hydrograph recorded in a certain point of the studied area, or in other worlds, the gauging station records. For each inflow data the modeller wants to use as input for the

```
ncols         3439
nrows         3657
xllcorner     735687.699999999953
yllcorner     7943090.700000000186
cellsize      30.000000000000
NODATA_value  -9999
```

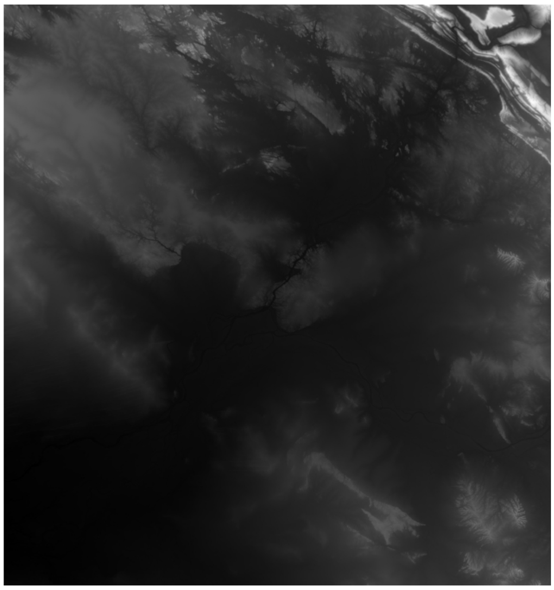

Figure 3.1. *An example of a DEM and labels of a raster file.*

simulation, for example in case of multiple gauge stations for a river with different branch or tributaries, it is necessary to specify the coordinates of the input point: that will be the cell where the flow will "spill" to initiate the simulation. Gauge stations are generally well distributed along river path and data are quite easily available despite they often show missing value and irregular time intervals. A good approach in implementing inflow data is to choose a suitable time interval of the input hydrograph and look for potential missing values: the lack can be filled applying an interpolation in order to obtain a regular input file.

3.1.3 Surface roughness

Another important data that affects considerably the model behaviour is the channel and floodplain friction that controls, in part, the wave speed and stage height in the model. The implementation of this parameter consists in the creation of a file, with same dimensions and resolution as the DEM file, containing a grid of floodplain Manning's values (n values) in ascii raster format (Appendix A.2). The Gauckler–Manning coefficient, or simply Manning's value, is an empirically derived coefficient, dependent on many factors, representing surface roughness and sinuosity of a territory. It is estimate with field inspection, or most commonly for large areas, using aerial photographs. Generally in natural streams n values vary along its reach, increasing where in the riverbed there is presence of boulder and vegetation. Typical values are between 0.01 and 0.05 and only in cases of high roughness n reaches values around the unit (Figure 3.2). In hydraulic models, the roughness is used as an effective parameter to compensate for other various sources of approximation, such as topography simplification and use of simplified equations. Its value is not measured in situ but has to be chosen physically plausible. Then, during model calibration, Manning's values are varied iteratively within the recommended range to attain a close agreement between observed and simulated discharge and stage height.

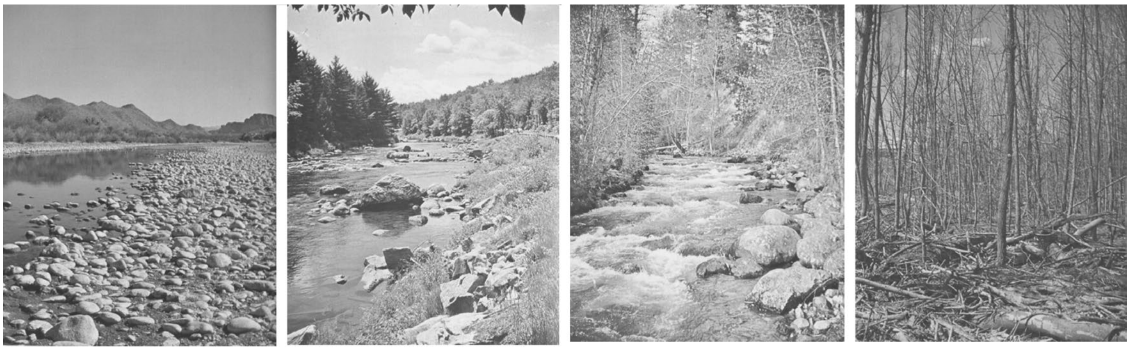

Figure 3.2. *Examples of Manning's values [27].*

3.1.4 Model solver typology

In paragraph 2.1.4 model solvers categories and their related time step have been described. As said before, the numerical code used in this study solves the inertial approximation of the shallow water equations, where only the convective acceleration term is assumed negligible. On the other side, inertial equation implies the use of an adaptive time step for which an optimum time step to maintain stability is calculated by the code.

3.2 Simulation and outputs

After having prepared all input files listed above it is possible to run a simulation through a DOS shell. The models presented later in Chapter 5 have been run using a machine with these specification: CPU Intel Core i7 6700T/2.8 GHz Quad-Core and 8 GB DDR4 SDRAM with memory speed 2133 MHz. Each event was simulated for a period longer than 15 days with an output time interval of 3 hours. The simulation generates different output results consisting in three typologies of files in ascii raster format, having the same headers of DEM file. They are:

- Discharge values in the x Cartesian directions (q_x)
- Discharge values in the y Cartesian directions (q_y)
- Water depths values (wd).

Each cell of discharge raster files contains a value of discharge in square meters per second whose sign indicates the direction of the flow. To obtain discharges in cubic meters per second it is necessary to multiply q_x and q_y values by the length of the DEM raster cell. Water depths file contains information of the water depth value over the terrain in meters for each cell of the raster.

3.2.1 Comparison with hydrometric measurements

The accuracy of two-dimensional hydrodynamic modelling results largely depends on a good match between observed and simulated discharge and water depth. A good match ensures that the model adequately reproduce the inundation dynamics and so input data chosen, particularly DEM and surface roughness, are suitable to reproduce the propagation of flow.
First step is to identify within the studied catchment gauge stations with available measurements for the temporal windows selected. Particularly these gauge stations have to be located downstream the input stations chosen as inflow points for the model. For the studied area, data have been obtained by the online archive of the Bureau of Meteorology of Australian Government [28]. This archive provides time series data collected from approximately 6000 measurement stations across Australia (Figure 3.3) allowing to download, for each station interested, values of discharge and water depth.

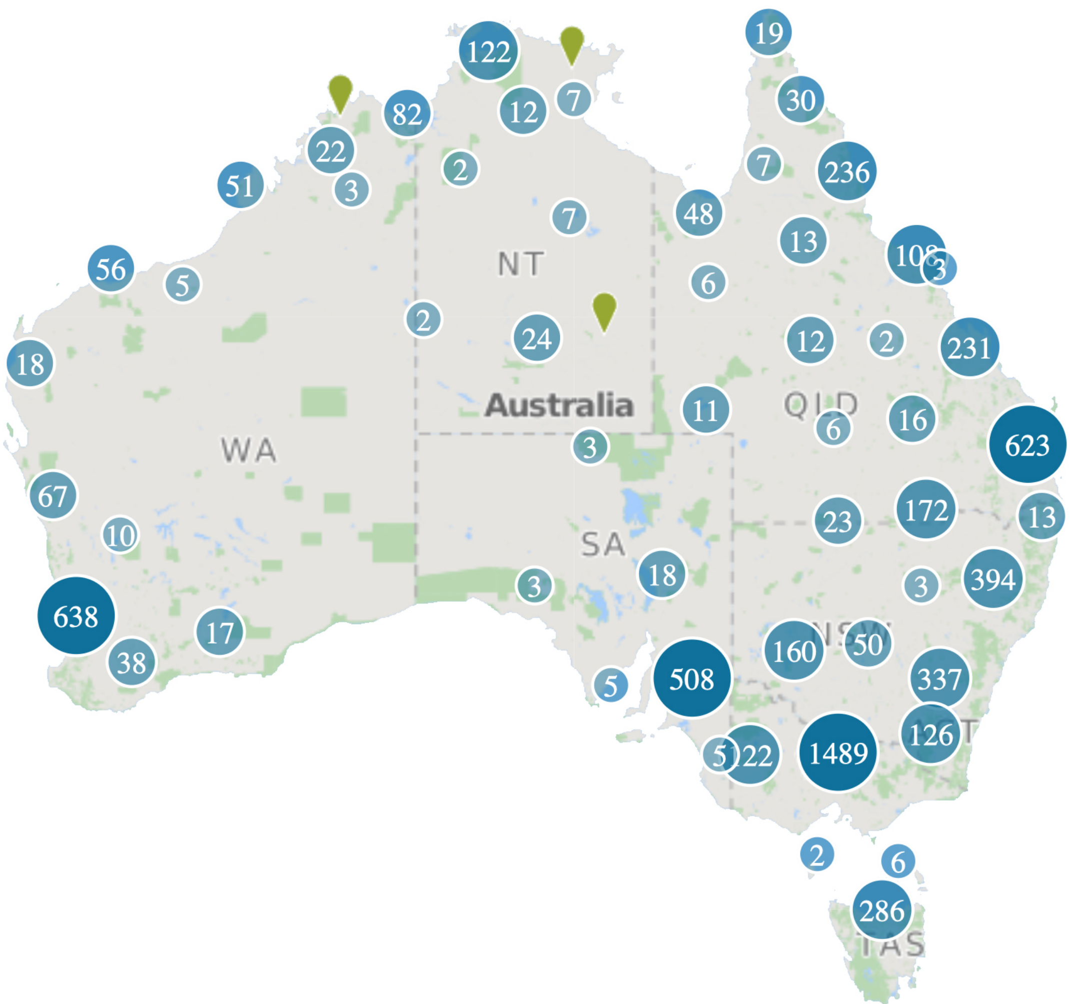

Figure 3.3. *The interactive map of the Bureau of Meteorology data archive showing the number of measurement station across Australia [28].*

After the control gauge stations have been selected, it is necessary to conveniently process the results of the model in order to read values of discharge and water depth in the same location where measurements are available.
For discharge values, first of all, it is necessary to read the results expressed in the two Cartesian coordinates in cells that define the cross section. Then, if the water flow in correspondence with the gauge station can be considered approximately unidirectional (horizontal or vertical motion in the raster grid), it is sufficient to calculate the sum of the values read along the cross section selected. Instead, in case of a diagonal flow, it needs to compose the values of q_x and q_y of each cell before computing the sum. In both cases the sum represents the data to compare with the observed measurement.
The evaluation of water depth is obtained reading for each output file the value of wd in the cell with the same geographical coordinates of the gauge station. Simulated values can be directly compared to the gauged ones since downloaded data have been already corrected taking into account the difference between CTF and zero gauge levels and assuming the zero gauge is positioned on the lowest point of the cross section. This assumption is considerably reasonable because of the well-known problems of water scarcity in Australia.
All the passages described above have to be made for each result in time in order to achieve the water depth and discharge profiles. Practically, the treatment of simulated data can be carried out using ad hoc code written in MATLAB software (Appendixes A.3 and A.4).
Once observed and simulated quantities (the observed ones have to be rewritten in order to have the same time step of the simulated) have been collected, it is possible to plot related hydrographs and water depth profiles and make visual comparisons. The comparison has to be concentrated in particular on differences related to these parts of the plot: the rising limb, the peak and the falling limb. The visual comparison can be supported by the analysis of the performance metrics described before. Moreover, for discharge graphs, a further comparison can be made in terms of volumes difference calculating the subtended area of the curves.

3.2.2 Comparison with RS - derived flood extent

With a view to a multi-objective analysis, a second approach of comparison between model and observation data has been adopted. Here the comparison is based on the use of remote sensing data described in paragraph 2.2.2 that offer two methods to evaluate the performance of the hydrodynamic model. The first one is a visual comparison of spatial inundation area between satellite image and model simulation to assess how the main inundation patterns are represented by the hydrodynamic model. The second one a quantitative assessment of spatial inundation metrics (whether the model correctly simulated an inundated pixel and vice versa) to assess how well the hydrodynamic model captures overall inundation extent. Below the practical steps to make the comparisons are listed:

1. First it is necessary to look for available images that capture flooded areas information within the interested perimeter for a instant contained in the time window of the studied event. Such images can be downloaded from the Geoscience Australia archive of Australian Government [29]. Remembering WOfS is a gridded dataset indicating areas where surface water has been observed, Figure 3.4 show an example of daily WOfS image and the legend describing the significance of each pixel.

2. Downloaded images generally require to be processed with a geographic information system application. Common operations are: merging of multiple images in order to cover the studied area; reprojection of composed image to the chosen coordinate system; resampling to the simulation results resolution; conversion to the simulation results format.

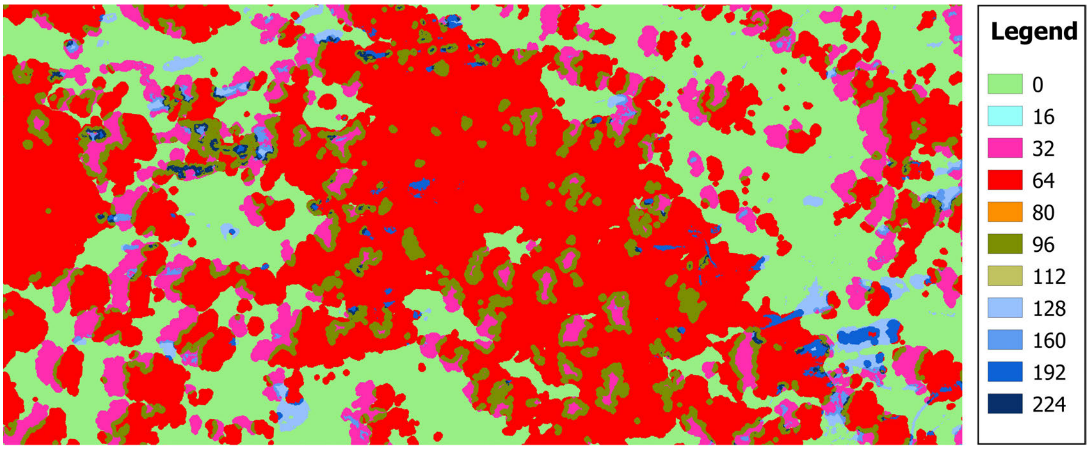

Flagging	Decimal Value	Description
no data	1	dec: 1 = pixel masked out due to NO_DATA in NBAR source, 0 = valid data in NBAR
contiguity	2	dec: 2 = pixel masked out due to lack of data contiguity
sea	4	dec: 4 = pixel masked out due to being over sea
terrain shadow	8	dec: 8 = pixel masked out due to terrain shadow
high slope	16	dec: 16 = pixel masked out due to high slop
cloud shadow	32	dec: 32 = pixel masked out due to cloud shadow
cloud	64	dec: 64 = pixel masked out due to cloud
water observed	128	dec: 128 = water present

Figure 3.4. *Example of daily WOfS image and its legend. For example, a value of 192 indicates water (128) and cloud (64) were observed for the pixel.*

3. A further treatment is applied to the processed images to remove the surface water areas not directly related to the flooding event such as local pools and errors in the Landsat acquisition. This "clearing" operation (Appendix A.5) is realized by comparing the WOfS image with a normalized DEM named HAND (Height Above the Nearest Drainage [30]). HAND is a raster file, obtained starting from the study of flow pathways in the original DEM, containing the values of the ground elevation difference between a location (grid cell) and its nearest stream reach. HAND cells values are grouped into different classes, or thresholds, in order to define a classification criteria. Common thresholds are 5, 10, 15 or 20 m, used to classify wet cells more or less distant from the nearest drainage reference level. In this thesis, a threshold of 20 m has been chosen with the purpose of processing the WOfS image including all possible flooded areas. An

example is shown in Figure 3.5. Now the WOfS file is ready for use, so it is possible to proceed with the two methods of performance evaluation.

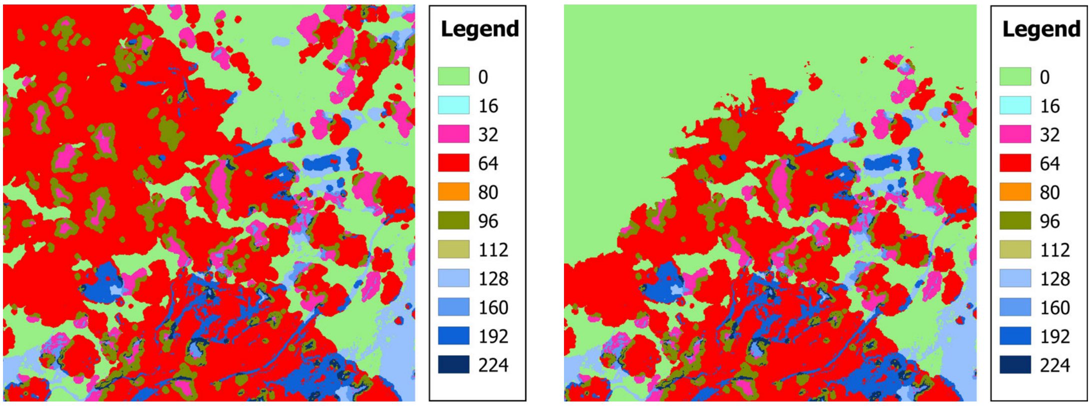

(a) *Pre-processing* (b) *Post-processing*

Figure 3.5. *Example of HAND index application to post-process the WOfS image.*

4. For the visual comparison the simulated water depth result corresponding to the time of the observed image have to be plotted (Appendix A.6). Comparing the two images, observed and simulated, a first approximate information of the model behaviour and the inundated area can be achieved.

5. On the other side, the quantitative assessment requires the use of a MATLAB script to calculate the real value of the flooded area extension of the observed and simulated files (Appendixes A.7 and A.8). The script reads from the simulated file the values of water depth and considers wet each cell of the grid with *wd* greater than a certain threshold value (in our case 1 cm has been chosen). Then, the total wet area is obtained by multiplying the number of wet cells by the area of a single cell (known from the resolution of the DEM). The procedure is similar for the observed file, but in this case the script will consider as wet cells whose value is greater than 128. The information about the total wet area and wet cells thus obtained can be used to calculate the performance metrics described in paragraph 2.2.2 (Appendix A.9).

Due to the limitations related to the satellite temporal resolution and the frequent difficulties of acquiring cloud-free images of the studied area, a common problem of using daily WOfS is that images containing usable information for the study time window are often unavailable. For these reasons it is effective to use an additional RS data provided by the Geoscience Australia archive: the WOfS filtered summary (Figure 3.6). As already seen before this product summarises all the information collected from 1987 to present, expressed as the percentage of time a pixel was wet, removing areas with less than 10% of Confidence (the probability that a water observation in that location is correct). Therefore, although the WOfS filtered summary does not represent specifically the study event, it is an important support tool for the visual and quantitative comparisons because of its continuous time window. To use this product and compare it to simulated data, same steps seen for the daily WOfS have to be executed. The difference is that now it needs to consider as simulated benchmark the maximum modelled flood extent of all the results of the simulation (Appendix A.10). The maximum modelled flood extent is obtained reading from all the simulated results which cells have been inundated and writing a new raster file that express this information with binary values (1 for wet cells and 0 for dry cells). Furthermore, to calculate the value of the flooded area extension in observed image, the script considers now as wet cells all the pixels having a percentage value greater than zero.

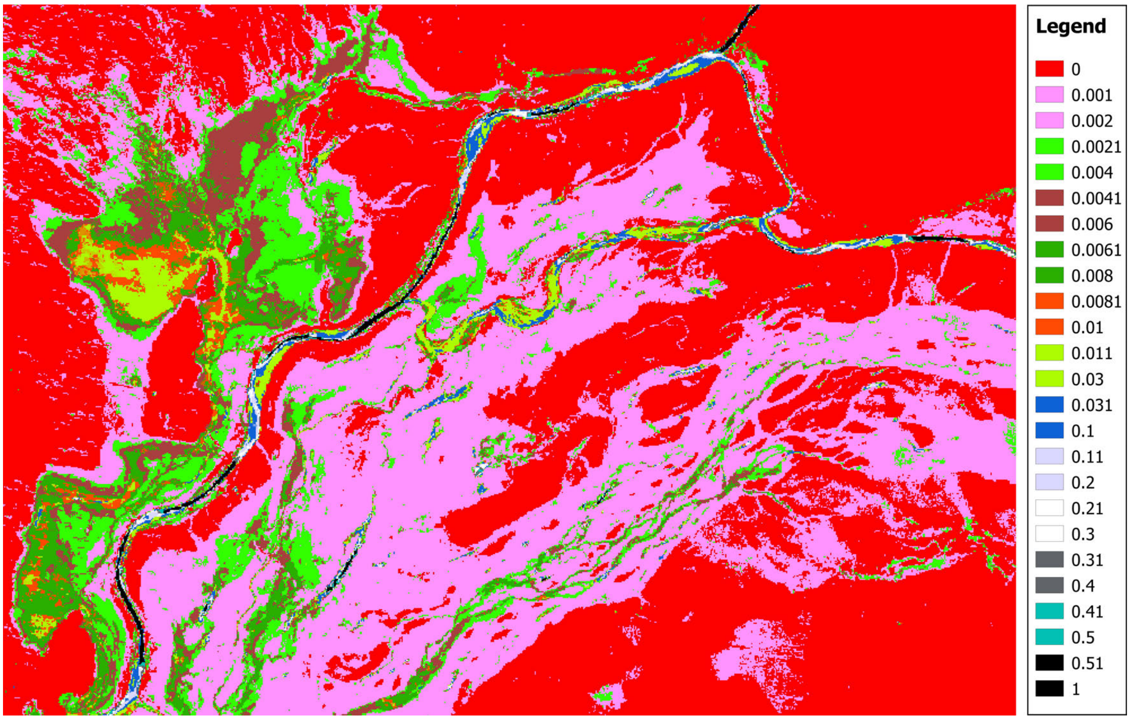

Figure 3.6. *Example of WOfS filtered summary image.*

Chapter 4

Case study: Fitzroy River (Western Australia)

During the month of December 2016 and January 2017 heavy rain affected many parts of Australia. The region of Kimberley in northern Western Australia and its main watercourse, the Fitzroy River, were especially stricken. During the event the water level rose 11 meters in only 5 days (Figure 4.1) provoking the flooding of huge areas that suffered from difficulties and economic losses.
In this chapter information about the Fitzroy River catchment and the characteristics of the specific event mentioned above are given in order to better know the main motivation of this thesis.

Figure 4.1. *Flooding condition at Fitzroy Crossing Bridge on 20th December 2016 (a), on 24th December 2016 (b) and on 25th December 2016 [31], [32].*

4.1 Study area

The Fitzroy River, also known to the local Aboriginal people as Raparapa, is located in the south west part of the Kimberley region, North West of Western Australia (Figure 4.2). The catchment occupies an area of 93,830 km^2, the river has a length of 733 km and it is characterised by an average discharge of 84.78 m^3/s [7].

Figure 4.2. *The Fitzroy River catchment [33].*

4.1.1 Geomorphology and land use

The territory is mainly flat with a total elevation difference in the catchment of around 1000 meters. The north eastern half of the catchment is part of an ancient plateau with elevated exposed igneous and metamorphic rocks while the south western part of the catchment (downstream of Fitzroy Crossing) is characterised by limited topographic reliefs (Figure 4.3). In the North-East part, for the presence of many faults and folds, the plateau has eroded over time forming relatively flat rugged terrain with a thin layer of sandy soils. This causes in case of heavy rainfall high runoff that flows quickly over the land surface due to rocky nature and steeper slope of the surface. Conversely, in the downstream part of the catchment, where plains and hills have more soils, slopes are less steep and valleys are broader, runoff results slower and water depth increases.
Common form of vegetation in the catchment include tall-grass savannah woodland, curly spinfex savannah woodland, tree savannah, pindan, and tall and short bunch grass savannah. The river floodplain ecosystems of the Fitzroy River provide a range of habitats

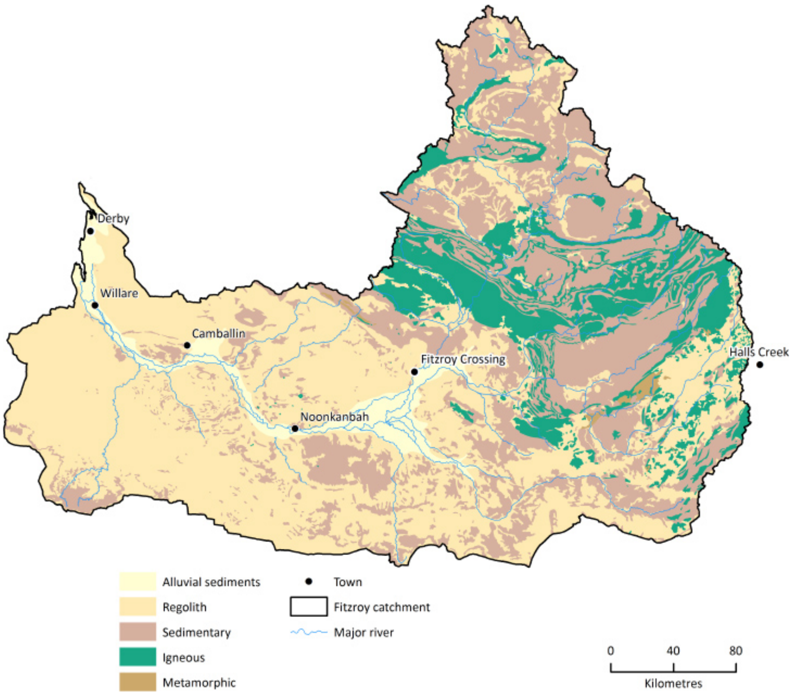

Figure 4.3. *Surface geology of the Fitzroy catchment [34].*

for rare and threatened flora and fauna considered to have high ecological value. Moreover its wetlands are important because they have historical significance or high cultural and economic value, particularly to Indigenous people (130 Aboriginal communities live throughout the valley).

For tens of thousands of years, Aboriginal peoples have been living in the Fitzroy River catchment with low population densities but, when European migration began in 1890s, most of the land of the catchment came under pastoral leases [35]. Now the main land use is still pastoralism (95%), with large grazing leases with cattle on native pastures, shrubs, and introduced forages and legumes. The two main prospects for land use change through agricultural development in the Fitzroy River Valley are increased intensity of grazing and irrigated agriculture for cropping.

The population in the catchment is sparse and the only major towns in the region are Derby and Fitzroy Crossing with an estimated populations of 1500 and 5000 people respectively. The key industries in the valley are resource extraction, service delivery, construction, primary production and tourism.

4.1.2 Climate and hydrology

The climate of the catchment is influenced by southern edge of the global monsoon system with two dominant seasons: a hot wet season from November to April followed by a warm dry winter. About 90% of annual rainfall occur during wet season with high-intensity rainfall considerably and spatially variable from North to South. Average values are around around 1000 mm/year to 500 mm/year (Figures 4.4 and 4.5) [33].

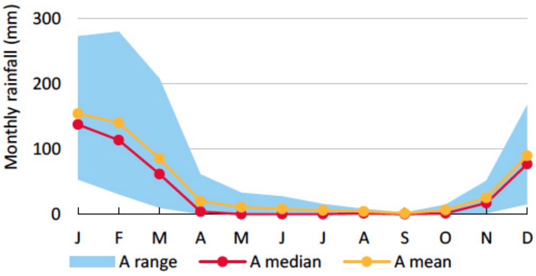

(a)

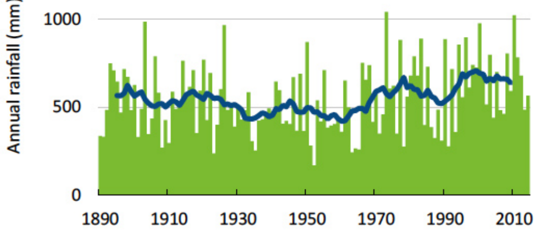

(b)

Figure 4.4. *Historical monthly rainfall (range is the 10th to 90th percentile monthly rainfall) (a) and historical annual rainfall (b) at Fitzroy Crossing [7].*

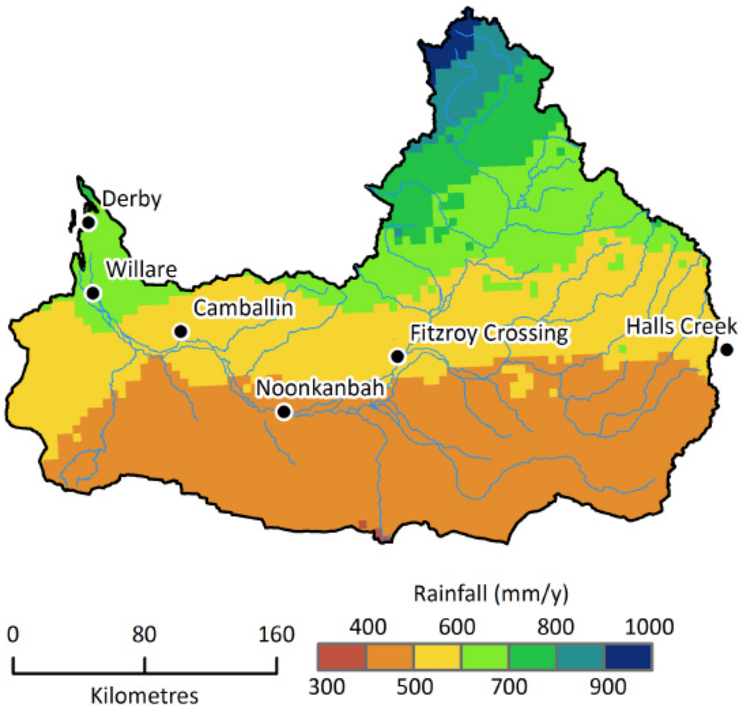

Figure 4.5. *Historical mean annual rainfall across the Fitzroy catchment [33].*

Areal potential evaporation in the Fitzroy catchment exhibits a strong seasonal pattern, ranging from 200 mm per month before and during the wet season, to about 100 mm per month during the middle of the dry season. In consequence to its high potential evaporation rates and its relatively low annual rainfall, a large proportion (95%) of the catchment results semi-arid during the year.
Mean average annual temperate ranges go from around 26 °C in the south to 24-25 °C in the north, with the highest mean annual temperatures around 27 °C in the middle of

the valley. Temperatures also vary substantially between dry and wet seasons. In the wet season mean temperatures range from 26 to 30 °C, while in the dry season mean temperatures range from 21 to 24 °C [34].
Streamflow (Figure 4.6) varies between perennial and intermittent in reaches downstream of Fitzroy Crossing, while flow in most other parts of the catchment is ephemeral. The Fitzroy has 20 tributaries where the most important are the Margaret River (with a contribution area of 16,561 km^2), the Leopold River (5820 km^2) and the Christmas Creek (11,446 km^2). The Fitzroy River is one of Australia's largest unregulated river systems and its overbank flows are generally governed by the topography of the floodplain. Over the past 35 years intense seasonal rains caused flooding and inundation in lots parts of the catchment, particularly in areas downstream Fitzroy Crossing (since 1981 there have been 18 floods). In the next paragraph the recent flooding event of 2016-2017 will be analyse in detail.

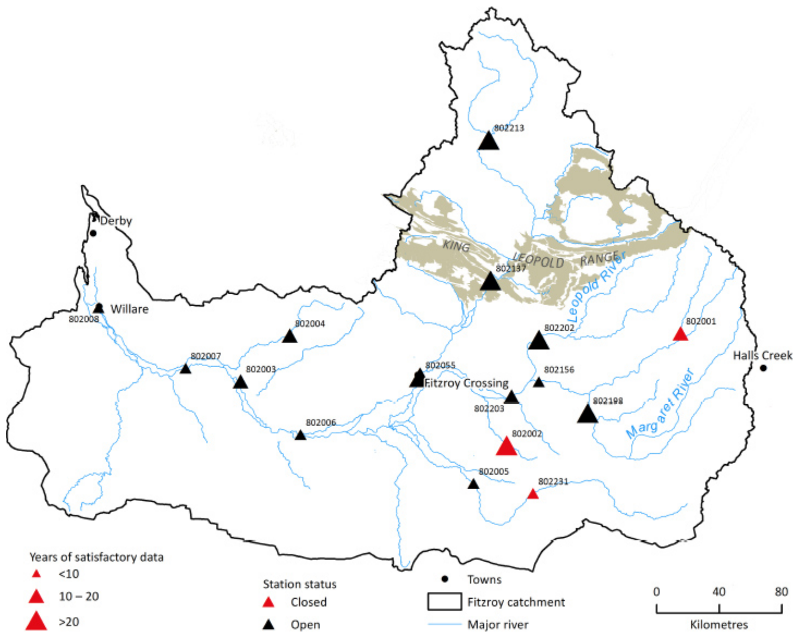

Figure 4.6. *Streamflow observation in the Fitzroy catchment [33].*

4.2 Study event

4.2.1 Synoptic analyses

During December 2016 much of Australia was influenced by broad surface troughs and low pressure systems that brought tropical conditions causing high temperatures, heavy rainfall at both short and longer durations and exceptionally high levels of atmospheric moisture. Heavy rain affected many parts of Western Australia region, extending from the Kimberley in north and progressively south through the eastern interior, resulting in substantial flooding.

The month started with a broad area of low pressure covering most of the continent that combined with a warm moist airmass, generated a middle-level cloud extending across central parts of the country (Figure 4.7). Broad troughs persisted through most of the

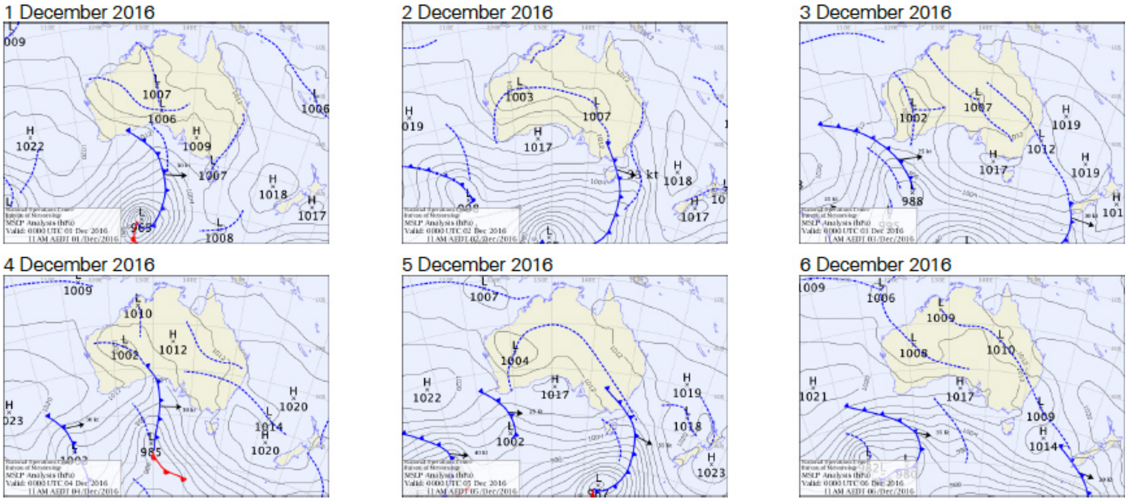

Figure 4.7. *Mean Sea Level Pressure (MSLP) Analysis for early December 2016 [36].*

month, leading to enhanced areas of thunderstorm activity across northern and central parts of the country. Later in the month thunderstorm activity increased over the waters in the north-west of the continent in association with two tropical lows and the monsoon trough. On the 21st (Figure 4.8), one of the tropical low intensified into a tropical cyclone continuing its way to the west-south. On the last days of the month the tropical

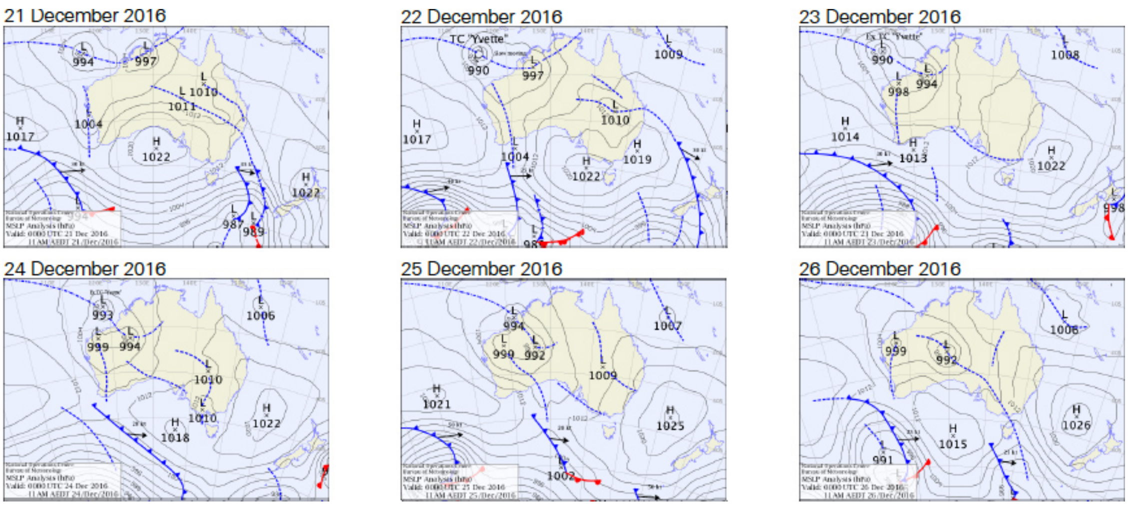

Figure 4.8. *MSLP Analysis for the end of December 2016 [36].*

cyclone, named Yvette, were absorbed into another low located over the Kimberley district of Western Australia. Then January began with an active monsoon extending over tropical Australia that brought squally thunderstorms to the Kimberley region. The month was mainly characterised by broad areas of low pressure weather, continuing to hit western territories with the heavy rainfall. The last few days of January saw a tropical low moving southeastward along the Kimberley coasts before moving offshore.

4.2.2 Temperature

Despite both maximum and minimum temperature during December 2016 were above average for Australia, with a national mean temperature anomaly of +0.71 °C, in large parts of Western Australia mean temperatures were below or around average (Figure 4.9).

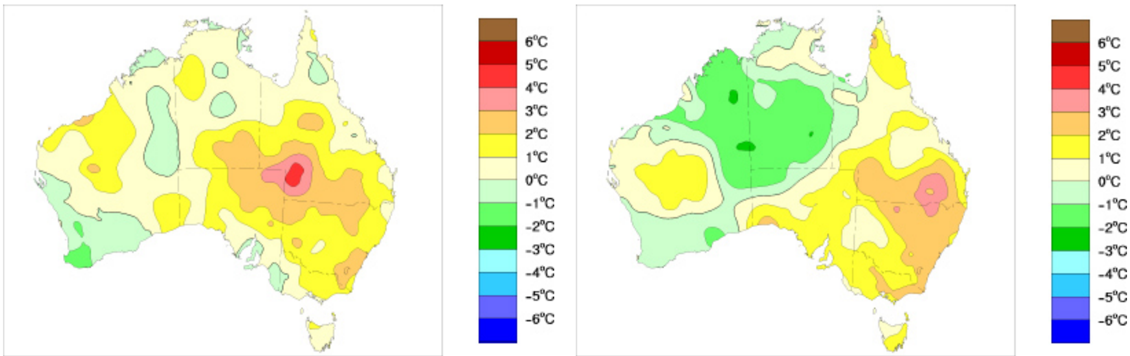

(a) (b)

Figure 4.9. *Anomalies of mean daily max (a) and min (b) temperatures for December 2016 [36].*

Same behaviour was observed for the month of January that saw both mean maximum and minimum temperatures warmer than average for Australia, with the national mean temperature 0.78 °C above average, but not in Western Australia territories that recorded cooler than average mean temperatures (Figure 4.10).

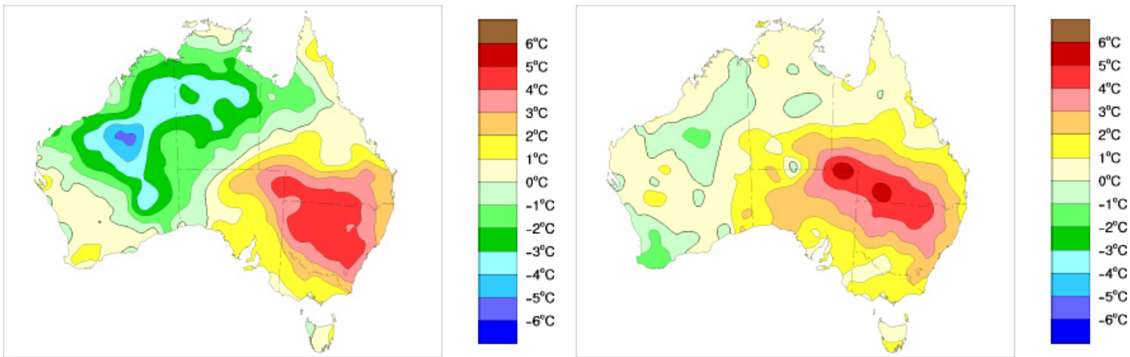

(a) (b)

Figure 4.10. *Anomalies of mean daily max (a) and min (b) temperatures for January 2017 [36].*

4.2.3 Rainfall

Nationally, December rainfall was 76% above average becoming so the fifth-wettest December on record with Western Australia reached its third-wettest December on record (Figure 4.11 (a)). Also January 2017 rainfall was particularly large: the fourth wettest on record for Australia with 66% above the long-term average and again the third-wettest January for Western Australia (Figure 4.11 (b)). The first significant rainfalls developed

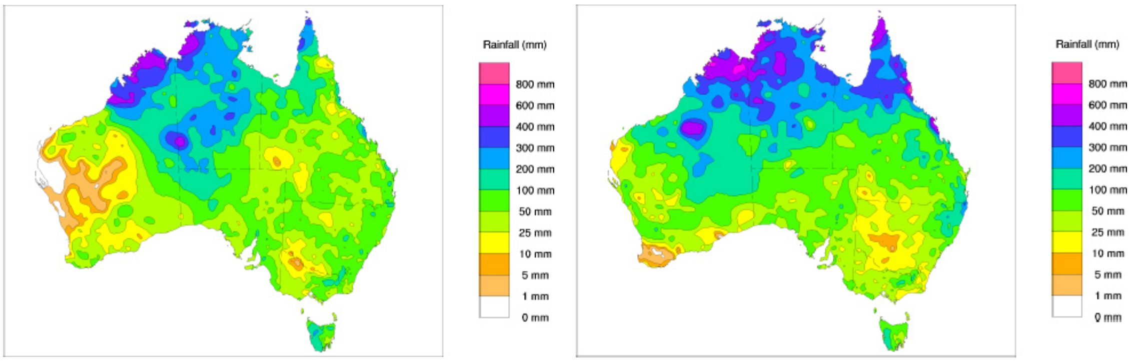

(a) (b)

Figure 4.11. *Total rainfall in December 2016 (a) and January 2017 (b) [36].*

on the 20th, when totals locally exceeded 50 millimetres over the east Kimberley. Then heavy rain became more extensive over the next two days with numerous totals above 100 millimetres on the 21st in the north Kimberley, extending to the west on the 22nd and 23rd. From 20 to 31 December (Figure 4.12) most parts of Kimberley were struck by falls between 200 and 400 millimetres.

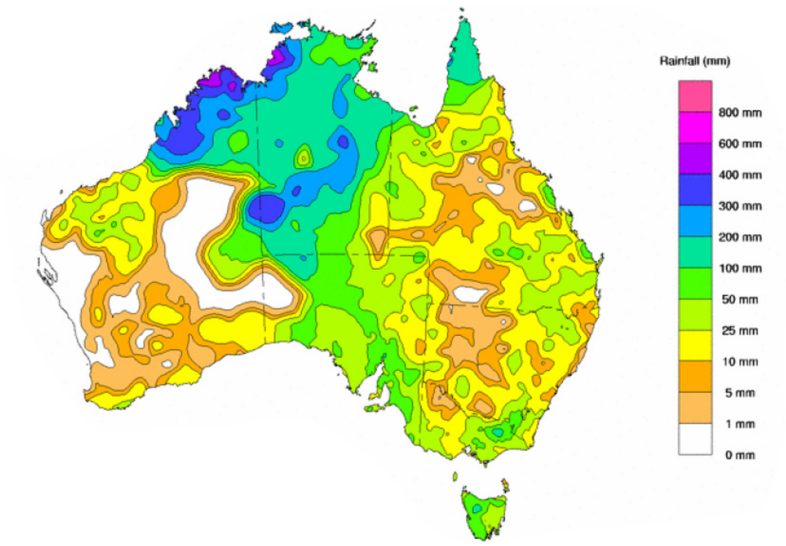

Figure 4.12. *Rainfall totals for the period from 20 to 31 December 2016 [37].*

4.3 Economic and social damages

The significant flooding of 2016-2017 occurred in Western Australia caused four deaths and only in Kimberley district eleven rescue interventions [8]. Low-lying houses in the town of Fitzroy Crossing have been evacuated and mainly roads to access to town have been cut. For these reasons emergency services have had to coordinate aerial food drops to remote pastoral stations and Aboriginal communities (Figure 4.13). The area's economy is primarily driven by pastoral, mining and tourism activities that underwent an interruption for several months.

Figure 4.13. *Floodplains around the town of Fitzroy Crossing isolated the area that requested the intervention of emergency services [9].*

The greatest economic damages were those related to circulation of traffic since the event needed the closure of the Fitzroy Crossing bridge, considered an hub of commercial and public passages for the communities of the Fitzroy Valley.

Chapter 5

Results

This chapter describes the steps of the methodology for implementation and results analysis presented in Chapter 3. Firstly we give an overview on the input data used to model the study case. After that, several cases of simulations tested and the comparisons necessary for the model evaluation will be reported.

5.1 Input and comparison data

Here data selection for the model implementation and the subsequent results analysis are presented. The fundamental data retrieved from online archives and prepared to be used are the DEM, the gauged data and the WOfS images.

5.1.1 DEM selection

For the purposes of this thesis a sub area of the total catchment has been chosen. The choice has been made in order to include the most relevant for economical and social aspects areas flooded during the event, reducing at the same time the computational costs of simulating the total DEM of the catchment. Moreover, it was important to include within the area selected the measurement stations available on the territory to have inflow discharge points for the simulation and gauge sections for results comparisons.
Therefore, the area chosen for the simulation has been selected firstly considering Fitzroy Crossing town, whose situation during the flooding event has been described in Chapter 4, and its available gauge station. Then the area has been extended from there to include four other stations listed in the Table 5.1. The resulting DEM selected is shown in Figure 5.1 and its characteristics are:

- Total area covered: 23 867 km^2.
- Number of rows: 4702.
- Number of columns: 5640.
- Resolution: 30 m.

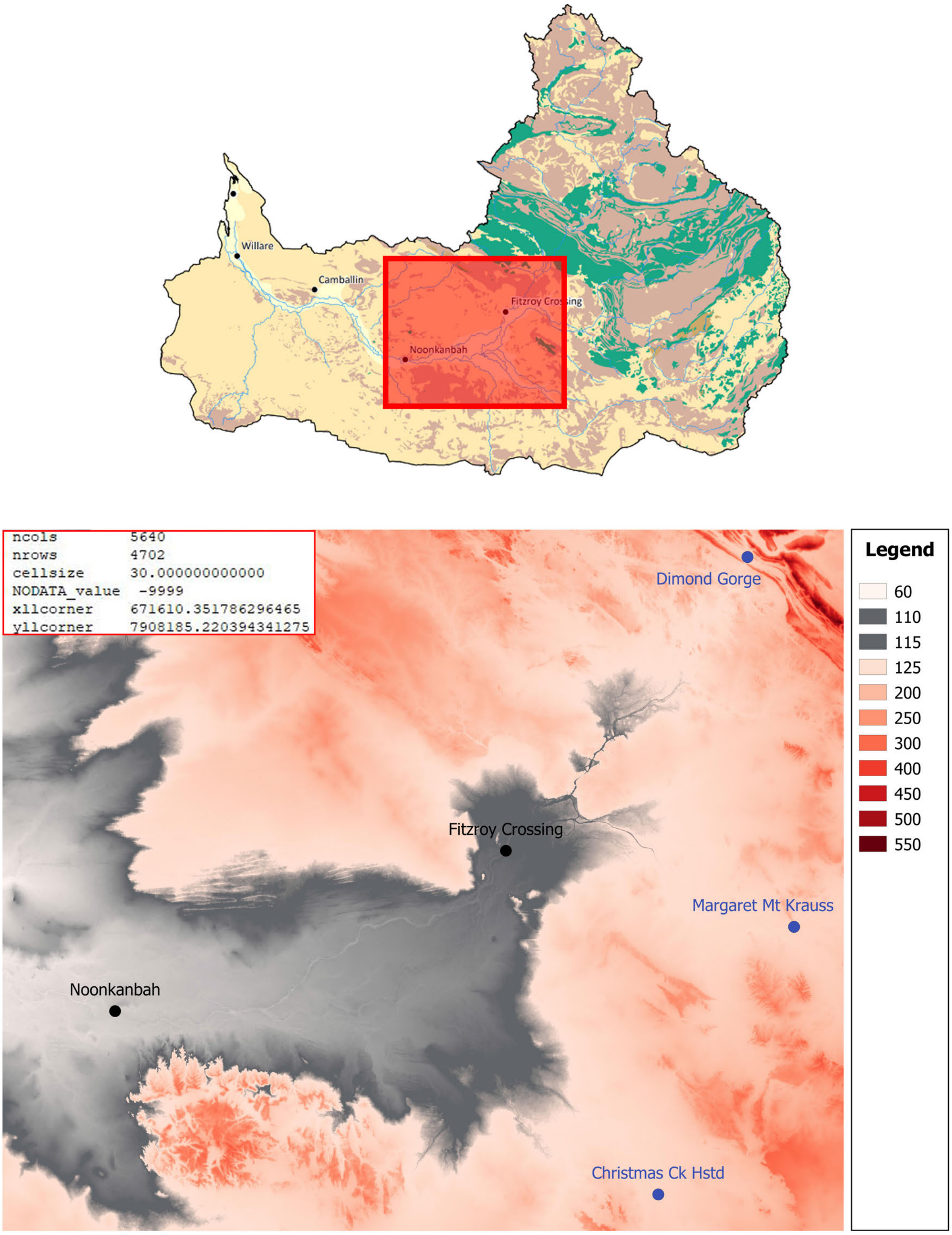

Figure 5.1. *Dem chosen as input for the model and its headers. Gauge stations used as inflow points (blue) and as comparison points (black) are marked.*

Gauge name	River name	Lat/Long	Period of record	Data used for
Dimond Gorge	Fitzroy River	-17.67/126.03	1962-2019	Inflow boundary
Mount Krauss	Margaret River	-18.34/126.13	1965-2019	Inflow boundary
Christmas Ck Hstd	Christmas Creek	-18.83/125.88	1997-2019	Inflow boundary
Fitzroy Crossing	Fitzroy River	-18.21/125.58	1955-2019	Comparisons
Noonkanbah	Fitzroy River	-18.51/124.84	1997-2019	Comparisons

Table 5.1. *Measurement stations included in the study area.*

5.1.2 Gauged and remote sensing data selection

As seen above, five gauge stations are available in the simulation area, three upstream used as inflow boundary conditions of the model and two downstream used as measurements for model evaluation. For each of them, gauged data profiles of discharge and water depth are reported in Figures 5.2 and 5.3. The rainfall event studied happened between the end of December 2016 and the end of February 2017 with a total duration of about 70 days. A time window of 16 days has been chosen to study the event, in particular the period between 20/12/2016 and 05/01/2017. Indeed, in these days high values of discharge and water depth have been recorded. In this way it is possible to focus on the peaks of the profiles, avoiding to simulate the whole event that imply high computational costs.

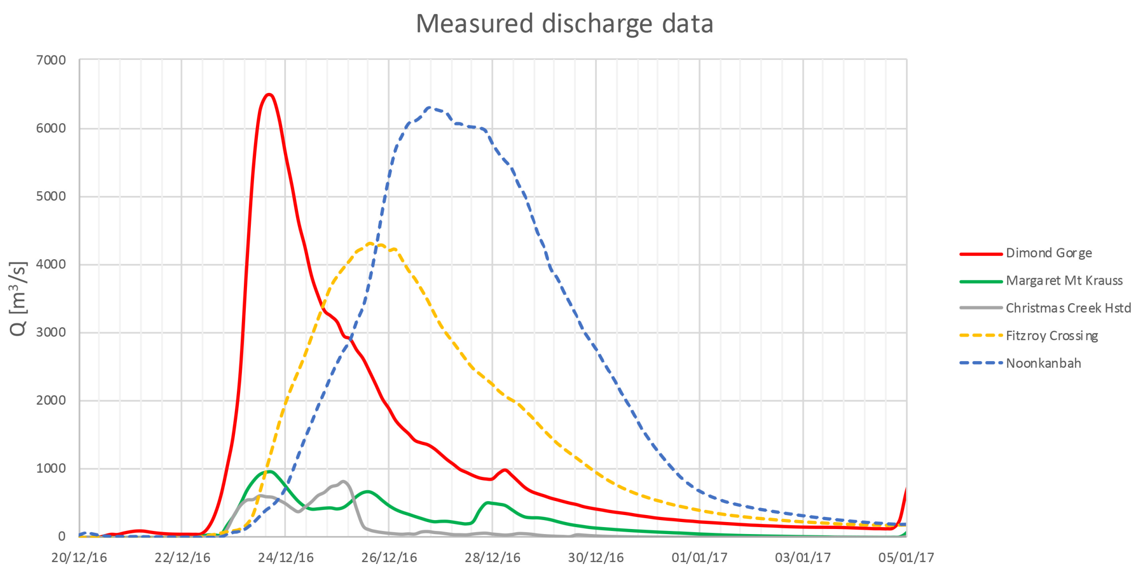

Figure 5.2. *Plot of gauged discharges.*

Moreover, the choice of the time window has been made taking into account the availability of usable WOfS images. In the aim of applying a multi-objective analysis and using remote sensing data as further results comparison, a search for WOfS images available for the event has been completed. Due to limitations of satellite temporal resolution and difficulties of

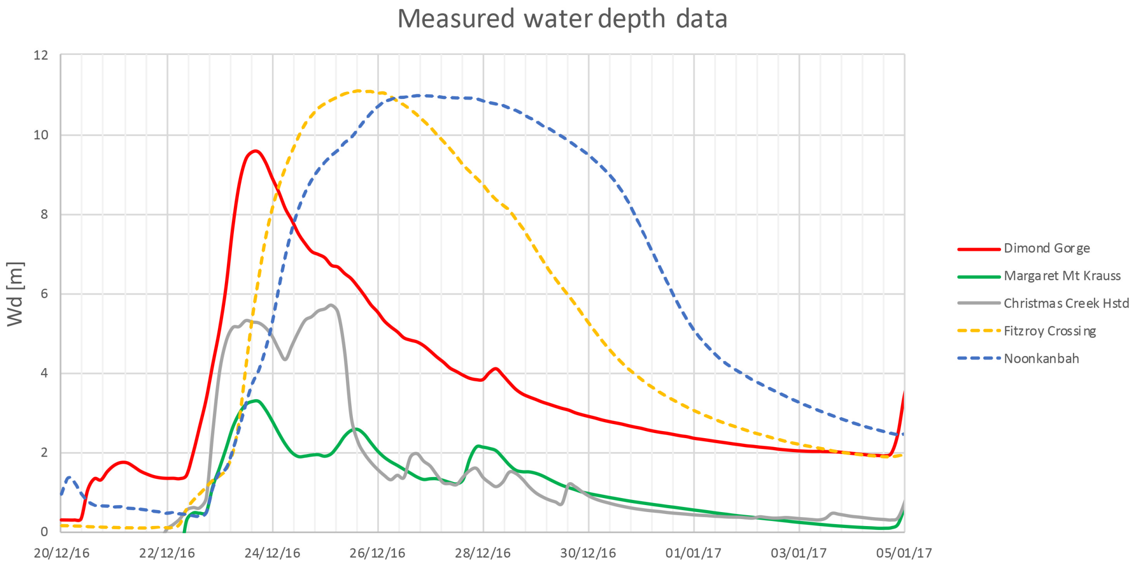

Figure 5.3. *Plot of gauged water depth.*

acquiring cloud-free images, only one acquisition containing usable information for the studied event has been found in WOfS archive. It consists in two images, captured on 28/12/2016 at 11:43, of the area around Noonkanbah station. These two images have been processed to obtain one merged, reprojected and resampled, usable for model evaluation. The result of the image processing, shown in Figure 5.4, consists in a map of about 4500 km^2.
As seen in the procedure described in paragraph 3.2.2, it is useful to take advantage of the WOfS filtered summary image for a further comparison. In the study case this product is fundamental to have an acquisition that covers all the area of interest. The image used, shown in Figure 5.5, has been obtained merging nine acquisitions of the studied area. The total image has been then reprojected, resampled and cut on the footprint of the DEM. Both WOfS products in Figures 5.4 and 5.5 need to be still processed with the HAND index procedure in order to to exclude errors in areas farther than 20 m from the main drainage network. The resulting post processed images will be presented in next paragraphs at the moment of results comparisons.

5.2 Initial simulations Dem0

The first scenario simulated used as input, according to the best practice, the DEM described in Figure 5.1. The three stations of Dimond Gorge, Margaret Mount Krauss and Christmas Creek have been selected as discharge inflow. Moreover a uniform roughness raster file has been chosen. It consists in a grid of Manning's values with the same dimension of DEM file. An average value of 0.025 m$^{-1/3}$·s, suitable for river applications, has been set. The name *Dem0_n0.025* has been assigned in order to label the case and distinguish it from other simulations. The results saving interval has been chosen equal to three hours, giving thus eight solutions for each day simulated. For each result, the discharge

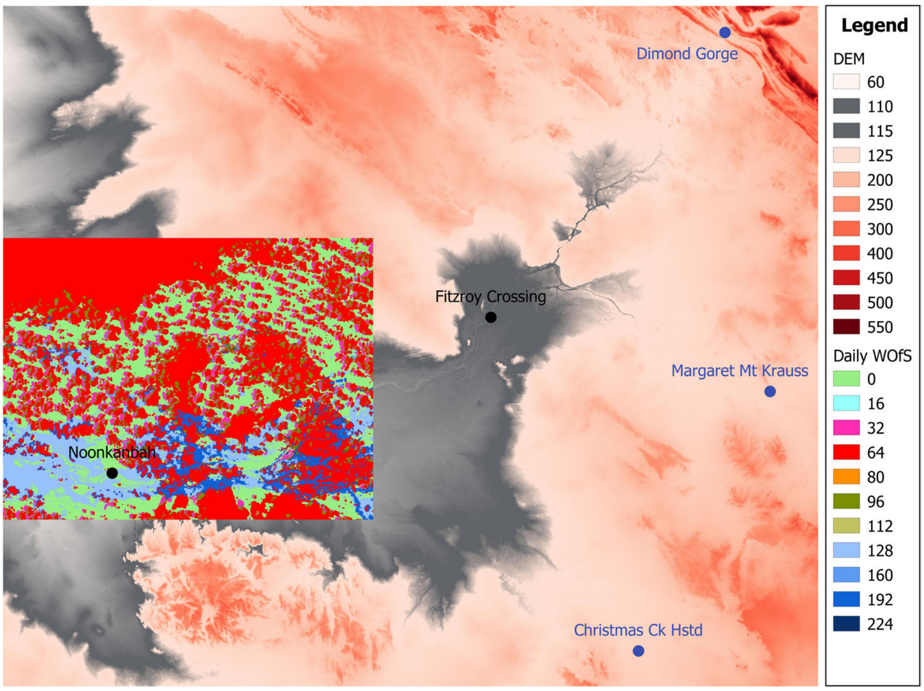

Figure 5.4. *The figure shows the WOfS image captured on 28/12/2016 laid on top of the DEM. The WOfS image covers the area around Noonkanbah station.*

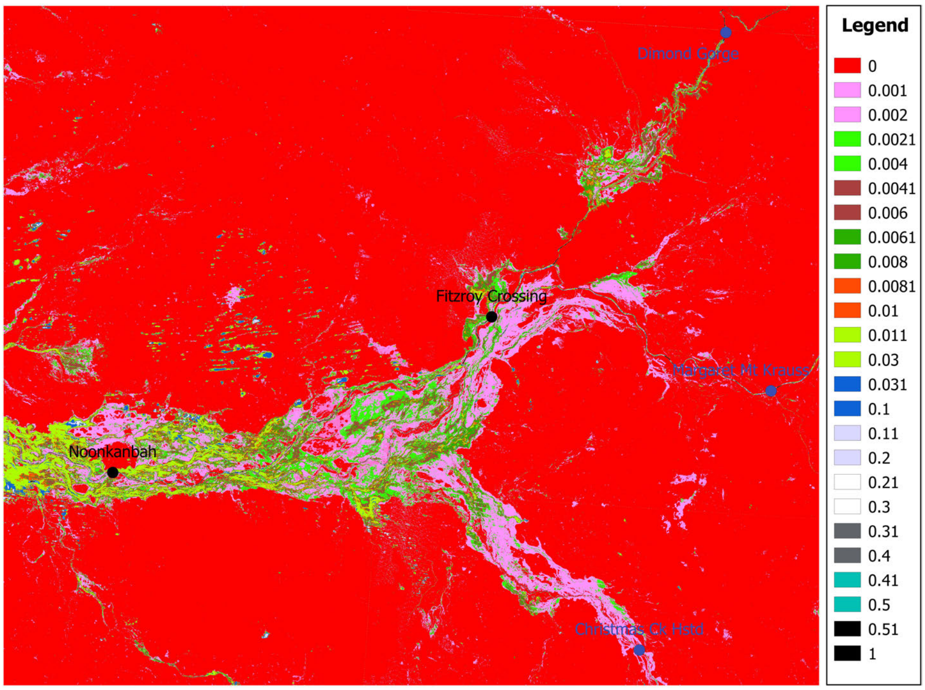

Figure 5.5. *The WOfS filtered summary image cut on the footprint of the DEM.*

and water depth values has been read in correspondence of Fitzroy Crossing and Noonkanbah stations according to the procedure described in paragraph 3.2.1. The comparisons between gauged data and simulated data profiles are displayed in Figures 5.6 and 5.7 and Tables blaaa. Hydrometric measurements comparisons show immediately the inability of the first simulation implemented to represent the behaviour of the river. In both gauge stations, the discharge and water depth simulated do not match at all the observed data. Particularly it is clear the difference between peaks reached, with a value, for example in terms of discharge, greater than 4000 m^3/s.

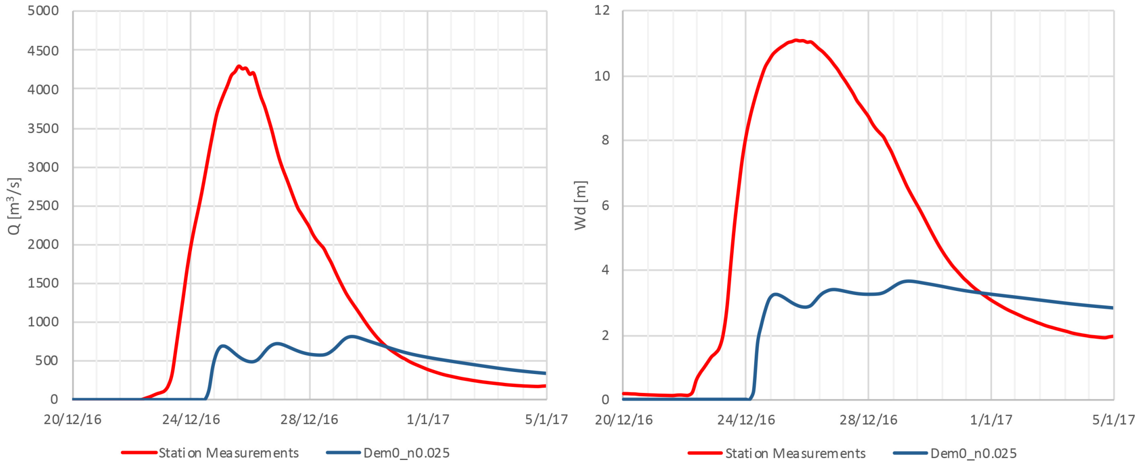

Figure 5.6. *Case Dem0_n0.025: gauged and simulated data comparisons at Fizroy Crossing station.*

Case	NSE	PBIAS	RMSE	RSR
Dem0_n0.025	-0.228	0.675	1118.448	1.108

Table 5.2. *Case Dem0_n0.025: performance metrics of gauged and simulated discharge comparison at Fitzroy Crossing station.*

Case	NSE	PBIAS	RMSE	RSR
Dem0_n0.025	-0.215	0.516	3.033	1.102

Table 5.3. *Case Dem0_n0.025: performance metrics of gauged and simulated water depth comparison at Fitzroy Crossing station.*

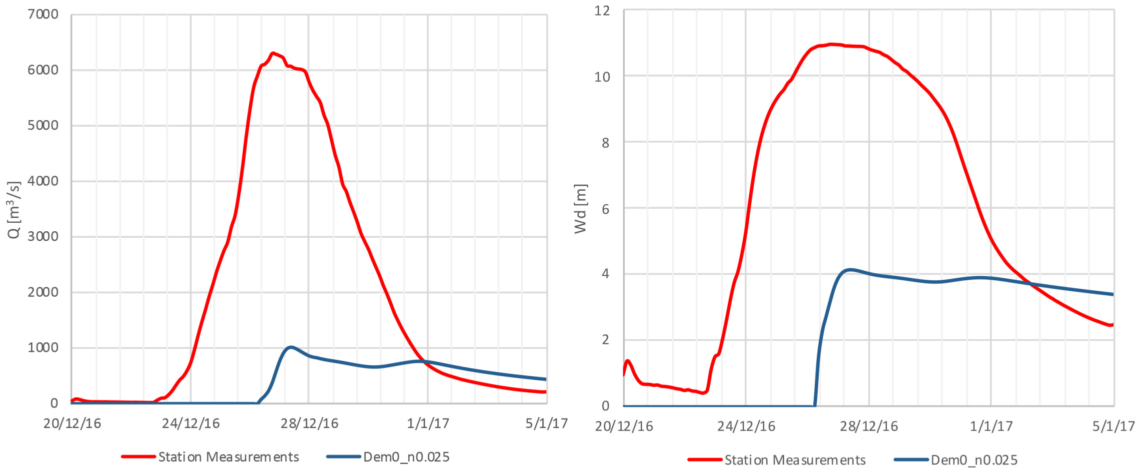

Figure 5.7. *Case Dem0_n0.025: gauged and simulated data comparisons at Noonkanbah station.*

Case	NSE	PBIAS	RMSE	RSR
Dem0_n0.025	-0.404	0.792	1872.140	1.185

Table 5.4. *Case Dem0_n0.025: performance metrics of gauged and simulated discharge comparison at Noonkanbah station.*

Case	NSE	PBIAS	RMSE	RSR
Dem0_n0.025	-0.747	0.615	3.729	1.322

Table 5.5. *Case Dem0_n0.025: performance metrics of gauged and simulated water depth comparison at Noonkanbah station.*

The visual and quantitative comparisons with RS data confirm the presence of errors in the model. The visual one, shown in Figures 5.8 and 5.9, compare the post-processing daily and summary filtered WOfS images with water depth plots. The comparison with daily WOfS image needs to select and plot the *wd* simulated result corresponding to the time of WOfS acquisition. Since the simulation starts on 20/12/2016 at 00:00 and the saving time interval is three hours, the *wd* result file to plot is the one computed by the model after 648 000 seconds from the beginning of the simulation, or in other words, after 7.5 days. The comparison with summary filtered WOfS needs instead to calculate and plot the maximum modelled flood extent considering all the water depth results of the simulation. Both the visual comparison are supported by the quantitative analysis of inundated areas, based on the creation of the contingency table and the calculation of performance metrics (Table 5.6 and 5.7). The comparison with daily WOfS image demonstrates visually and quantitatively the underestimation of the model in terms of wet areas in the area around Noonkanbah station. $BIAS$ value, very below the unit value, confirms the model underestimates the real behaviour. CSI low value indicates false alarms and miss in contingency table are numerous. $F^{<3>}$ highlights the difference between hits and miss; in this case it assumes a negative value that denotes model miss are greater than hits, or in other words the times the model does not consider cells effectively wet are greater than the times it does. $F^{<4>}$ highlights the difference between hits and false alarms; in this case it is a low but positive value, so false alarms are numerous but at least less than hits. H index describes the trade-off between hits and miss and its optimum value should be equal to one. Finally, the very low value of F implies a large number of correct non-event that indicates the high presence of dry cells, both in the simulation and in the WOfS image. Even the comparison with summary filtered WOfS image shows similar values of performance metrics.

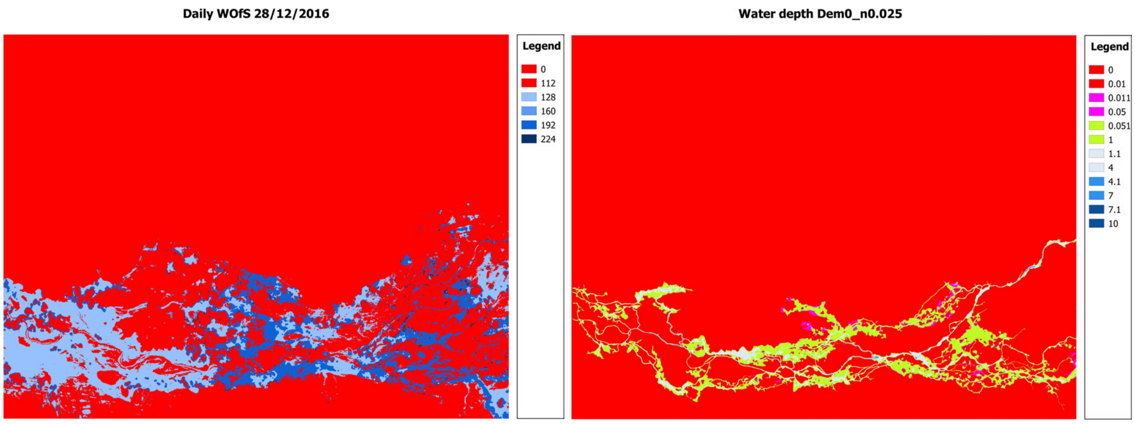

Figure 5.8. *Case Dem0_n0.025: visual comparison between daily WOfS image and correspondent water depth plot.*

	Present in observation	Absent in observation
Present in model	214 841	92 827
Absent in model	509 404	4 155 065

BIAS	PC	CSI	$F^{<3>}$	$F^{<4>}$	H	F
0.424	0.878	0.262	-0.360	0.149	0.296	0.021

Table 5.6. *Case Dem0_n0.025: quantitative comparison (contingency table and performance metrics) between daily WOfS image and correspondent water depth plot.*

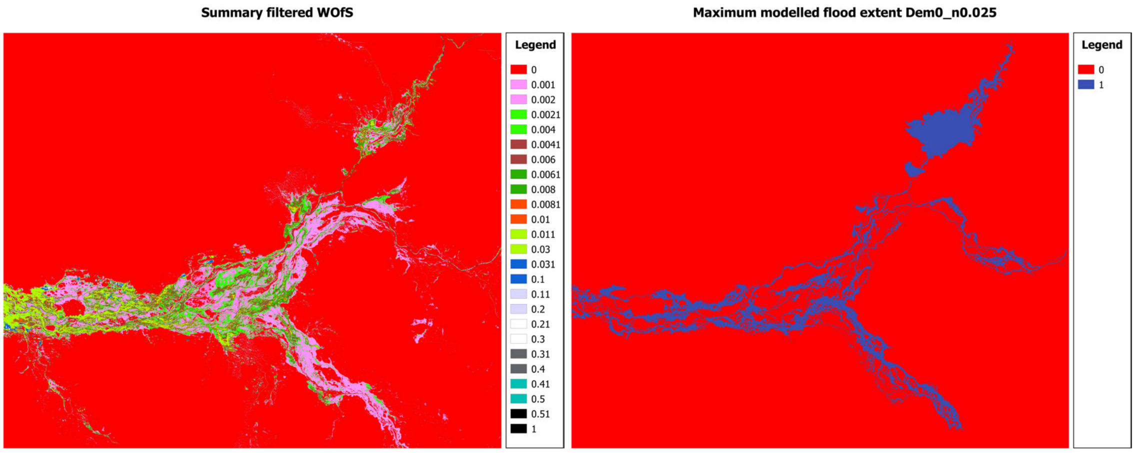

Figure 5.9. *Case Dem0_n0.025: visual comparison between summary filtered WOfS image and maximum modelled flood extent plot.*

	Present in observation	Absent in observation
Present in model	1 181 027	280 957
Absent in model	2 047 356	23 009 940

BIAS	PC	CSI	$F^{<3>}$	$F^{<4>}$	H	F
0.452	0.912	0.336	-0.246	0.256	0.365	0.012

Table 5.7. *Case Dem0_n0.025: quantitative comparison (contingency table and performance metrics) between summary filtered WOfS image and maximum modelled flood extent plot.*

In order to understand the model behaviour under different conditions, two further simulations have been implemented using the same DEM studied above and two roughness input file with Manning's values of 0.018 and 0.075. As it is possible to observe in the Figures 5.10 and 5.11, assuming lower values of roughness allows to anticipate the rising limb of discharge and water depth profiles. On the other side, as expected, the discharge peak values slightly increase, whereas water depth peak values are subjected to a further drop. However, also for these cases the match between observed and simulated data is far from being considered acceptable.
Comparisons with RS data bring approximately to the same considerations made for the case with n equal to 0.025. Actually in these cases, assuming lower values of roughness, it increases the underestimation of the model and leads to have performance metrics values further from their optimal targets. Visual comparison plots and performance metrics tables are reported below.

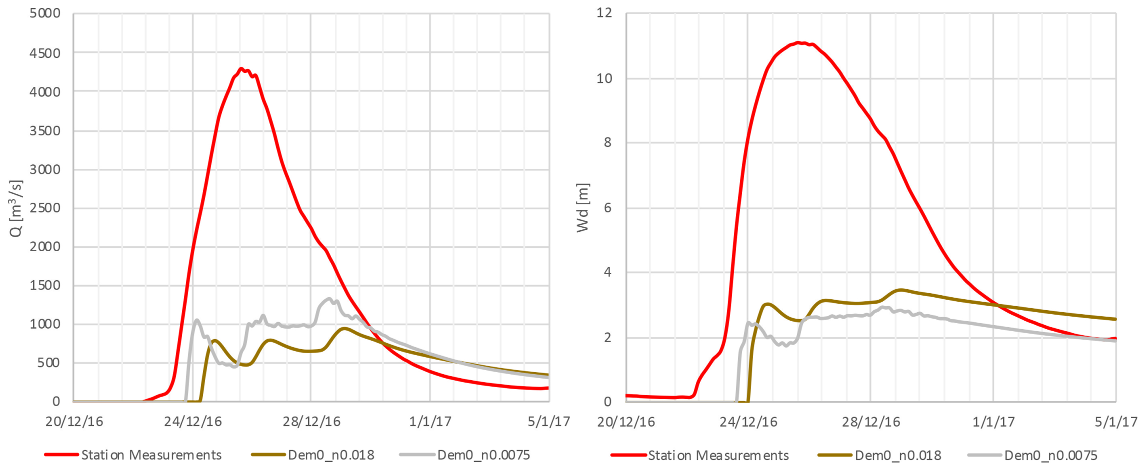

Figure 5.10. *Cases Dem0: observed and simulated data comparisons at Fizroy Crossing station.*

Case	NSE	PBIAS	RMSE	RSR
Dem0_n0.018	-0.154	0.634	1084.096	1.074
Dem0_n0.0075	0.037	0.537	990.379	0.981

Table 5.8. *Cases Dem0: performance metrics of gauged and simulated discharge comparisons at Fitzroy Crossing station.*

Case	NSE	PBIAS	RMSE	RSR
Dem0_n0.018	-0.234	0.543	3.056	1.111
Dem0_n0.0075	-0.370	0.625	3.220	1.170

Table 5.9. *Cases Dem0: performance metrics of gauged and simulated water depth comparisons at Fitzroy Crossing station.*

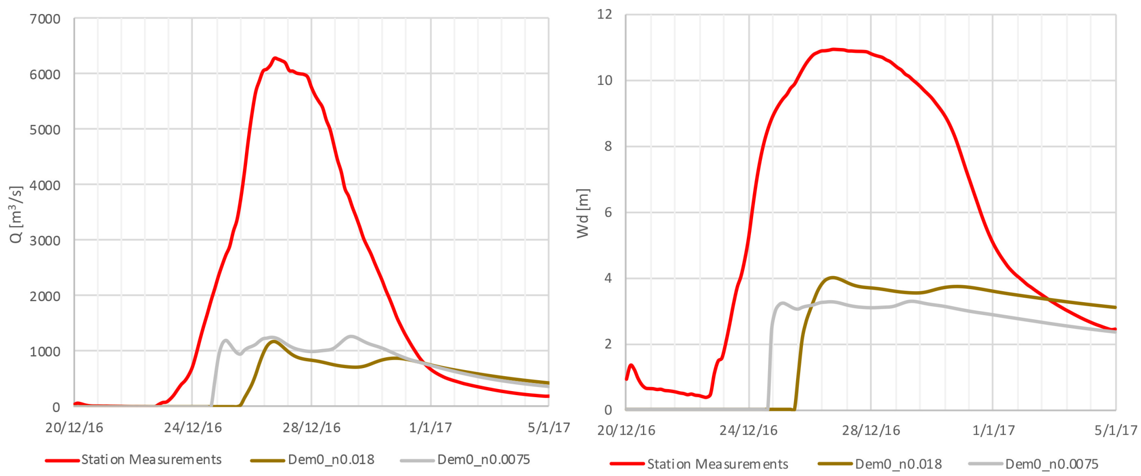

Figure 5.11. *Cases Dem0: observed and simulated data comparisons at Noonkanbah station.*

Case	NSE	PBIAS	RMSE	RSR
Dem0_n0.018	-0.282	0.759	1788.877	1.132
Dem0_n0.0075	-0.082	0.686	1643.511	1.040

Table 5.10. *Cases Dem0: performance metrics of gauged and simulated discharge comparisons at Noonkanbah station.*

Case	NSE	PBIAS	RMSE	RSR
Dem0_n0.018	-0.598	0.611	3.567	1.264
Dem0_n0.0075	-0.576	0.647	3.542	1.255

Table 5.11. *Cases Dem0: performance metrics of gauged and simulated water depth comparisons at Noonkanbah station.*

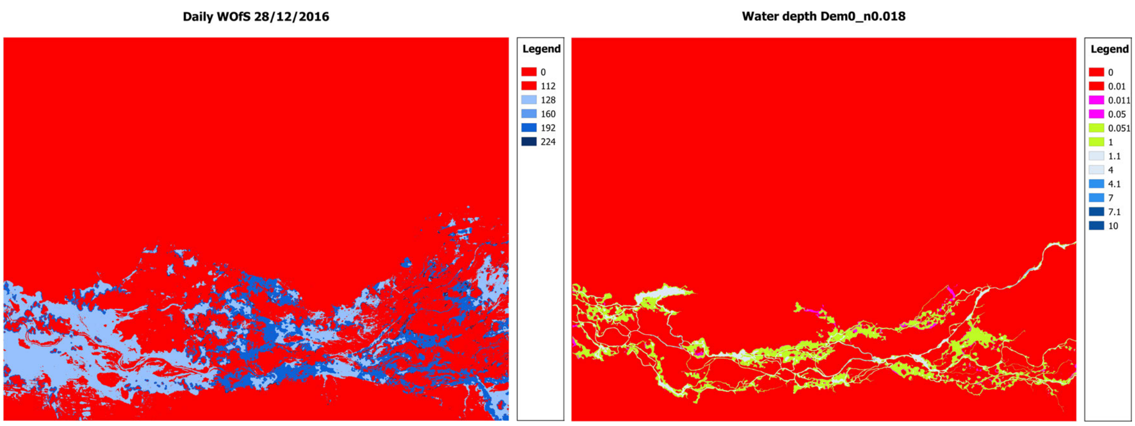

Figure 5.12. *Case Dem0_n0.018: visual comparison between daily WOfS image and correspondent water depth plot.*

	Present in observation	Absent in observation
Present in model	199 213	79 998
Absent in model	525 032	4 167 894

BIAS	PC	CSI	$F^{<3>}$	$F^{<4>}$	H	F
0.385	0.878	0.247	-0.405	0.148	0.275	0.018

Table 5.12. *Case Dem0_n0.018: quantitative comparison (contingency table and performance metrics) between daily WOfS image and correspondent water depth plot.*

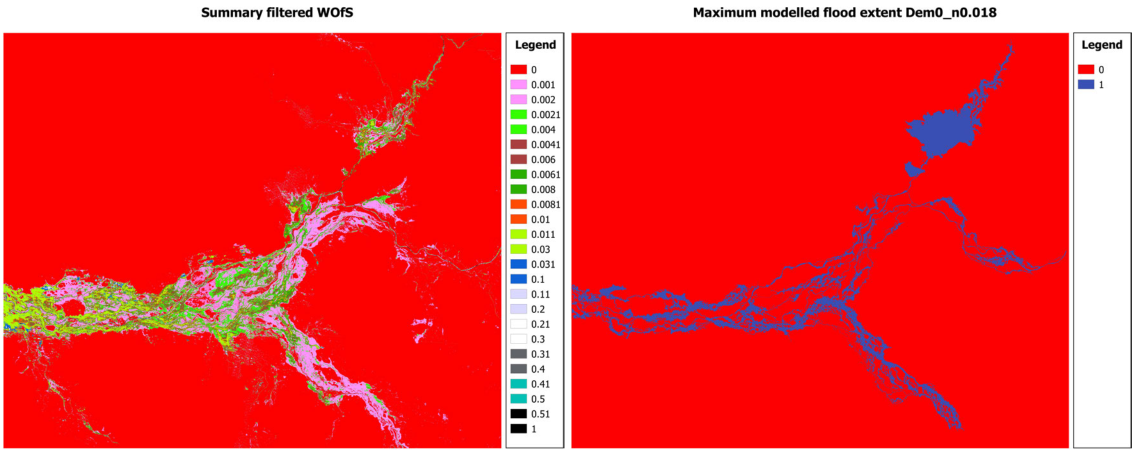

Figure 5.13. *Case Dem0_n0.018: visual comparison between summary filtered WOfS image and maximum modelled flood extent plot.*

	Present in observation	Absent in observation
Present in model	1 068 731	251 096
Absent in model	2 159 652	23 039 801

BIAS	PC	CSI	$F^{<3>}$	$F^{<4>}$	H	F
0.408	0.909	0.307	-0.313	0.234	0.331	0.010

Table 5.13. *Case Dem0_n0.018: quantitative comparison (contingency table and performance metrics) between summary filtered WOfS image and maximum modelled flood extent plot.*

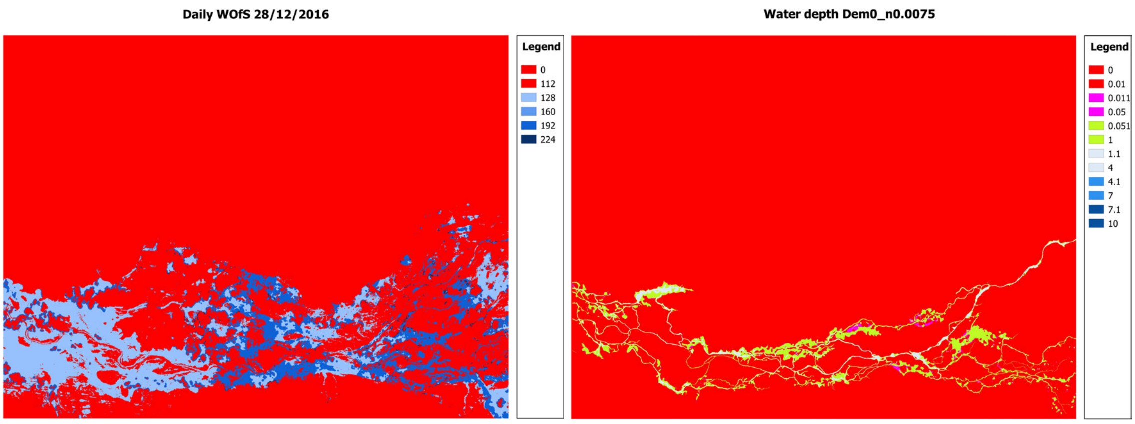

Figure 5.14. *Case Dem0_n0.0075: visual comparison between daily WOfS image and correspondent water depth plot.*

	Present in observation	Absent in observation
Present in model	126 939	50 203
Absent in model	597 306	4 197 689

BIAS	PC	CSI	$F^{<3>}$	$F^{<4>}$	H	F
0.244	0.869	0.163	-0.607	0.099	0.175	0.011

Table 5.14. *Case Dem0_n0.0075: quantitative comparison (contingency table and performance metrics) between daily WOfS image and correspondent water depth plot.*

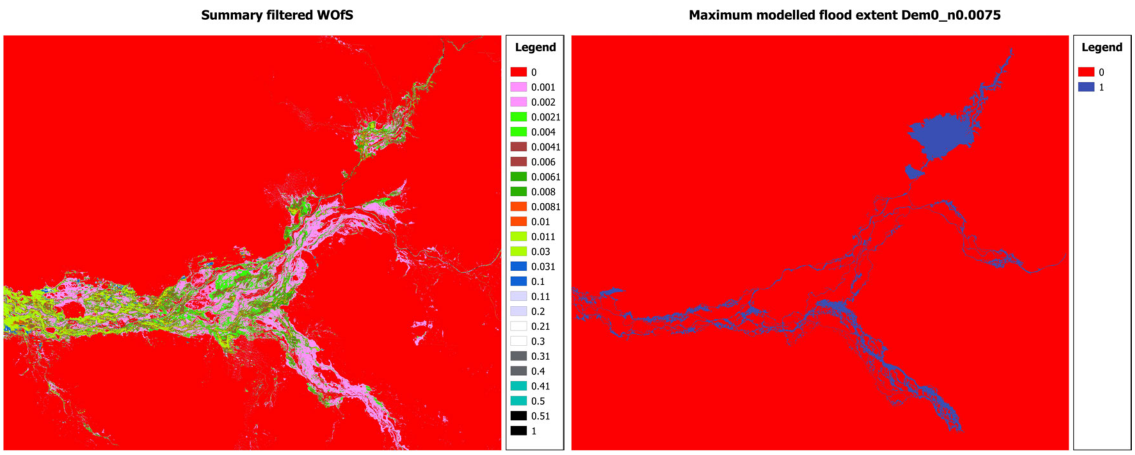

Figure 5.15. *Case Dem0_n0.0075: visual comparison between summary filtered WOfS image and maximum modelled flood extent plot.*

	Present in observation	Absent in observation
Present in model	728 019	191 456
Absent in model	2 500 364	23 099 441

BIAS	PC	CSI	$F^{<3>}$	$F^{<4>}$	H	F
0.284	0.898	0.212	-0.518	0.156	0.225	0.008

Table 5.15. *Case Dem0_n0.0075: quantitative comparison (contingency table and performance metrics) between summary filtered WOfS image and maximum modelled flood extent plot.*

5.3 Dem correction

Results analysis executed for cases *Dem0* showed the inability of the model, under the conditions chosen, to represent the studied flooding event. In order to understand the possible source of errors and visualize the water flow propagation, the series of daily water depth has been plotted. Figure 5.17 shows the water depth plots for the first eight days of simulation *Dem0_n0.025*. It is possible to notice, starting from the third day, a particular effect of back water flow in the reach of the Fitzroy River downstream Dimond Gorge station. Going into detail as shown in Figure 5.18, a presence of an obstruction causing the interruption of the flow between Dimond Gorge and Fitzroy Crossing stations can be supposed. This obstruction could be a real natural barrier created by the terrain slope, but most likely it can be associated to the low accuracy and precision of the DEM in the specific area of study. The hypothesis of an obstruction is supported then by another fact. It is possible to notice the simulated profiles of cases *Dem0* present a fluctuating trend similar to those gauged at Margaret Mt Krauss and Christmans Creek stations. This could indicate that the simulated values of q and wd read at Fitzroy Crossing and Noonkanbah stations correspond to the contribution of only the tributaries Margaret River and Christmas Creek, whereas the part of flow related to Fitzroy River is blocked upstream.

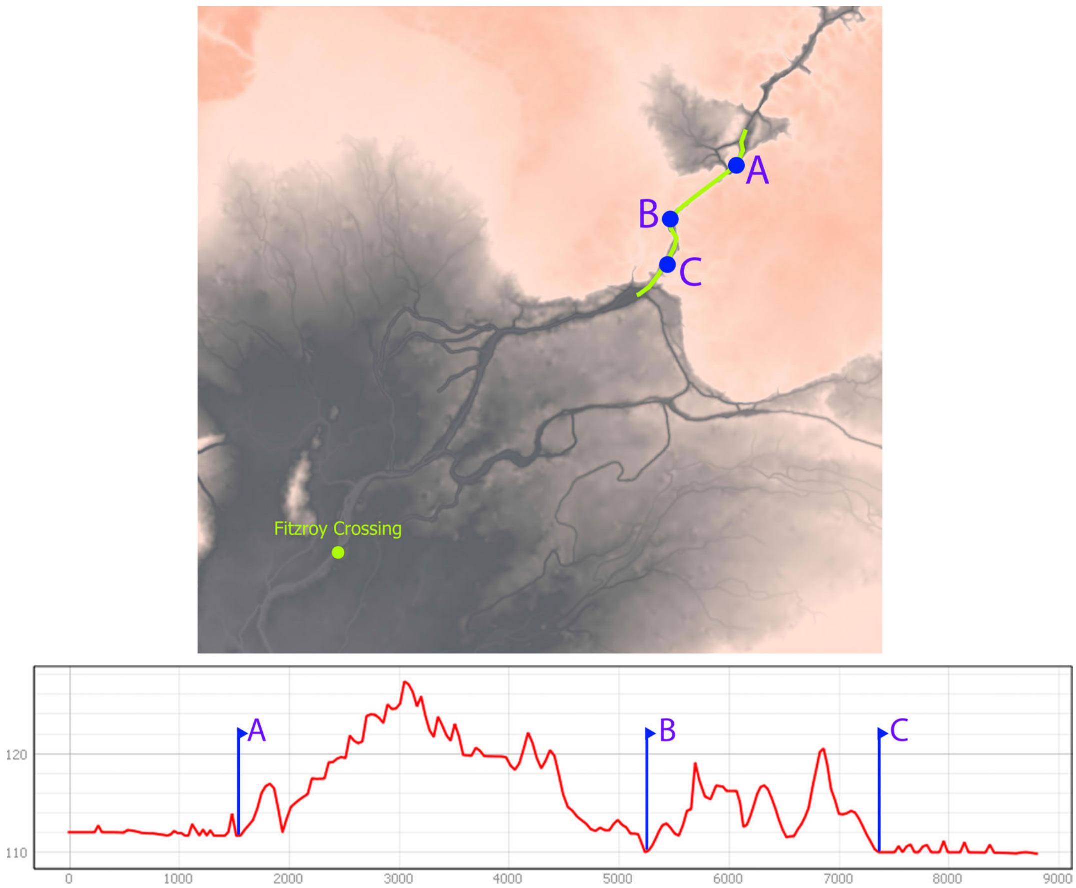

Figure 5.16. *Reach interested by the increase of the bottom slope and its terrain profile.*

In order to verify the real presence of an obstruction, the terrain profile of the DEM in the critic area has been studied using a geographic information system. In this way, a local increase of the river bottom has been discovered (Figure 5.16). Particularly, the river slope increases in two stretches: the first one, *A*-*B*, characterised by a raising of terrain of about 15 meters for a length of 4 km and the second one, *B*-*C*, by a raising of about 10 meters for a length of 2 km. On the basis of this information, it has been chosen to locally modify the DEM file to simulate several configurations without the obstruction. Following steps described in paragraph 3.1.1, the two critic stretches have been levelled to obtain a DEM with a regular downhill slope. Practically, two typologies of DEM correction have been tested. One levelling only the first stretch with greater raising of slope *A*-*B* and the other levelling the whole reach interested *A*-*C*. The latter will be labelled *extended*. Then, for both typologies, it was necessary to chose the width of the levelling realized, corresponding to the number of adjacent pixels modified in the direction perpendicular to the flow. Three configurations of "digging" width have been selected. The first one, that will be named *Dem1*, with a width of one pixel; the second one, named *Dem3*, with a width of three pixels; and the third one, named *Dem9*, with a width of nine pixels.
All the configurations described have been implemented and tested in the model. In next paragraphs, as it has been done for the case *Dem0*, results of simulations are reported.

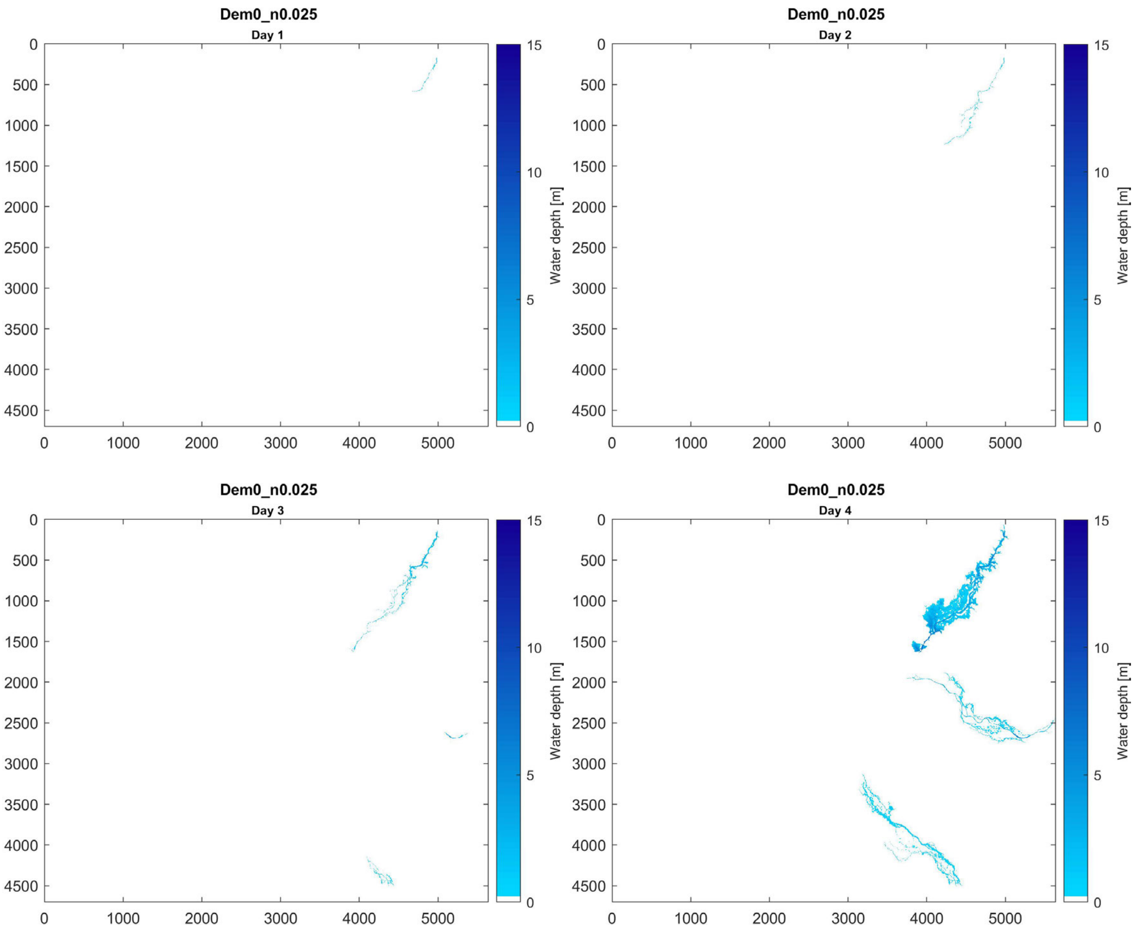

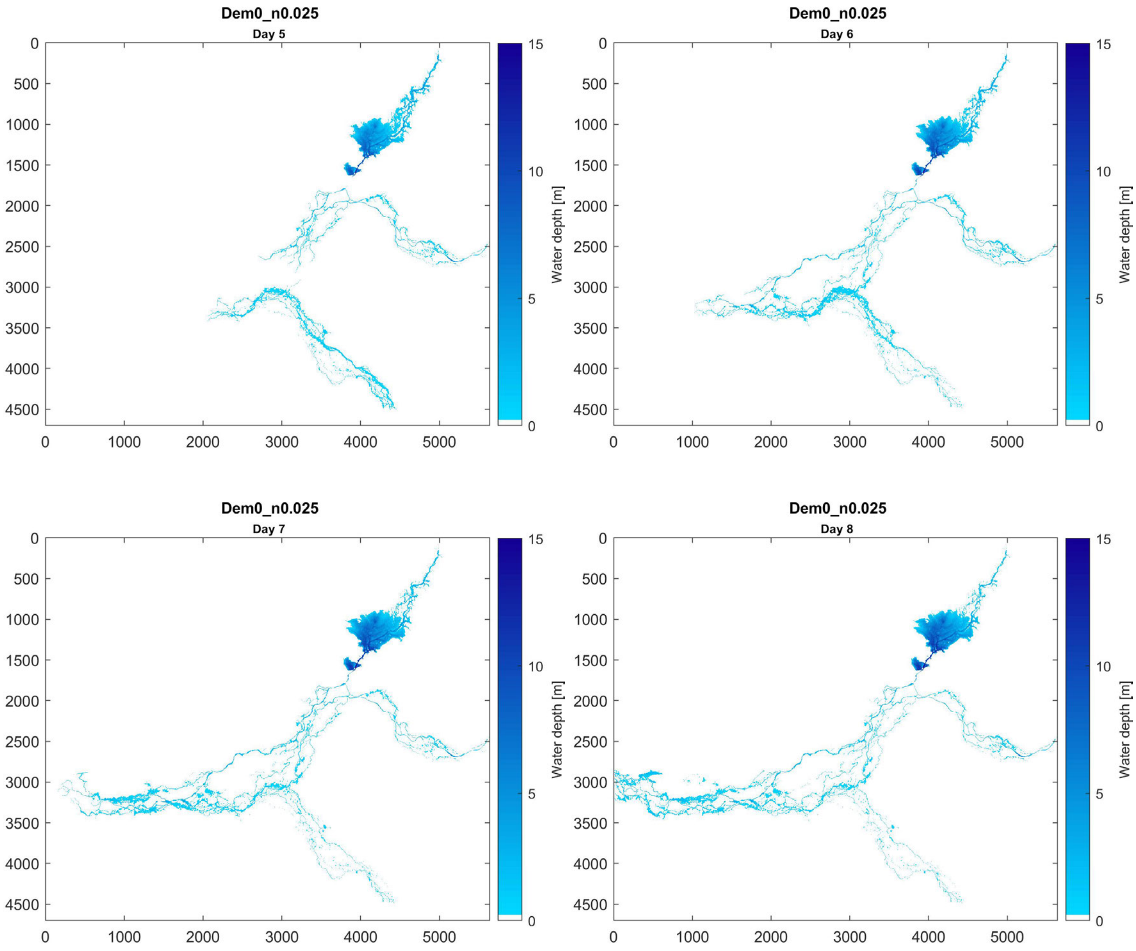

Figure 5.17. *Water depth plots of the first eight days of simulation Dem0_n0.025.*

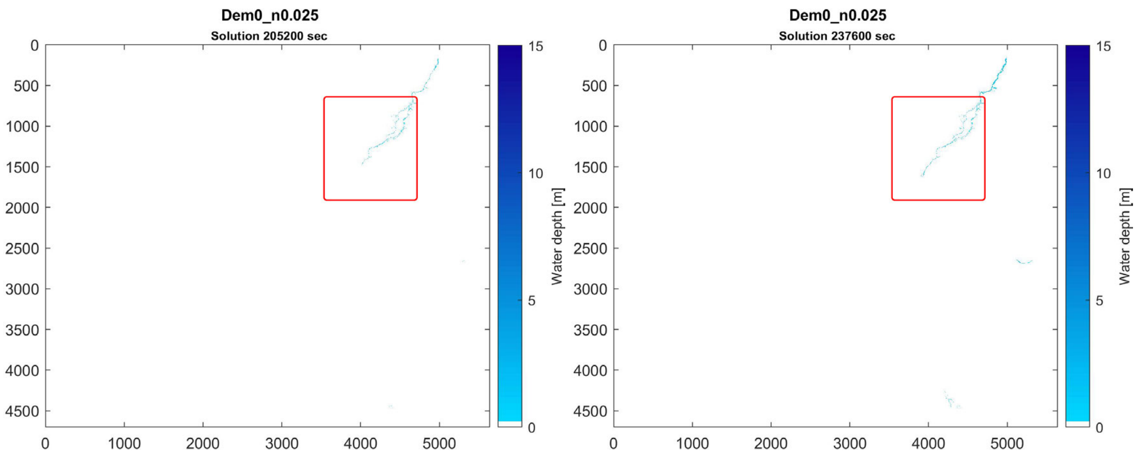

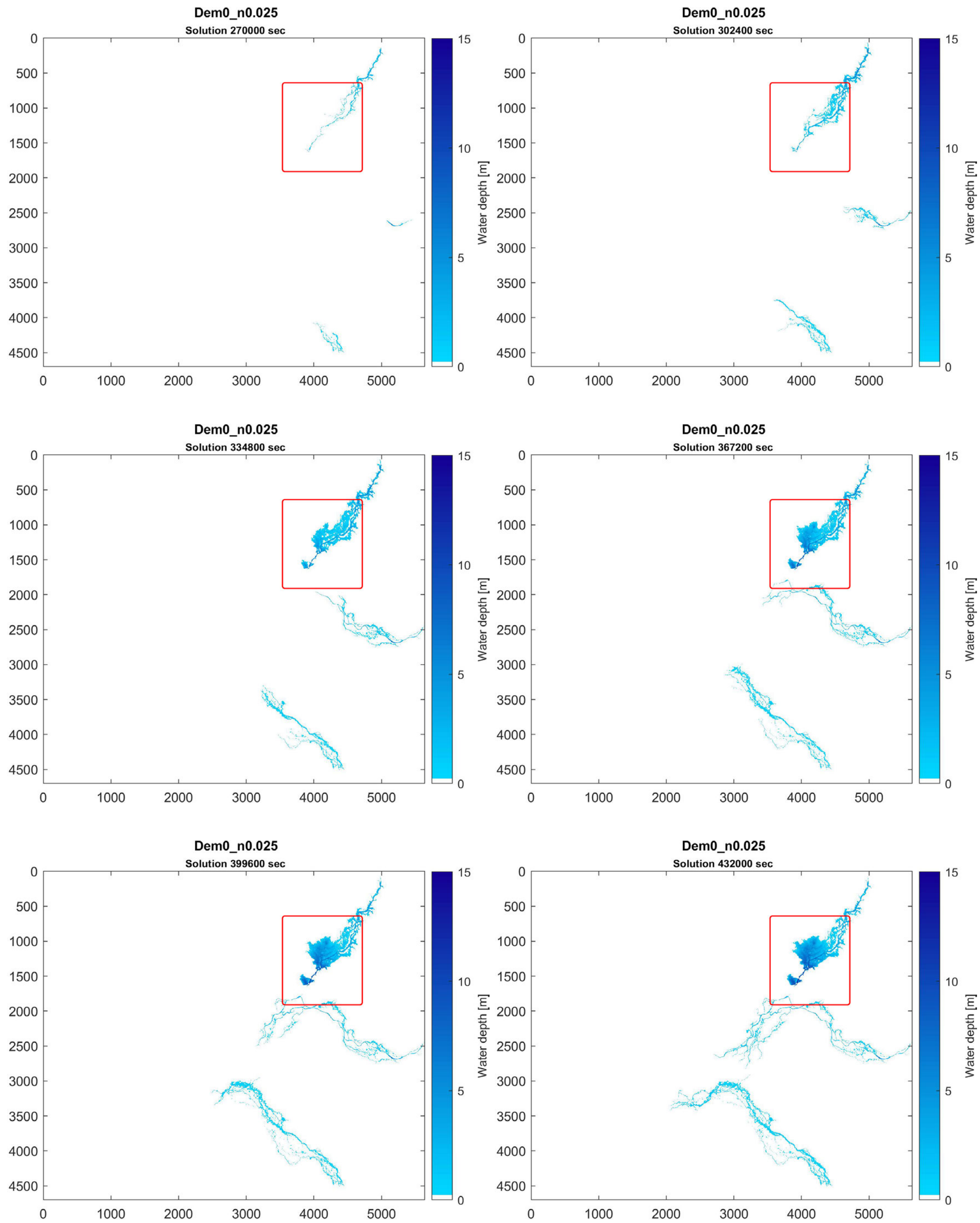

Figure 5.18. *Detail of water depth plots. The area marked with red indicates the zone where the water flow stops.*

5.4 Simulations Dem1

The first modified tests run uses a DEM where the local obstruction is solved realizing a strip of levelled terrain with a width of 30 meters. Figure 5.20 shows the two typologies of modified DEM tested.

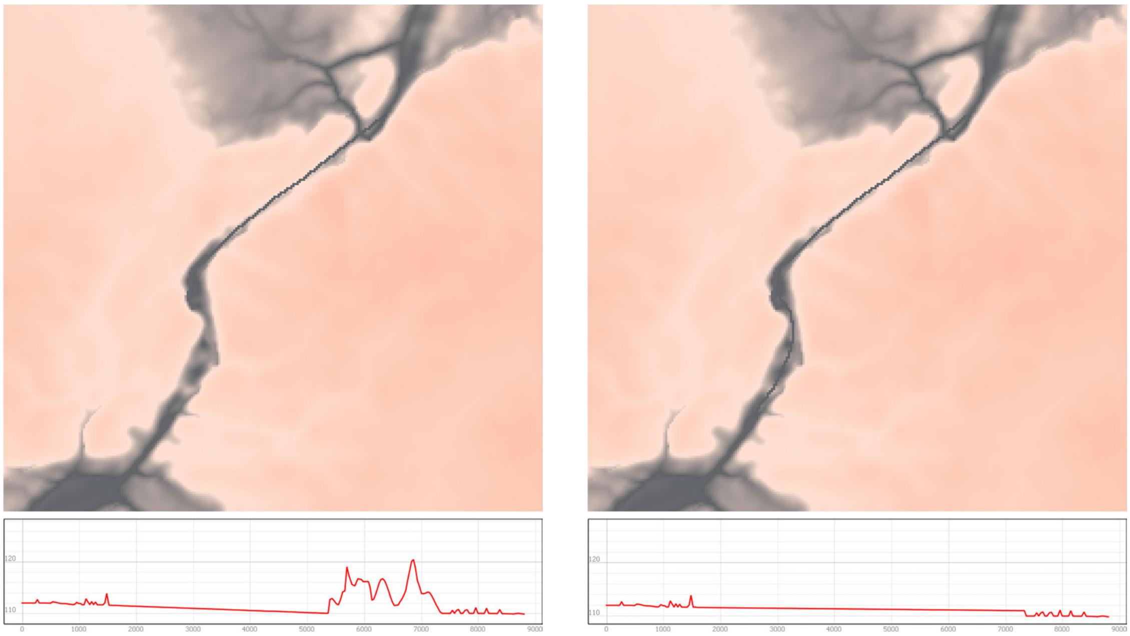

(a) *No extended* (b) *Extended*

Figure 5.20. *Local DEM modifications and related terrain profiles of the stretch interested for case one pixels width digging.*

Firstly, a no extended with roughness equal to 0.025, labelled case *Dem1_n0.025*, has been tested. Immediately the results analysis showed an improvement of the model behaviour compared to the initial simulations with *Dem0*. Both at Fitzroy Crossing and Noonkanbah stations peaks values read increase and the particular fluctuation of the profiles disappears, indicating the contributions of Margaret River and Christmas Creek is now joined with that of Fitzroy River. Therefore, simulated profiles fits better the observed ones, suggesting the hypothesis of the presence of an error in the DEM file was correct. Even the visual and quantitative comparisons with WOfS image show a significant improvement. The wet cells simulated of the area around Noonkanbah better correspond to those captured by the daily WOfS image and performance metrics confirm the improvement of model prediction (Figure 5.23 and Table 5.20). The comparison with summary filtered WOfS (Figure 5.24 and Table 5.21) indicates the model still underestimates the real behaviour. Nevertheless, a margin of underestimation is acceptable remembering the summary filtered WOfS takes into account of all the historical events and it cannot considered a direct comparison with a specific event.
As done for cases *Dem0* a test changing the roughness value input has been run. The case *Dem1_n0.018* chosen as new simulation allowed to achieve a general further improvement

of model behaviour. Moreover, in order to understand the influence of the second stretch with raising slope, an extended *Dem1* has been tested. Here the no extended and the extended cases show approximately the same results. It is possible thus to say, at least for case with excavation width equal to one pixel, the obstruction of the stretch AB is that with greater effect on the model.
In next paragraphs all the comparisons described are groped for each case of simulation run.

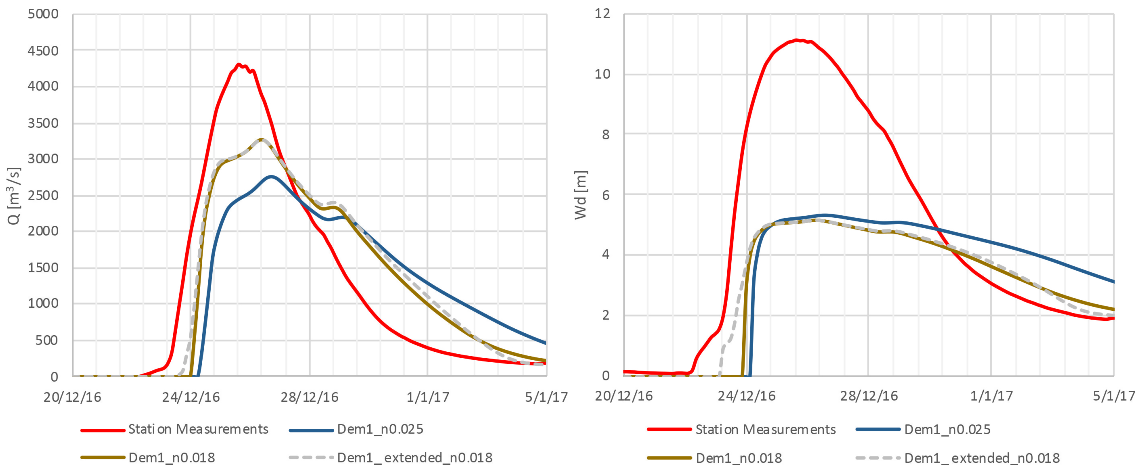

Figure 5.21. *Cases Dem1: gauged and simulated data comparisons at Fizroy Crossing station.*

Case	NSE	PBIAS	RMSE	RSR
Dem1_n0.025	0.534	0.015	688.803	0.682
Dem1_n0.018	0.788	-0.017	464.735	0.460
Dem1_extended_n0.018	0.792	-0.050	460.626	0.456

Table 5.16. *Cases Dem1: performance metrics of gauged and simulated discharge comparisons at Fitzroy Crossing station.*

Case	NSE	PBIAS	RMSE	RSR
Dem1_n0.025	0.271	0.305	2.350	0.854
Dem1_n0.018	0.335	0.374	2.243	0.815
Dem1_extended_n0.018	0.397	0.355	2.137	0.777

Table 5.17. *Cases Dem1: performance metrics of gauged and simulated water depth comparisons at Fitzroy Crossing station.*

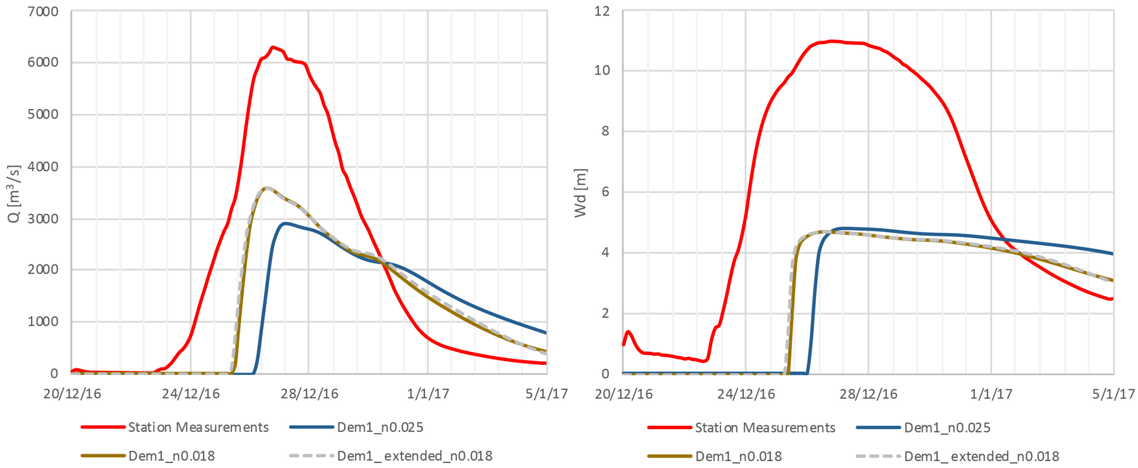

Figure 5.22. *Cases Dem1: gauged and simulated data comparisons at Noonkanbah station.*

Case	NSE	PBIAS	RMSE	RSR
Dem1_n0.025	0.534	0.015	688.803	0.682
Dem1_n0.018	0.788	-0.017	464.735	0.460
Dem1_extended_n0.018	0.792	-0.050	460.626	0.456

Table 5.18. *Cases Dem1: performance metrics of gauged and simulated discharge comparisons at Noonkanbah station.*

Case	NSE	PBIAS	RMSE	RSR
Dem1_n0.025	-0.492	0.533	3.446	1.221
Dem1_n0.018	-0.296	0.534	3.212	1.139
Dem1_extended_n0.018	-0.265	0.527	3.174	1.125

Table 5.19. *Cases Dem1: performance metrics of gauged and simulated water depth comparisons at Noonkanbah station.*

5.4.1 Case Dem1_n0.025

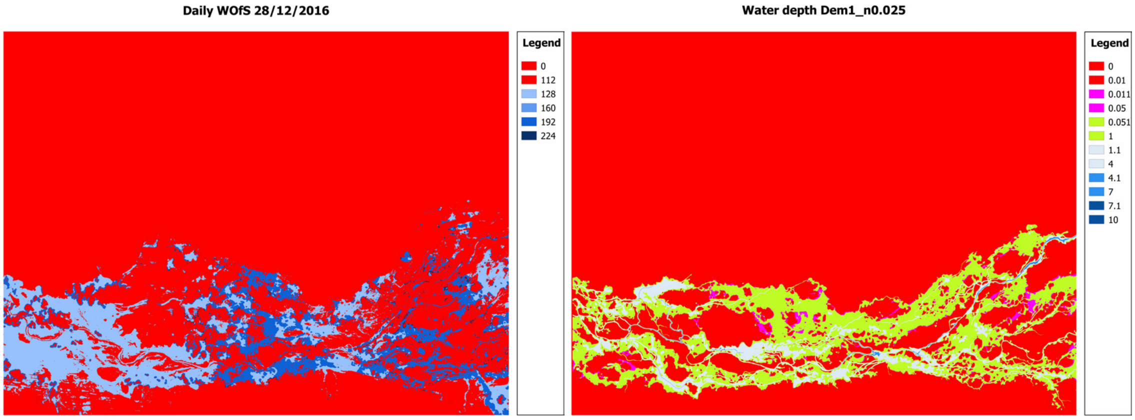

Figure 5.23. *Case Dem1_n0.025: visual comparison between daily WOfS image and correspondent water depth plot.*

	Present in observation	Absent in observation
Present in model	472 093	322 369
Absent in model	252 152	3 925 523

BIAS	PC	CSI	F <3>	F<4>	H	F
1.096	0.884	0.451	0.210	0.143	0.651	0.075

Table 5.20. *Case Dem1_n0.025: quantitative comparison (contingency table and performance metrics) between daily WOfS image and correspondent water depth plot.*

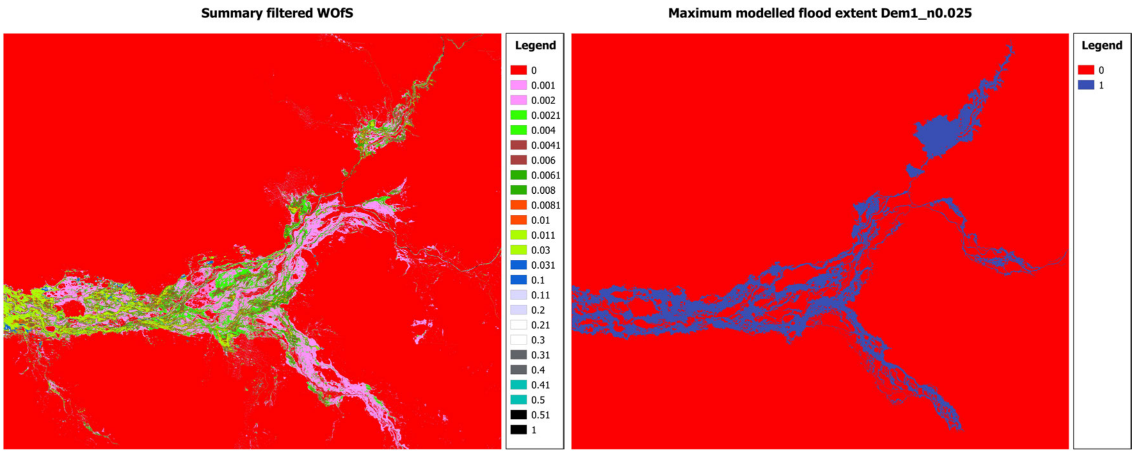

Figure 5.24. *Case Dem1_n0.025: visual comparison between summary filtered WOfS image and maximum modelled flood extent plot.*

	Present in observation	Absent in observation
Present in model	1 629 146	255 005
Absent in model	1 599 237	23 035 892

BIAS	PC	CSI	$F^{<3>}$	$F^{<4>}$	H	F
0.583	0.930	0.467	0.008	0.394	0.504	0.010

Table 5.21. *Case Dem1_n0.025: quantitative comparison (contingency table and performance metrics) between summary filtered WOfS image and maximum modelled flood extent plot.*

5.4.2 Case Dem1_n0.018

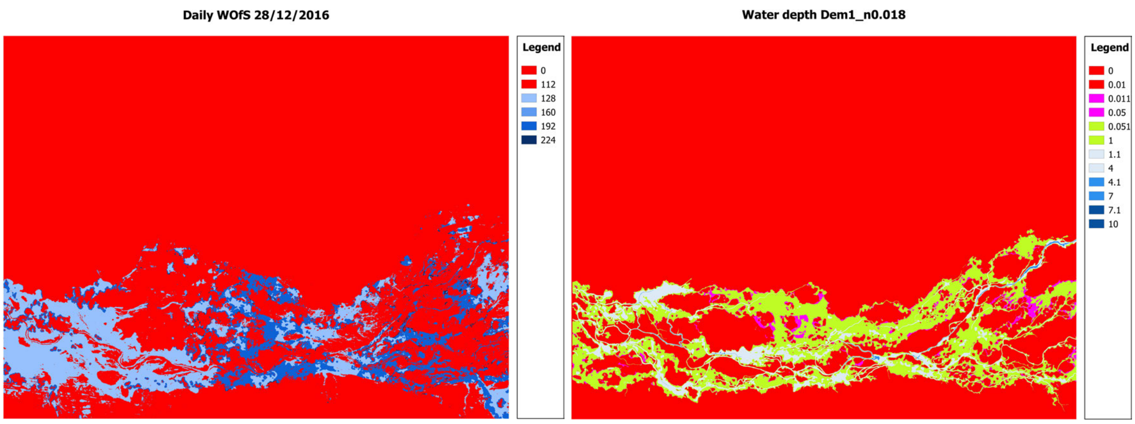

Figure 5.25. *Case Dem1_n0.018: visual comparison between daily WOfS image and correspondent water depth plot.*

	Present in observation	Absent in observation
Present in model	447 020	281 549
Absent in model	277 225	3 966 343

BIAS	PC	CSI	$F^{<3>}$	$F^{<4>}$	H	F
1.005	0.887	0.444	0.168	0.164	0.617	0.066

Table 5.22. *Case Dem1_n0.018: quantitative comparison (contingency table and performance metrics) between daily WOfS image and correspondent water depth plot.*

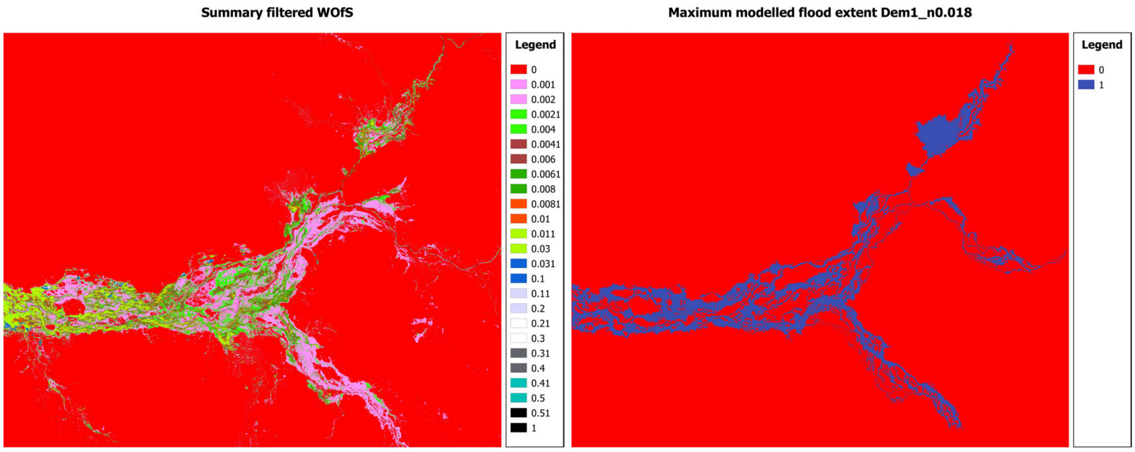

Figure 5.26. *Case Dem1_n0.018: visual comparison between summary filtered WOfS image and maximum modelled flood extent plot.*

	Present in observation	Absent in observation
Present in model	1 519 610	212 052
Absent in model	1 708 773	23 078 845

BIAS	PC	CSI	$F^{<3>}$	$F^{<4>}$	H	F
0.536	0.927	0.441	-0.054	0.380	0.470	0.009

Table 5.23. *Case Dem1_n0.018: quantitative comparison (contingency table and performance metrics) between summary filtered WOfS image and maximum modelled flood extent plot.*

5.4.3 Case Dem1_extended_n0.018

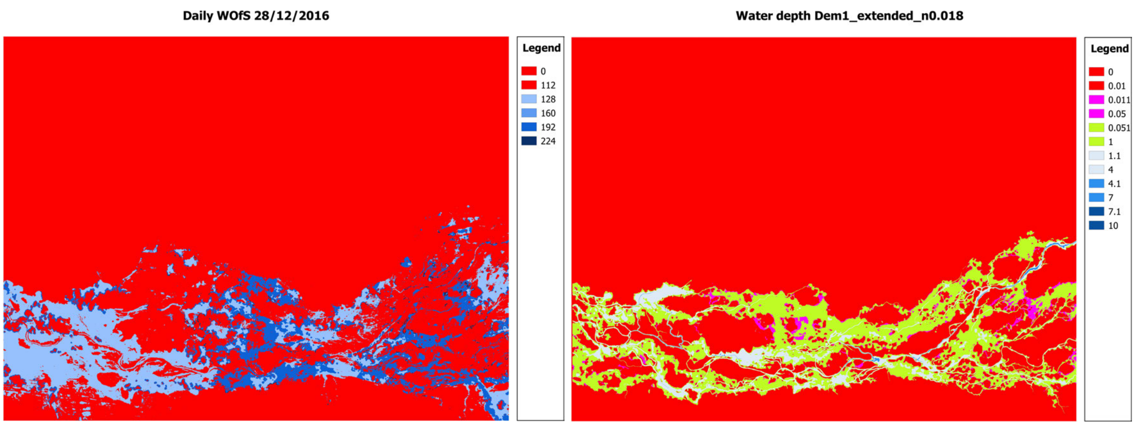

Figure 5.27. *Case Dem1_extended_n0.018: visual comparison between daily WOfS image and correspondent water depth plot.*

	Present in observation	Absent in observation
Present in model	447 410	282 210
Absent in model	276 835	3 965 682

BIAS	PC	CSI	$F^{<3>}$	$F^{<4>}$	H	F
1.007	0.887	0.444	0.169	0.164	0.617	0.066

Table 5.24. *Case Dem1_extended_n0.018: quantitative comparison (contingency table and performance metrics) between daily WOfS image and correspondent water depth plot.*

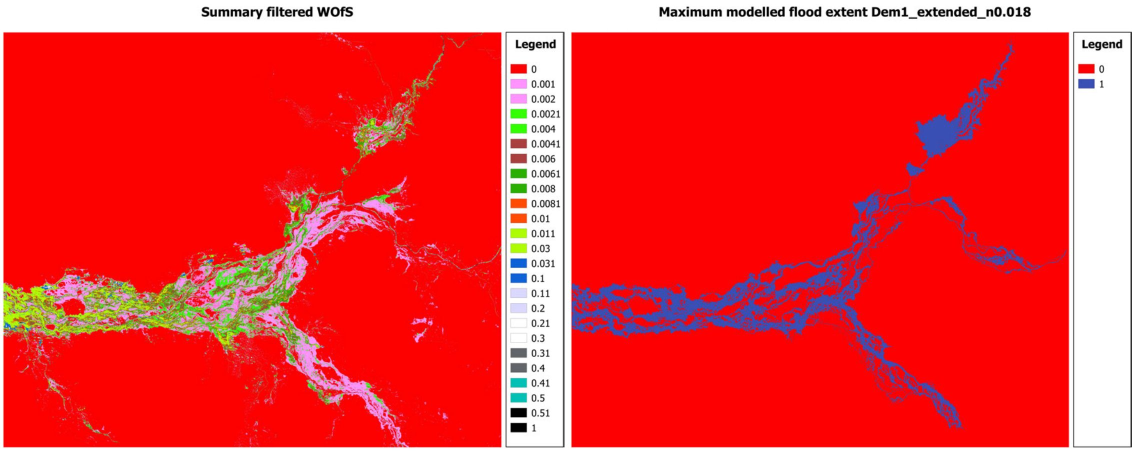

Figure 5.28. *Case Dem1_extended_n0.018: visual comparison between summary filtered WOfS image and maximum modelled flood extent plot.*

	Present in observation	Absent in observation
Present in model	1 520 463	209 817
Absent in model	1 707 920	23 081 080

BIAS	PC	CSI	$F^{<3>}$	$F^{<4>}$	H	F
0.535	0.927	0.442	-0.054	0.381	0.470	0.009

Table 5.25. *Case Dem1_extended_n0.018: quantitative comparison (contingency table and performance metrics) between summary filtered WOfS image and maximum modelled flood extent plot.*

5.5 Simulations Dem3

After having seen the improvements of the results thanks to the modification of the DEM, a second group of simulations with excavation has been studied. Particularly it was interesting to evaluate the effects of considering a larger width of levelling in the critic reach. Therefore, as done for case *Dem1*, two typologies of modified DEM have been prepared, one no extended and one extended (Figure 5.30). However, this time it has been chosen to test a width of excavation of 3 cells, equal to 90 meters.

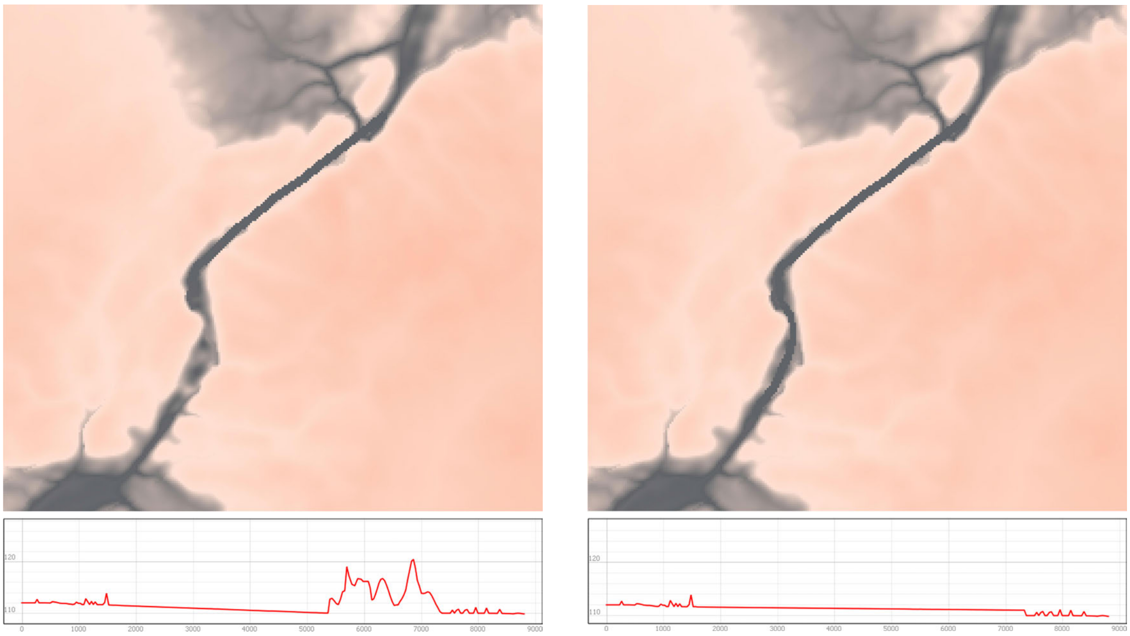

(a) *No extended* (b) *Extended*

Figure 5.30. *Local DEM modifications and related terrain profiles of the stretch interested for case three pixels width digging.*

The first test run uses a no extended modification and a roughness file with Manning's value set to 0.025. The peak of discharge read at Fitzroy Crossing station starts to assume a value comparable with the observed one. The comparison with daily WOfS shows that this model slightly overestimates the wet areas, whereas the performance metrics related to the comparison with summary filtered WOfS improve compared to the cases *Dem1*. The corresponding extended case, named *Dem3_extended_n0.025*, shows a further improvement in term of match between gauged and simulated data. On the other side, the comparison with daily WOfS indicates the overestimation increases considering an extended excavation.
In order to evaluate also the influence of the roughness combined to the levelling type, the couple of simulations no extended and extended with *Dem3* and Manning's value equal to 0.018 has been implemented. Their results follow the behaviour already seen for the couple with roughness 0.025, but with peak values increased and anticipated in time.
Despite the results obtained for cases *Dem3_n0.018* and *Dem3_extended_n0.018* were

already quite satisfactory, a third test with lower roughness value has been run to complement the sensitivity analysis and evaluate the modelled flooding behaviour at Noonkanbah station. Actually the simulation with Manning's value of 0.0075 implemented generates a profile with peak value increased and anticipated, but its general behaviour lower match with data. Indeed, this scenario highly underestimates the flooded area such as first simulations with original *Dem0*.
Also in this case, next paragraphs contain all the images and tables for results comparisons described above.

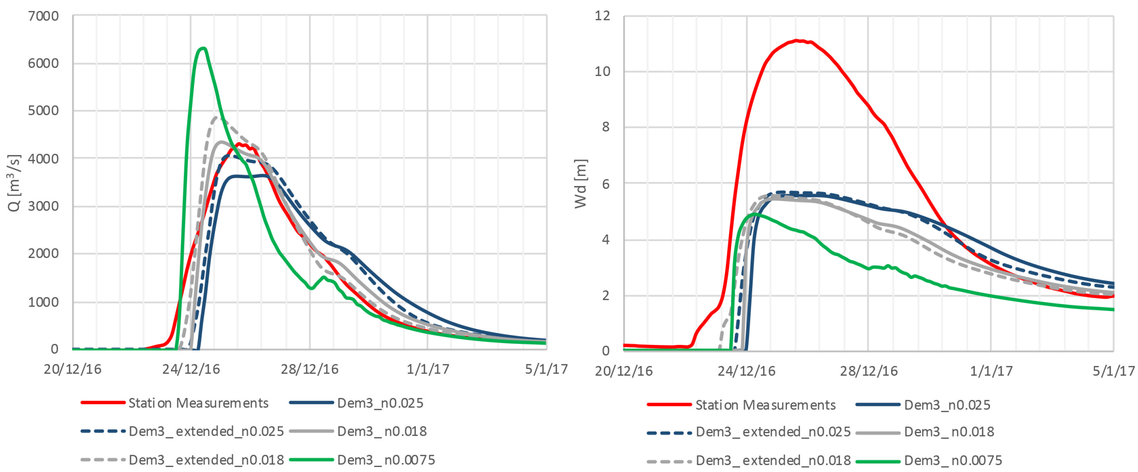

Figure 5.31. *Comparisons between observed and simulated data for Dem3 cases at Fizroy Crossing station.*

Case	NSE	PBIAS	RMSE	RSR
Dem3_n0.025	0.801	-0.006	450.589	0.446
Dem3_extended_n0.025	0.883	-0.039	345.585	0.342
Dem3_n0.018	0.935	-0.018	258.285	0.256
Dem3_extended_n0.018	0.938	-0.048	252.123	0.250
Dem3_n0.0075	0.562	-0.033	668.369	0.662

Table 5.26. *Cases Dem3: performance metrics of gauged and simulated discharge comparisons at Fitzroy Crossing station.*

Case	NSE	PBIAS	RMSE	RSR
Dem3_n0.025	0.382	0.345	2.162	0.786
Dem3_extended_n0.025	0.472	0.346	1.999	0.727
Dem3_n0.018	0.370	0.409	2.184	0.794
Dem3_extended_n0.018	0.435	0.401	2.069	0.752
Dem3_n0.0075	0.078	0.552	2.642	0.960

Table 5.27. *Cases Dem3: performance metrics of gauged and simulated water depth comparisons at Fitzroy Crossing station.*

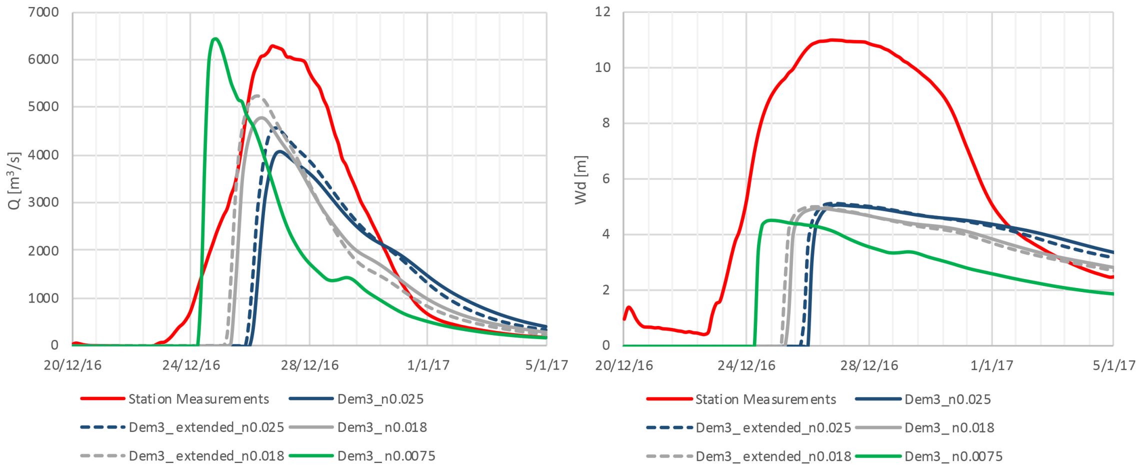

Figure 5.32. *Comparisons between observed and simulated data for Dem3 cases at Noonkanbah station.*

Case	NSE	PBIAS	RMSE	RSR
Dem3_n0.025	0.455	0.369	1166.118	0.738
Dem3_extended_n0.025	0.580	0.342	1024.511	0.648
Dem3_n0.018	0.702	0.351	863.065	0.546
Dem3_extended_n0.018	0.743	0.330	801.745	0.507
Dem3_n0.0075	0.298	0.339	1324.213	0.838

Table 5.28. *Cases Dem3: performance metrics of gauged and simulated discharge comparisons at Noonkanbah station.*

Case	NSE	PBIAS	RMSE	RSR
Dem3_n0.025	-0.414	0.536	3.356	1.189
Dem3_extended_n0.025	-0.343	0.533	3.269	1.159
Dem3_n0.018	-0.254	0.546	3.160	1.120
Dem3_extended_n0.018	-0.208	0.544	3.101	1.099
Dem3_n0.0075	-0.304	0.610	3.222	1.142

Table 5.29. *Cases Dem3: performance metrics of gauged and simulated water depth comparisons at Noonkanbah station.*

5.5.1 Case Dem3_n0.025

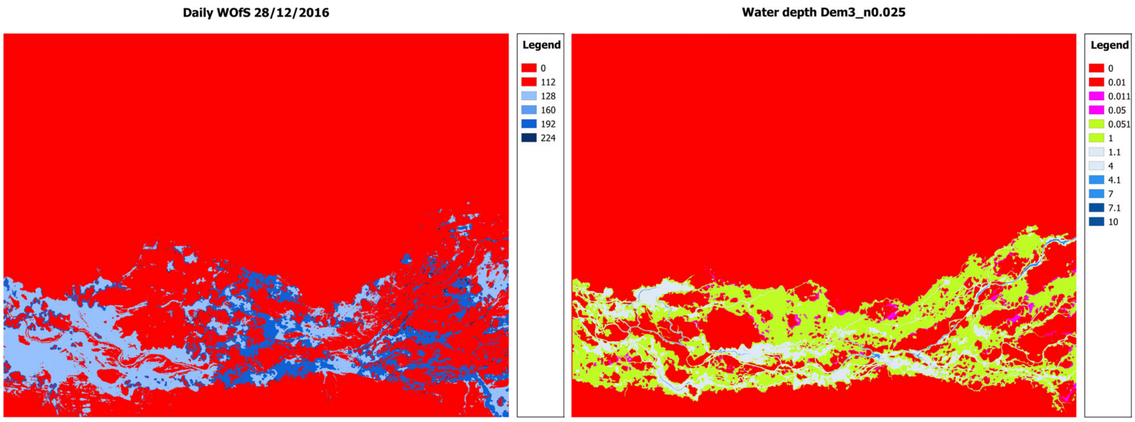

Figure 5.33. *Case Dem3_n0.025: visual comparison between daily WOfS image and correspondent water depth plot.*

	Present in observation	Absent in observation
Present in model	528 629	392 746
Absent in model	195 616	3 855 146

BIAS	PC	CSI	$F^{<3>}$	$F^{<4>}$	H	F
1.272	0.881	0.473	0.298	0.121	0.729	0.092

Table 5.30. *Case Dem3_n0.025: quantitative comparison (contingency table and performance metrics) between daily WOfS image and correspondent water depth plot.*

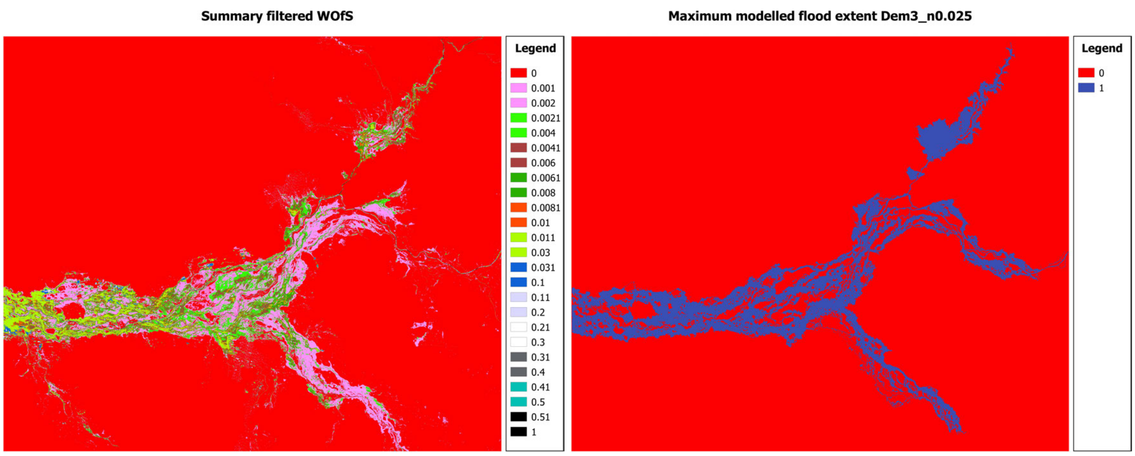

Figure 5.34. *Case Dem3_n0.025: visual comparison between summary filtered WOfS image and maximum modelled flood extent plot.*

		Present in observation		Absent in observation		
Present in model		1 940 927		350 973		
Absent in model		1 287 456		22 939 924		
BIAS	PC	CSI	$F^{<3>}$	$F^{<4>}$	H	F
0.709	0.938	0.542	0.182	0.444	0.601	0.015

Table 5.31. *Case Dem3_n0.025: quantitative comparison (contingency table and performance metrics) between summary filtered WOfS image and maximum modelled flood extent plot.*

5.5.2 Case Dem3_extended_n0.025

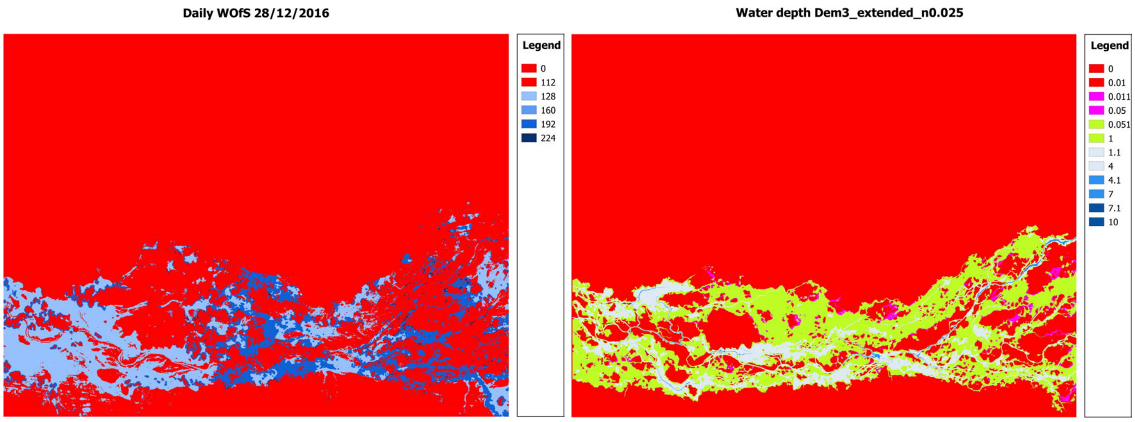

Figure 5.35. *Case Dem3_extended_n0.025: visual comparison between daily WOfS image and correspondent water depth plot.*

		Present in observation		Absent in observation		
Present in model		542 873		413 513		
Absent in model		181 372		3 834 379		
BIAS	PC	CSI	$F^{<3>}$	$F^{<4>}$	H	F
1.320	0.880	0.477	0.317	0.113	0.749	0.097

Table 5.32. *Case Dem3_extended_n0.025: quantitative comparison (contingency table and performance metrics) between daily WOfS image and correspondent water depth plot.*

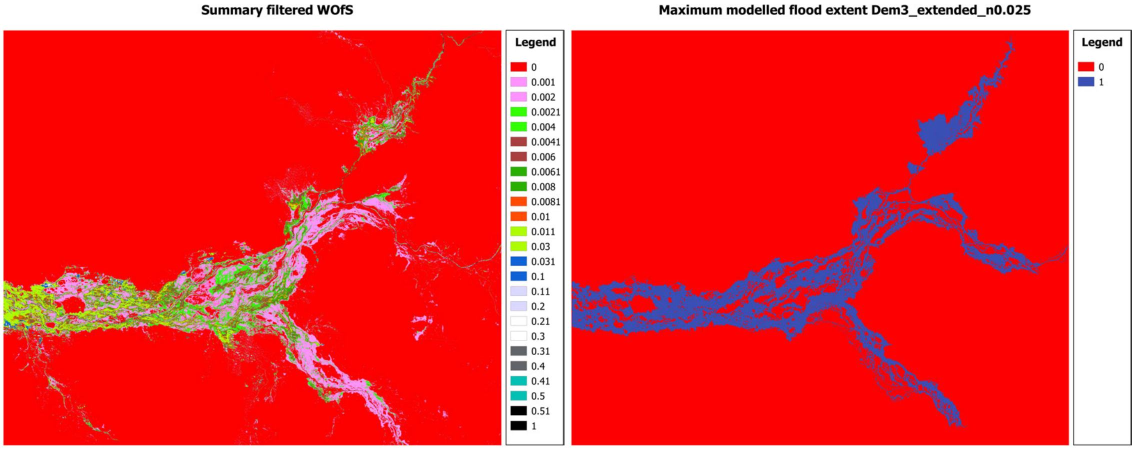

Figure 5.36. *Case Dem3_extended_n0.025: visual comparison between summary filtered WOfS image and maximum modelled flood extent plot.*

	Present in observation	Absent in observation
Present in model	1 997 798	350 383
Absent in model	1 230 585	22 940 514

BIAS	PC	CSI	$F^{<3>}$	$F^{<4>}$	H	F
0.7273	0.940	0.558	0.214	0.460	0.618	0.015

Table 5.33. *Case Dem3_extended_n0.025: quantitative comparison (contingency table and performance metrics) between summary filtered WOfS image and maximum modelled flood extent plot.*

5.5.3 Case Dem3_n0.018

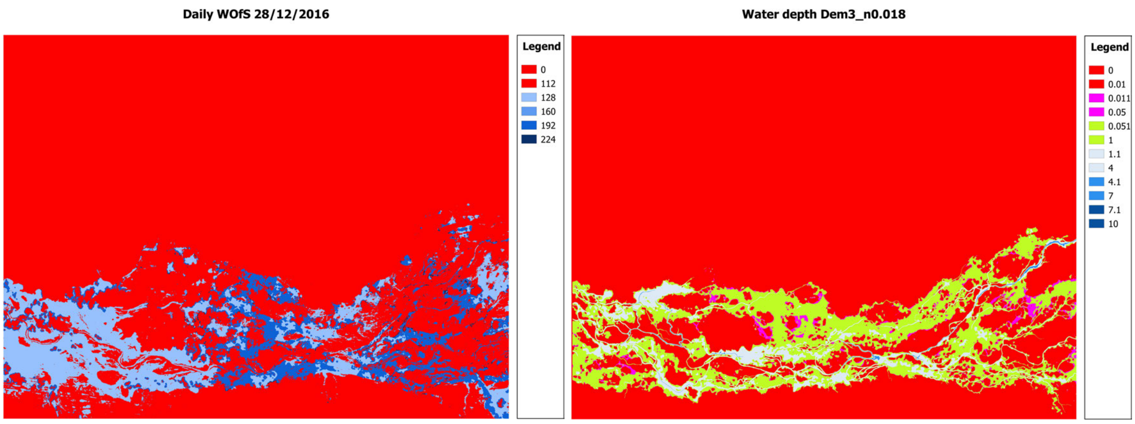

Figure 5.37. *Case Dem3_n0.018: visual comparison between daily WOfS image and correspondent water depth plot.*

	Present in observation	Absent in observation
Present in model	477 026	311 211
Absent in model	247 219	3 936 681

BIAS	PC	CSI	F <3>	F<4>	H	F
1.088	0.887	0.460	0.221	0.160	0.658	0.073

Table 5.34. *Case Dem3_n0.018: quantitative comparison (contingency table and performance metrics) between daily WOfS image and correspondent water depth plot.*

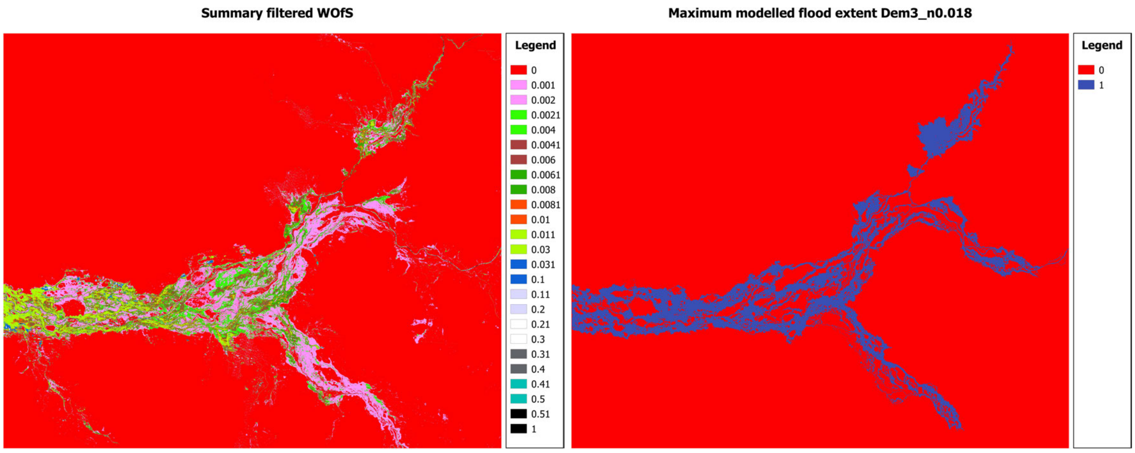

Figure 5.38. *Case Dem3_n0.018: visual comparison between summary filtered WOfS image and maximum modelled flood extent plot.*

	Present in observation	Absent in observation
Present in model	1 786 645	291 124
Absent in model	1 441 738	22 999 773

BIAS	PC	CSI	F <3>	F<4>	H	F
0.643	0.934	0.507	0.097	0.424	0.553	0.012

Table 5.35. *Case Dem3_n0.018: quantitative comparison (contingency table and performance metrics) between summary filtered WOfS image and maximum modelled flood extent plot.*

5.5.4 Case Dem3_extended_n0.018

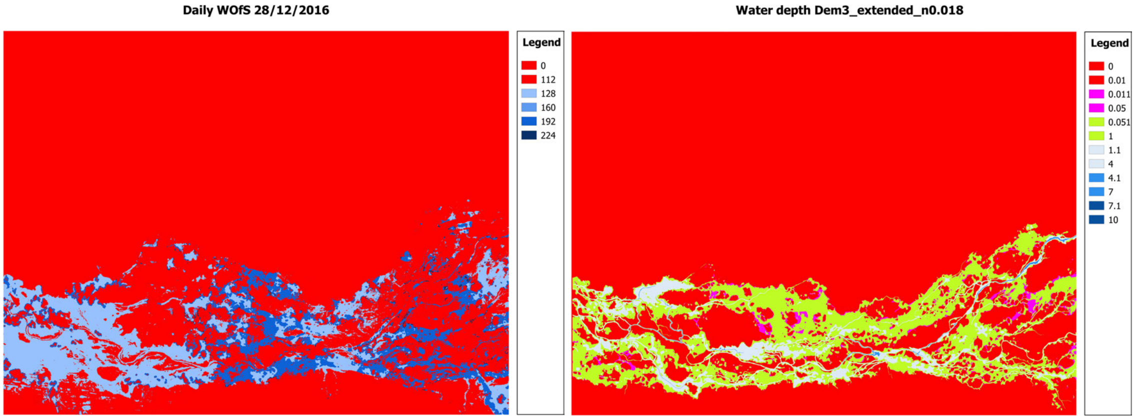

Figure 5.39. *Case Dem3_extended_n0.018: visual comparison between daily WOfS image and correspondent water depth plot.*

	Present in observation	Absent in observation
Present in model	484 286	318 773
Absent in model	239 959	3 929 119

BIAS	PC	CSI	F $^{<3>}$	F $^{<4>}$	H	F
1.108	0.887	0.464	0.234	0.158	0.668	0.075

Table 5.36. *Case Dem3_extended_n0.018: quantitative comparison (contingency table and performance metrics) between daily WOfS image and correspondent water depth plot.*

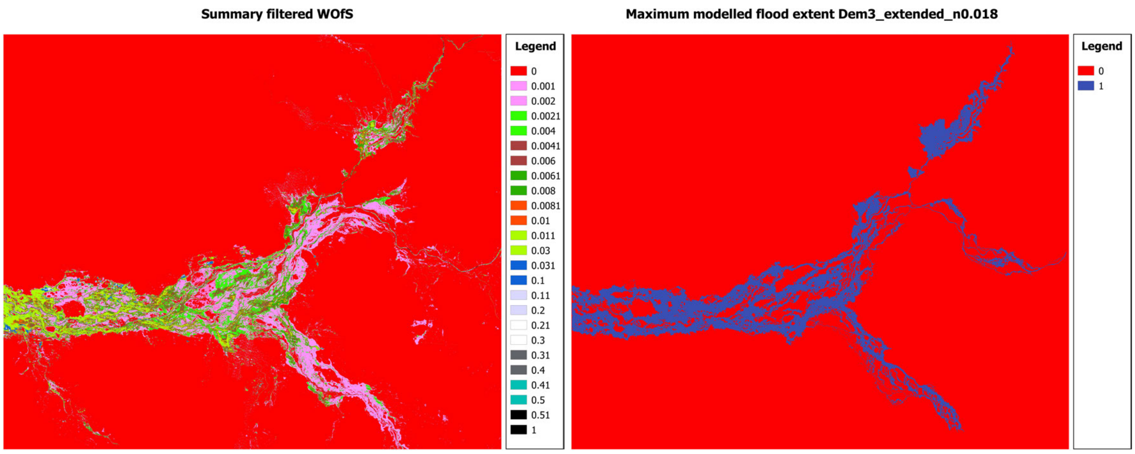

Figure 5.40. *Case Dem3_extended_n0.018: visual comparison between summary filtered WOfS image and maximum modelled flood extent plot.*

	Present in observation	Absent in observation
Present in model	1 730 796	216 207
Absent in model	1 497 587	23 074 690

BIAS	PC	CSI	$F^{<3>}$	$F^{<4>}$	H	F
0.603	0.935	0.502	0.067	0.439	0.536	0.009

Table 5.37. *Case Dem3_extended_n0.018: quantitative comparison (contingency table and performance metrics) between summary filtered WOfS image and maximum modelled flood extent plot.*

5.5.5 Case Dem3_n0.0075

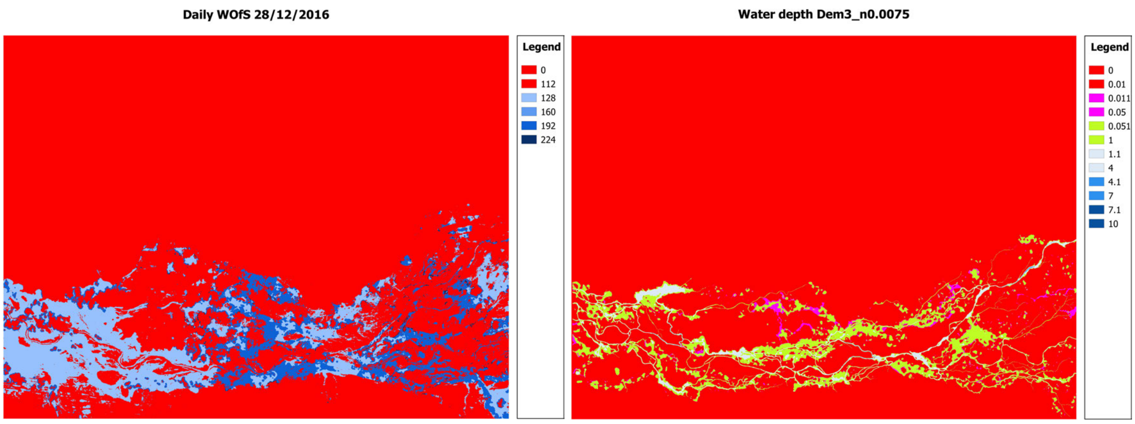

Figure 5.41. *Case Dem3_n0.0075: visual comparison between daily WOfS image and correspondent water depth plot.*

	Present in observation	Absent in observation
Present in model	238 549	109 110
Absent in model	485 696	4 138 782

BIAS	PC	CSI	$F^{<3>}$	$F^{<4>}$	H	F
0.480	0.880	0.286	-0.296	0.155	0.329	0.025

Table 5.38. *Case Dem3_n0.0075: quantitative comparison (contingency table and performance metrics) between daily WOfS image and correspondent water depth plot.*

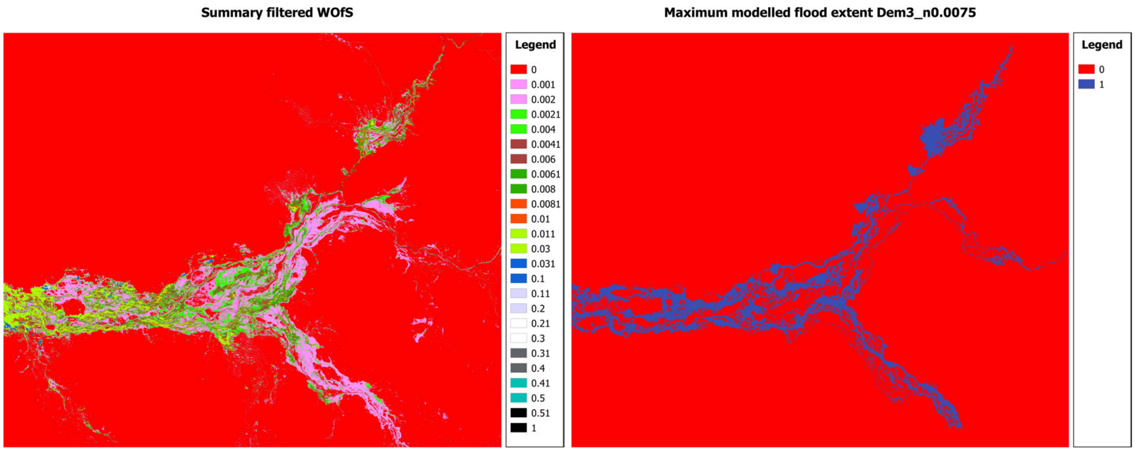

Figure 5.42. *Case Dem3_n0.0075: visual comparison between summary filtered WOfS image and maximum modelled flood extent plot.*

	Present in observation	Absent in observation
Present in model	1 323 506	129 737
Absent in model	1 904 877	23 161 160

BIAS	PC	CSI	$F^{<3>}$	$F^{<4>}$	H	F
0.450	0.923	0.394	-0.173	0.355	0.409	0.005

Table 5.39. *Case Dem3_n0.0075: quantitative comparison (contingency table and performance metrics) between summary filtered WOfS image and maximum modelled flood extent plot.*

5.6 Simulations Dem9

Finally the third group of simulations implemented use a modified DEM with a levelling excavation of nine pixels width equal to 270 meters (Figure 5.44).
Two tests, one no extended and one extended, were run using a modified DEM combined with a roughness file with 0.025 values. Results show a significant improvement compared to the initial case, both in terms of profile and WOfS comparisons. As it has been noted from previous simulations reducing the Manning's input values causes an increase of discharge peak. Since the simulated discharge values read at Fitzroy Crossing were already higher than the observed ones for cases with roughness 0.025, it has been chosen to not proceed with further simulations with lower roughness input.
In the next paragraphs the results of these two simulation are reported.

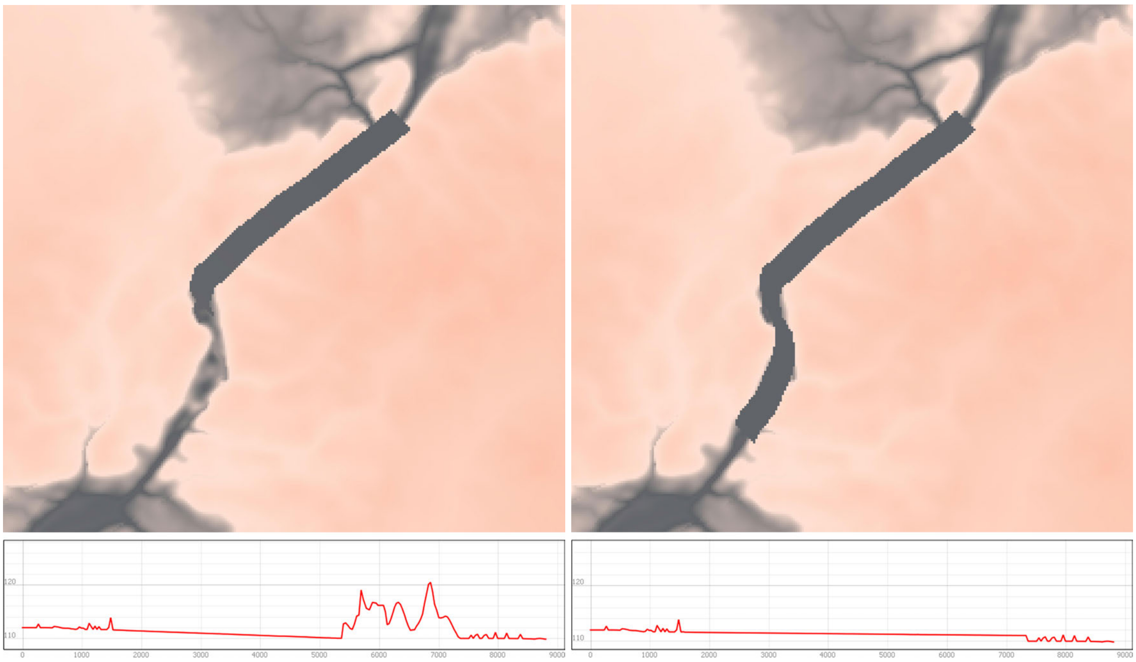

(a) *No extended* (b) *Extended*

Figure 5.44. *Local DEM modifications and related terrain profiles of the stretch interested for case nine pixels width digging.*

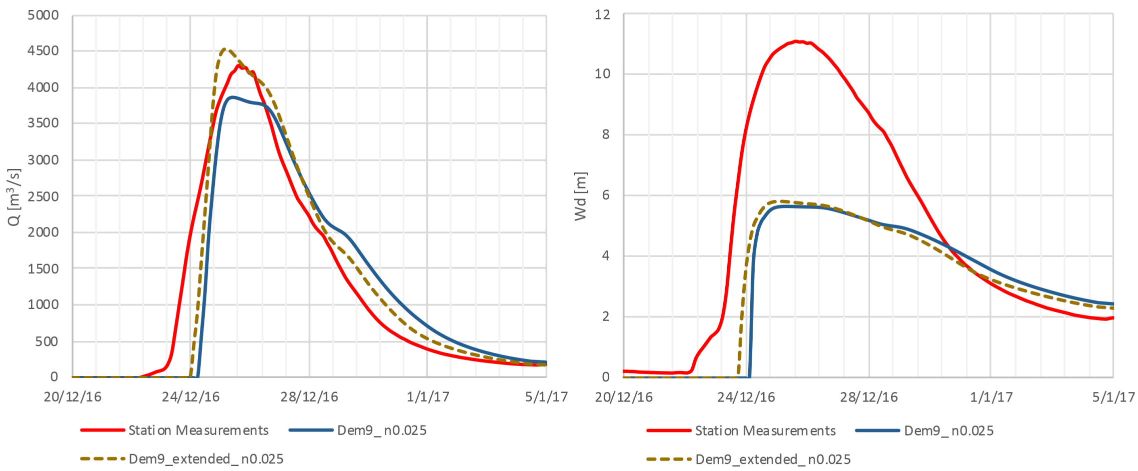

Figure 5.45. *Comparisons between observed and simulated data for Dem9 cases at Fizroy Crossing station.*

Case	NSE	PBIAS	RMSE	RSR
Dem9_n0.025	0.828	-0.001	418.518	0.415
Dem9_extended_n0.025	0.906	-0.035	308.844	0.306

Table 5.40. *Cases Dem9: performance metrics of gauged and simulated discharge comparisons at Fitzroy Crossing station.*

Case	NSE	PBIAS	RMSE	RSR
Dem9_n0.025	0.370	0.354	2.183	0.793
Dem9_extended_n0.025	0.462	0.354	2.018	0.733

Table 5.41. *Cases Dem9: performance metrics of gauged and simulated water depth comparisons at Fitzroy Crossing station.*

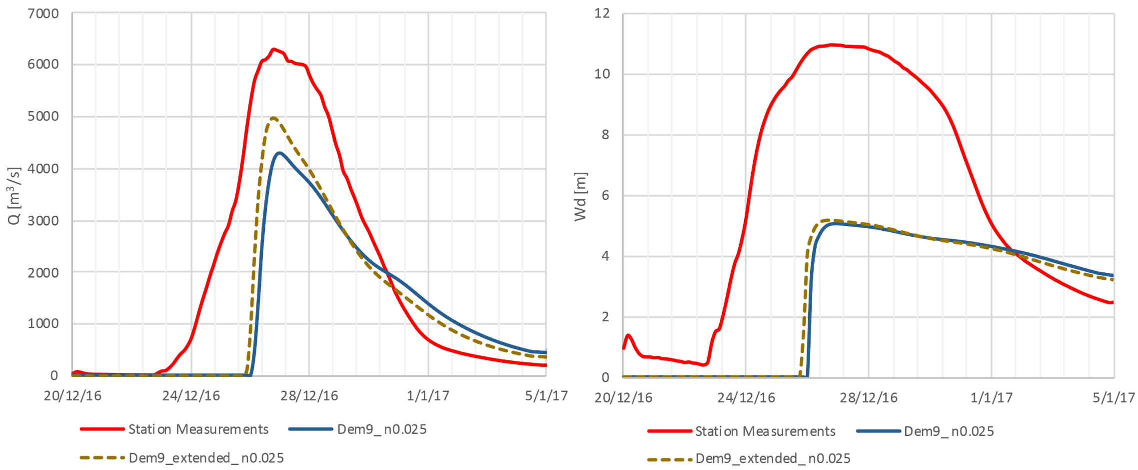

Figure 5.46. *Comparisons between observed and simulated data for Dem9 cases at Noonkanbah station.*

Case	NSE	PBIAS	RMSE	RSR
Dem9_n0.025	0.828	-0.001	418.518	0.415
Dem9_extended_n0.025	0.906	-0.035	308.844	0.306

Table 5.42. *Cases Dem9: performance metrics of gauged and simulated discharge comparisons at Noonkanbah station.*

Case	NSE	PBIAS	RMSE	RSR
Dem9_n0.025	0.370	0.354	2.183	0.793
Dem9_extended_n0.025	0.462	0.354	2.018	0.733

Table 5.43. *Cases Dem9: performance metrics of gauged and simulated water depth comparisons at Noonkanbah station.*

5.6.1 Case Dem9_n0.025

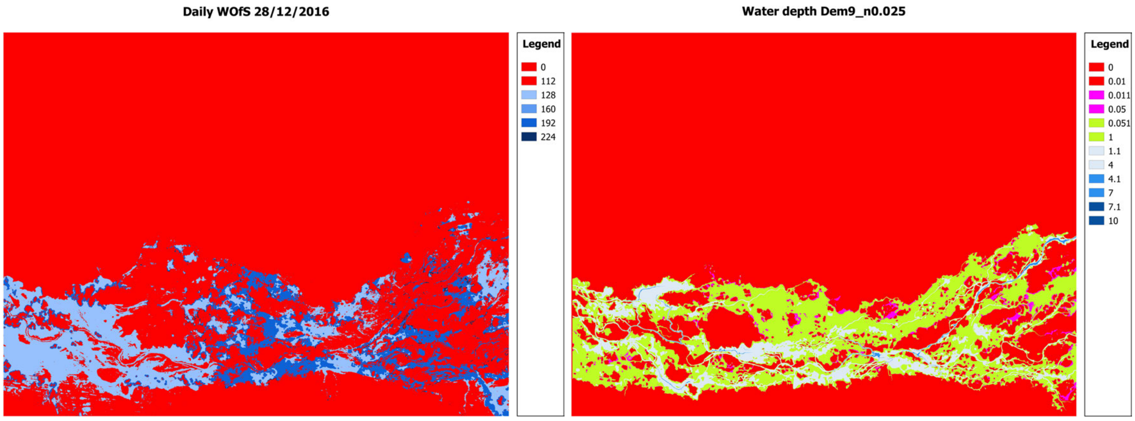

Figure 5.47. *Case Dem9_n0.025: visual comparison between daily WOfS image and correspondent water depth plot.*

	Present in observation	Absent in observation
Present in model	535 502	401 561
Absent in model	188 743	3 846 331

BIAS	PC	CSI	$F^{<3>}$	$F^{<4>}$	H	F
1.293	0.881	0.475	0.308	0.118	0.739	0.094

Table 5.44. *Case Dem9_n0.025: quantitative comparison (contingency table and performance metrics) between daily WOfS image and correspondent water depth plot.*

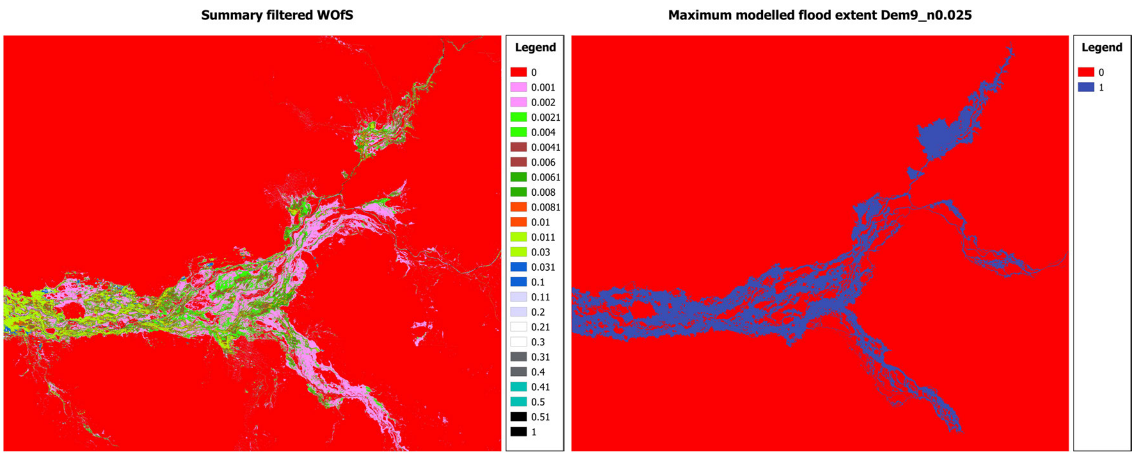

Figure 5.48. *Case Dem9_n0.025: visual comparison between summary filtered WOfS image and maximum modelled flood extent plot.*

	Present in observation	Absent in observation
Present in model	1 842 474	267 537
Absent in model	1 385 909	23 023 360

BIAS	PC	CSI	$F^{<3>}$	$F^{<4>}$	H	F
0.653	0.937	0.527	0.130	0.450	0.570	0.011

Table 5.45. *Case Dem9_n0.025: quantitative comparison (contingency table and performance metrics) between summary filtered WOfS image and maximum modelled flood extent plot.*

5.6.2 Case Dem9_extended_n0.025

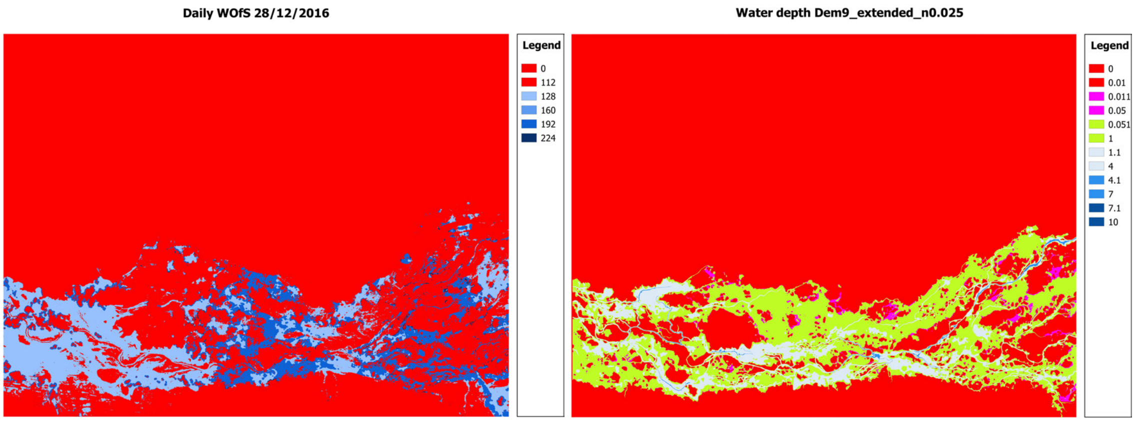

Figure 5.49. *Case Dem9_extended_n0.025: visual comparison between daily WOfS image and correspondent water depth plot.*

	Present in observation	Absent in observation
Present in model	548 968	423 174
Absent in model	175 277	3 824 718

BIAS	PC	CSI	$F^{<3>}$	$F^{<4>}$	H	F
1.342	0.879	0.478	0.325	0.109	0.757	0.099

Table 5.46. *Case Dem9_extended_n0.025: quantitative comparison (contingency table and performance metrics) between daily WOfS image and correspondent water depth plot.*

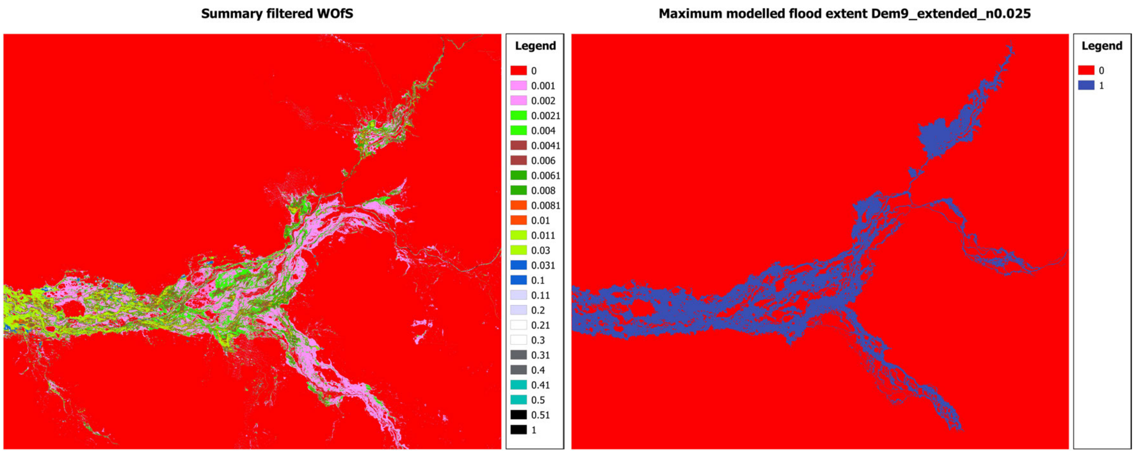

Figure 5.50. *Case Dem9_extended_n0.025: visual comparison between summary filtered WOfS image and maximum modelled flood extent plot.*

	Present in observation	Absent in observation
Present in model	1 929 008	69 210
Absent in model	1 299 375	23 021 687

BIAS	PC	CSI	$F^{<3>}$	$F^{<4>}$	H	F
0.680	0.940	0.551	0.180	0.474	0.597	0.011

Table 5.47. *Case Dem9_extended_n0.025: quantitative comparison (contingency table and performance metrics) between summary filtered WOfS image and maximum modelled flood extent plot.*

5.7 Flood event 2016-2017: summary of the results

In this paragraph all the results reported above for each case of simulation are summarised in order to give a general framework of the work done.
Starting from the discharge and water depth profiles (Figures 5.51 and 5.52) and related performance metrics (Tables 5.48, 5.49, 5.50 and 5.51) it is possible to observe how the model behaviour improved adopting the DEM correction. In particular, the comparison between flow rates clearly shows the change in behaviour of the simulations. Instead, the water depth comparisons is more difficult to perform since *wd* have less pronounced peaks. The similarity between *wd* profiles is related to the low accuracy of the DEM with respect to which they were read. It should be remembered that the bathymetry used in the model derives from satellite images. DEM obtained with satellites, unlike ones more accurate derived by surveys such as the Lidar, are not able to describe the local excursions of the terrain. Therefore, the simulated *wd* has been read with respect to a smoothed ground, not able to highlights the behaviour differences between the simulated scenarios. For the same reason, the difference between gauged and simulated water depth peaks is so pronounced. In fact, the gauged data is referred to a real observation sensitive to the local terrain depression whereas the simulated one suffer of the inaccuracy of the

DEM. Moreover, it is necessary to note that the inability of the implemented models to match the observations, particularly evident for the results read at Noonkanbah station, is justified by the fact that only gauged inflows were used as input. Indeed, it would be necessary to implement an hydrological model, that uses also precipitation input, in order to obtain a more accurate model.

The comparisons between observed and simulated peak values (peaks time, discharge peaks and water depth peaks in Table 5.52 and 5.53 allow to define which are the best configurations to represent the study event. This decision is supported by the information related to the study of the WOfS images and the relative performance metrics (Table 5.54, 5.55 and 5.56). In particular, ensuring a good match with RS data is crucial to know the real behaviour of the river and the extension of wet areas in order to apply an intervention policy for future events. Based on the results comparisons and the comments made above, two scenarios can be selected as which with best behaviour compared to the real one: *Dem3_extended_n0.025* and *Dem3_extended_n0.018*.

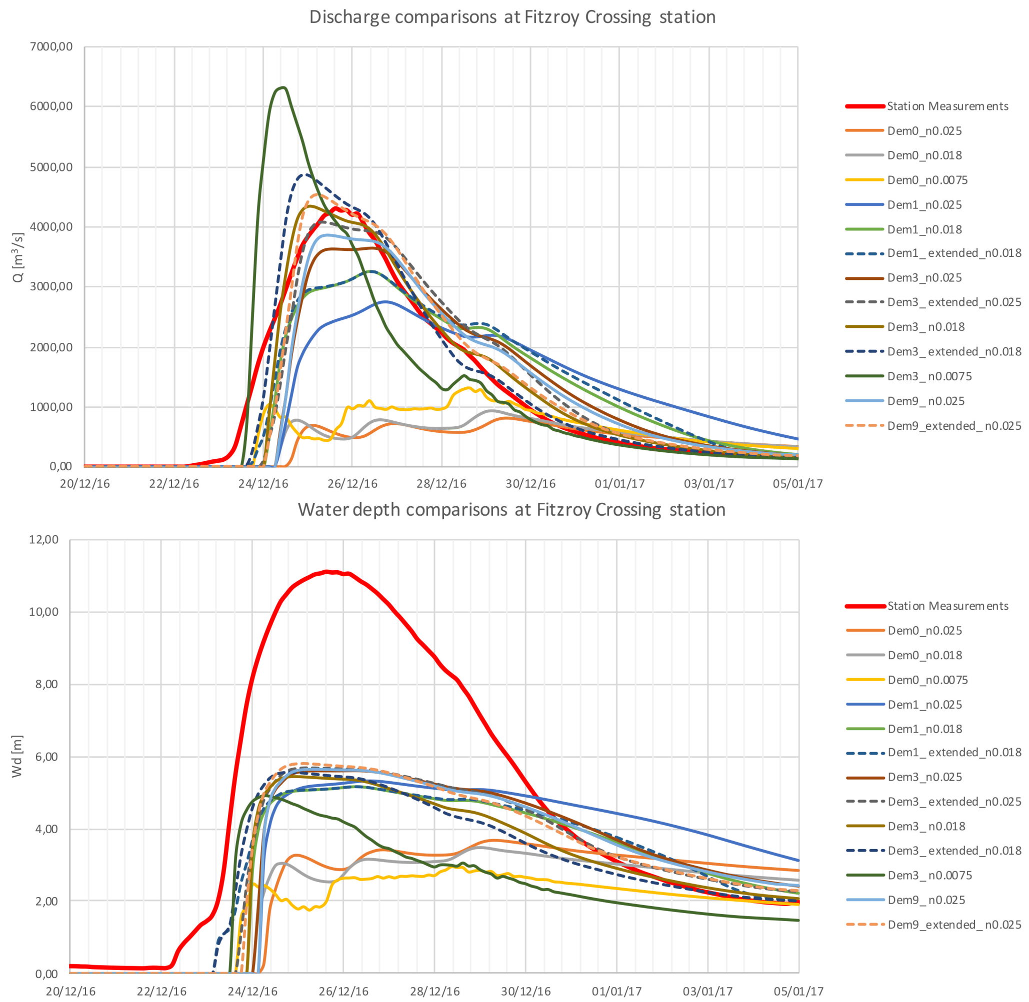

Figure 5.51. *Comparisons between gauged and simulated data for all cases at Fizroy Crossing station.*

Case	NSE	PBIAS	RMSE	RSR
Dem0_n0.025	-0.228	0.675	1.118.448	1.108
Dem0_n0.018	-0.154	0.634	1.084.096	1.074
Dem0_n0.0075	0.037	0.537	990.379	0.981
Dem1_n0.025	0.534	0.015	688.803	0.682
Dem1_n0.018	0.788	-0.017	464.735	0.460
Dem1_extended_n0.018	0.792	-0.050	460.626	0.456
Dem3_n0.025	0.801	-0.006	450.589	0.446
Dem3_extended_n0.025	0.883	-0.039	345.585	0.342
Dem3_n0.018	0.935	-0.018	258.285	0.256
Dem3_extended_n0.018	0.938	-0.048	252.123	0.250
Dem3_n0.0075	0.562	-0.033	668.369	0.662
Dem9_n0.025	0.828	-0.001	418.518	0.415
Dem9_extended_n0.025	0.906	-0.035	308.844	0.306

Table 5.48. *Performance metrics of gauged and simulated discharge comparisons for all cases at Fitzroy Crossing station.*

Case	NSE	PBIAS	RMSE	RSR
Dem0_n0.025	-0.215	0.516	3.033	1.102
Dem0_n0.018	-0.234	0.543	3.056	1.111
Dem0_n0.0075	-0.370	0.625	3.220	1.170
Dem1_n0.025	0.271	0.305	2.350	0.854
Dem1_n0.018	0.335	0.374	2.243	0.815
Dem1_extended_n0.018	0.397	0.355	2.137	0.777
Dem3_n0.025	0.382	0.345	2.162	0.786
Dem3_extended_n0.025	0.472	0.346	1.999	0.727
Dem3_n0.018	0.370	0.409	2.184	0.794
Dem3_extended_n0.018	0.435	0.401	2.069	0.752
Dem3_n0.0075	0.078	0.552	2.642	0.960
Dem9_n0.025	0.370	0.354	2.183	0.793
Dem9_extended_n0.025	0.462	0.354	2.018	0.733

Table 5.49. *Performance metrics of gauged and simulated water depth comparisons for all cases at Fitzroy Crossing station.*

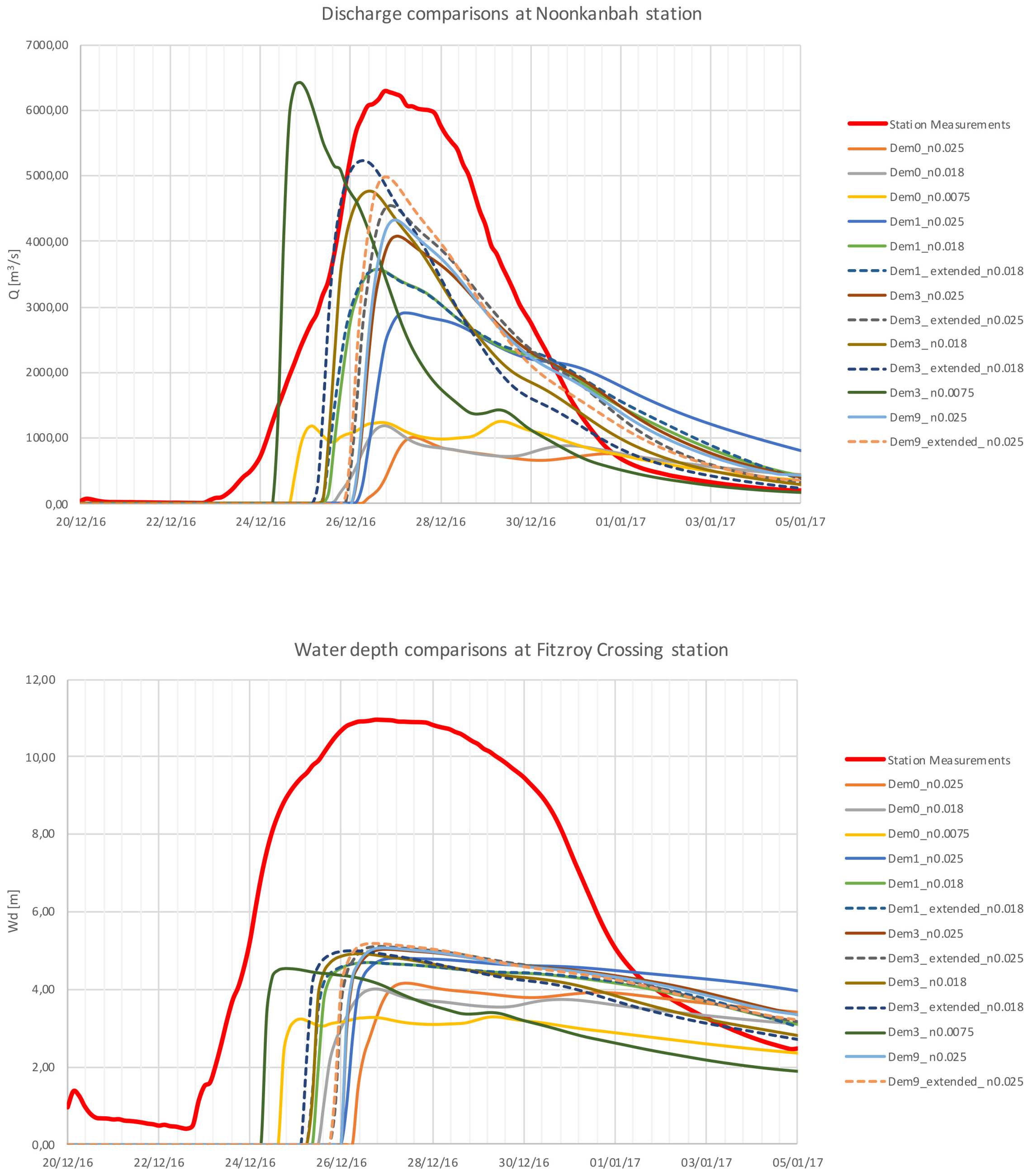

Figure 5.52. *Comparisons between gauged and simulated data for all cases at Noonkanbah station.*

Case	NSE	PBIAS	RMSE	RSR
Dem0_n0.025	-0.404	0.792	1.872.140	1.185
Dem0_n0.018	-0.282	0.759	1.788.877	1.132
Dem0_n0.0075	-0.082	0.686	1.643.511	1.040
Dem1_n0.025	0.189	0.408	1422.860	0.901
Dem1_n0.018	0.543	0.357	1068.028	0.676
Dem1_extended_n0.018	0.561	0.332	1047.222	0.663
Dem3_n0.025	0.455	0.369	1.166.118	0.738
Dem3_extended_n0.025	0.580	0.342	1024.511	0.648
Dem3_n0.018	0.702	0.351	863.065	0.546
Dem3_extended_n0.018	0.743	0.330	801.745	0.507
Dem3_n0.0075	0.298	0.339	1324.213	0.838
Dem9_n0.025	0.487	0.370	1.131.854	0.716
Dem9_extended_n0.025	0.626	0.343	966.499	0.612

Table 5.50. *Performance metrics of gauged and simulated discharge comparisons for all cases at Noonkanbah station.*

Case	NSE	PBIAS	RMSE	RSR
Dem0_n0.025	-0.747	0.615	3.729	1.322
Dem0_n0.018	-0.598	0.611	3.567	1.264
Dem0_n0.0075	-0.576	0.647	3.542	1.255
Dem1_n0.025	-0.492	0.533	3.446	1.221
Dem1_n0.018	-0.296	0.534	3.212	1.139
Dem1_extended_n0.018	-0.265	0.527	3.174	1.125
Dem3_n0.025	-0.414	0.536	3.356	1.189
Dem3_extended_n0.025	-0.343	0.533	3.269	1.159
Dem3_n0.018	-0.254	0.546	3.160	1.120
Dem3_extended_n0.018	-0.208	0.544	3.101	1.099
Dem3_n0.0075	-0.304	0.610	3.222	1.142
Dem9_n0.025	-0.410	0.538	3.350	1.187
Dem9_extended_n0.025	-0.335	0.534	3.261	1.156

Table 5.51. *Performance metrics of gauged and simulated water depth comparisons for all cases at Noonkanbah station.*

Case	Peak time	Q peak [m^3/s]	Wd peak [m]
Observed	25/12/16 15:00	4301.58	11.10
Dem0_n0.025	29/12/16 12:00	806.29	3.68
Dem0_n0.018	29/12/16 03:00	941.26	3.48
Dem0_n0.0075	28/12/16 15:00	1324.89	2.94
Dem1_n0.025	26/12/16 18:00	2761.57	5.31
Dem1_n0.018	26/12/16 09:00	3259.47	5.14
Dem1_extended_n0.018	26/12/16 09:00	3259.52	5.14
Dem3_n0.025	26/12/16 09:00	3640.71	5.58
Dem3_extended_n0.025	25/12/16 09:00	4066.30	5.69
Dem3_n0.018	25/12/16 00:00	4331.19	5.44
Dem3_extended_n0.018	24/12/16 21:00	4873.88	5.55
Dem3_n0.0075	24/12/16 09:00	6303.10	4.92
Dem9_n0.025	25/12/16 12:00	3860.85	5.64
Dem9_extended_n0.025	25/12/16 06:00	4531.26	5.79

Table 5.52. *Values of peak time, discharge peak and water depth peak for Fitzroy Crossing station.*

Case	Peak time	Q peak [m^3/s]	Wd peak [m]
Observed	26/12/16 21:00	6283.27	10.97
Dem0_n0.025	27/12/16 12:00	1014.22	4.16
Dem0_n0.018	26/12/16 21:00	1178.29	4.02
Dem0_n0.0075	29/12/16 12:00	1255.90	3.28
Dem1_n0.025	27/12/16 09:00	2900.08	4.79
Dem1_n0.018	26/12/16 18:00	3566.73	4.70
Dem1_extended_n0.018	26/12/16 18:00	3579.32	4.70
Dem3_n0.025	27/12/16 03:00	4079.05	5.05
Dem3_extended_n0.025	27/12/16 00:00	4556.26	5.12
Dem3_n0.018	26/12/16 12:00	4764.30	4.92
Dem3_extended_n0.018	26/12/16 09:00	5230.68	4.99
Dem3_n0.0075	25/12/16 00:00	6414.00	4.52
Dem9_n0.025	27/12/16 03:00	4313.88	5.09
Dem9_extended_n0.025	26/12/16 21:00	4976.49	5.17

Table 5.53. *Values of peak time, discharge peak and water depth peak for Noonkanbah station.*

Case	BIAS	PC	CSI	$F^{<3>}$	$F^{<4>}$	H	F
Dem0_n0.025	0.424	0.878	0.262	-0.360	0.149	0.296	0.021
Dem0_n0.018	0.385	0.878	0.247	-0.405	0.148	0.275	0.018
Dem0_n0.0075	0.244	0.869	0.163	-0.607	0.099	0.175	0.011
Dem1_n0.025	1.096	0.884	0.451	0.210	0.143	0.651	0.075
Dem1_n0.018	1.005	0.887	0.444	0.168	0.164	0.617	0.066
Dem1_extended_n0.018	1.007	0.887	0.444	0.169	0.164	0.617	0.066
Dem3_n0.025	1.272	0.881	0.473	0.298	0.121	0.729	0.092
Dem3_extended_n0.025	1.320	0.880	0.477	0.317	0.113	0.749	0.097
Dem3_n0.018	1.088	0.887	0.460	0.221	0.160	0.658	0.073
Dem3_extended_n0.018	1.108	0.887	0.464	0.234	0.158	0.668	0.075
Dem3_n0.0075	0.480	0.880	0.286	-0.296	0.155	0.329	0.025
Dem9_n0.025	1.293	0.881	0.475	0.308	0.118	0.739	0.094
Dem9_extended_n0.025	1.342	0.879	0.478	0.325	0.109	0.757	0.099

Table 5.54. *Performance metrics summary for comparison with daily WOfS.*

Case	BIAS	PC	CSI	$F^{<3>}$	$F^{<4>}$	H	F
Dem0_n0.025	0.452	0.912	0.336	-0.246	0.256	0.365	0.012
Dem0_n0.018	0.408	0.909	0.307	-0.313	0.234	0.331	0.010
Dem0_n0.0075	0.284	0.898	0.212	-0.518	0.156	0.225	0.008
Dem1_n0.025	0.583	0.930	0.467	0.008	0.394	0.504	0.010
Dem1_n0.018	0.536	0.927	0.441	-0.054	0.380	0.470	0.009
Dem1_extended_n0.018	0.535	0.927	0.442	-0.054	0.381	0.470	0.009
Dem3_n0.025	0.709	0.938	0.542	0.182	0.444	0.601	0.015
Dem3_extended_n0.025	0.727	0.940	0.558	0.214	0.460	0.618	0.015
Dem3_n0.018	0.643	0.934	0.507	0.097	0.424	0.553	0.012
Dem3_extended_n0.018	0.603	0.935	0.502	0.067	0.439	0.536	0.009
Dem3_n0.0075	0.450	0.923	0.394	-0.173	0.355	0.409	0.005
Dem9_n0.025	0.653	0.937	0.527	0.130	0.450	0.570	0.011
Dem9_extended_n0.025	0.680	0.940	0.551	0.180	0.474	0.597	0.011

Table 5.55. *Performance metrics summary for comparison with summary filtered WOfS.*

Case	Total wet area Daily WOfS [km^2]	Total wet area Summary filtered WOfS [km^2]
Observed	651.82	2905.54
Dem0_n0.025	276.90	1315.79
Dem0_n0.018	251.29	1187.84
Dem0_n0.0075	159.43	827.53
Dem1_n0.025	715.02	1695.74
Dem1_n0.018	655.71	1558.50
Dem1_extended_n0.018	656.66	1557.25
Dem3_n0.025	829.24	2062.71
Dem3_extended_n0.025	860.75	2113.36
Dem3_n0.018	709.41	1869.99
Dem3_extended_n0.018	722.75	1752.30
Dem3_n0.0075	312.89	1307.92
Dem9_n0.025	843.36	1899.01
Dem9_extended_n0.025	874.93	1798.40

Table 5.56. *Values of total wet area for Daily and Summary filtered WOfS footprints.*

Chapter 6

Historical data analysis

In Chapter 5 we saw the importance of using satellite images as a support tool for assessing the quality of the model. However, as already mentioned, this approach has limitations due to the availability of useful images depending on the temporal resolution. In the study case, in fact, the only usable daily WOfS image represented the area limited to Noonkanbah without providing useful information on the remaining study area. This problem was partially overcome by using the comparison with the summary filtered WOfS image. This one provides information on the entire study area but does not represent a specific event.
For these reasons, in order to have a further support tool for the simulation analysis, it has been decided to carry out a search for historical data that are characterized by flood events of intensity comparable to that of the 2016-2017 event. Among these historical events it is necessary to find acquisitions that capture the flooded area between Dimond Gorge and Fitzroy Crossing stations, particularly affected by an extensive flooding area and not represented by the 2016-2017 daily WOfS (Figure 6.1).

6.1 Data research

The selection of the useful data took place first of all considering all the historical events recorded from 1987 (WOfS archive start date) to 2017 with peak flow rates greater than 3000 m^3/s, in order to exclude events incomparable with the intense study one (Dimond Gorge has been arbitrarily chosen as station control). For each of them a possible satellite image representing the upstream interest area has been sought from the WOfS archive. The research led to the selection of five usable images relating to the events of years: 1991, 1995, 1997, 2001 and 2009 (Figure 6.2). A further skimming was carried out by comparing the date of acquisition of the WOfS image and the date of the peak flow. Indeed, the interest is in using acquisitions made in the time span of the peak flow, able thus to capture the flooded areas at the peak of the event. The Figure 6.3, 6.4, 6.5, 6.6, 6.7 show the hydrograms and WOfS images available for historical events with relative acquisition date. As it possible to see, the satellite images of the event 1991 was acquired at an instant away from the recorded peak. The 2001 image, instead, is strongly characterized by presence of clouds that impede to have usable information about flooded areas. For this reason they have been excluded from the selection. Summing up, between all the events of the past, only three events (1995, 1997 and 2009) can be used as indirect comparison for the study case 2016-2017.

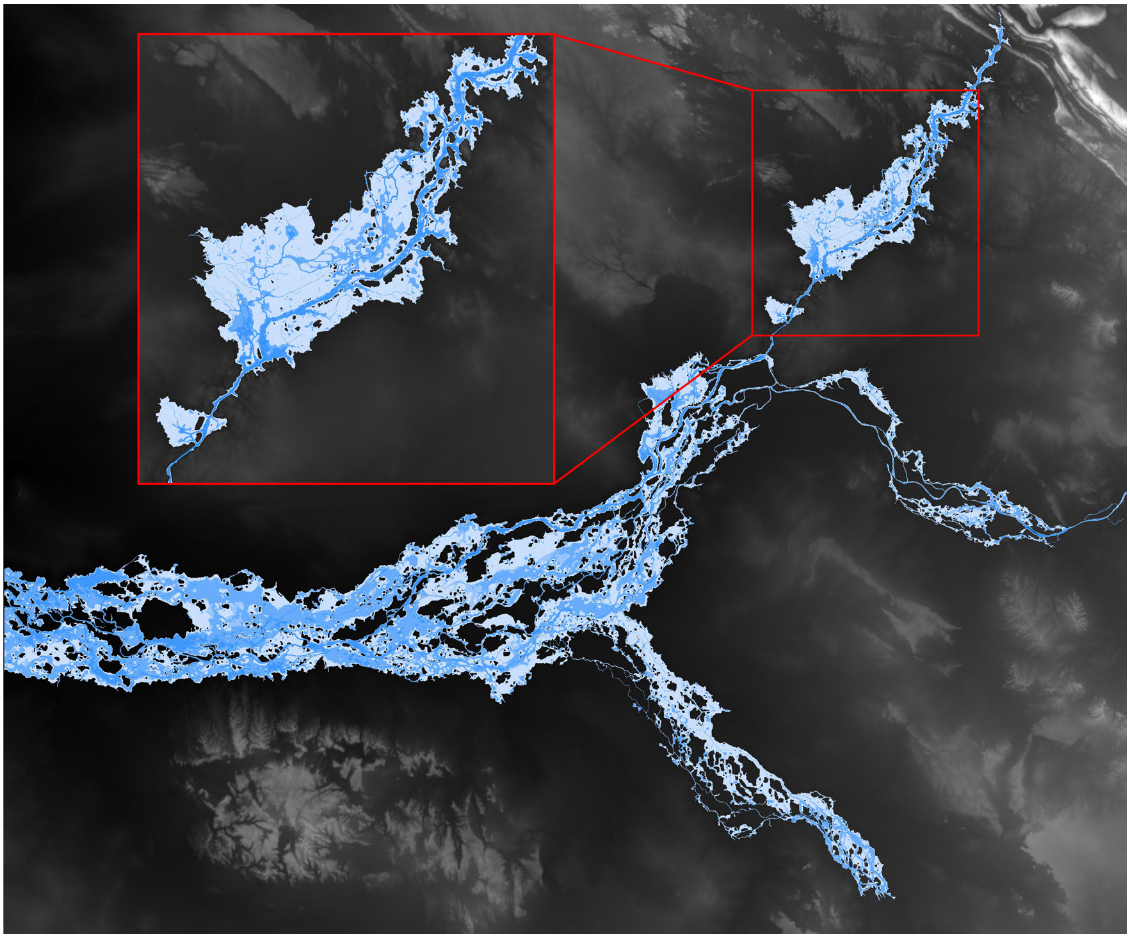

Figure 6.1. *Detail of flooded area between Dimond Gorge and Fitzroy Crossing stations.*

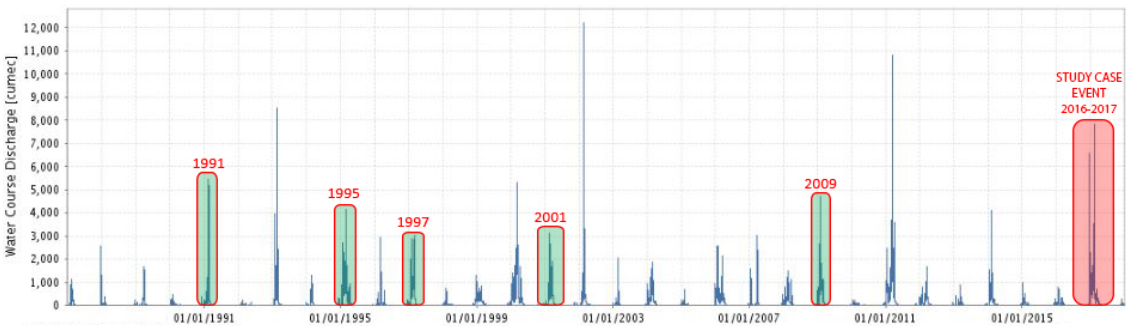

Figure 6.2. *Five hystorical events (green marked) with discharge peak greater than 2000 m^3/s have been selected due to related availability of daily WOfS images capturing the interested area.*

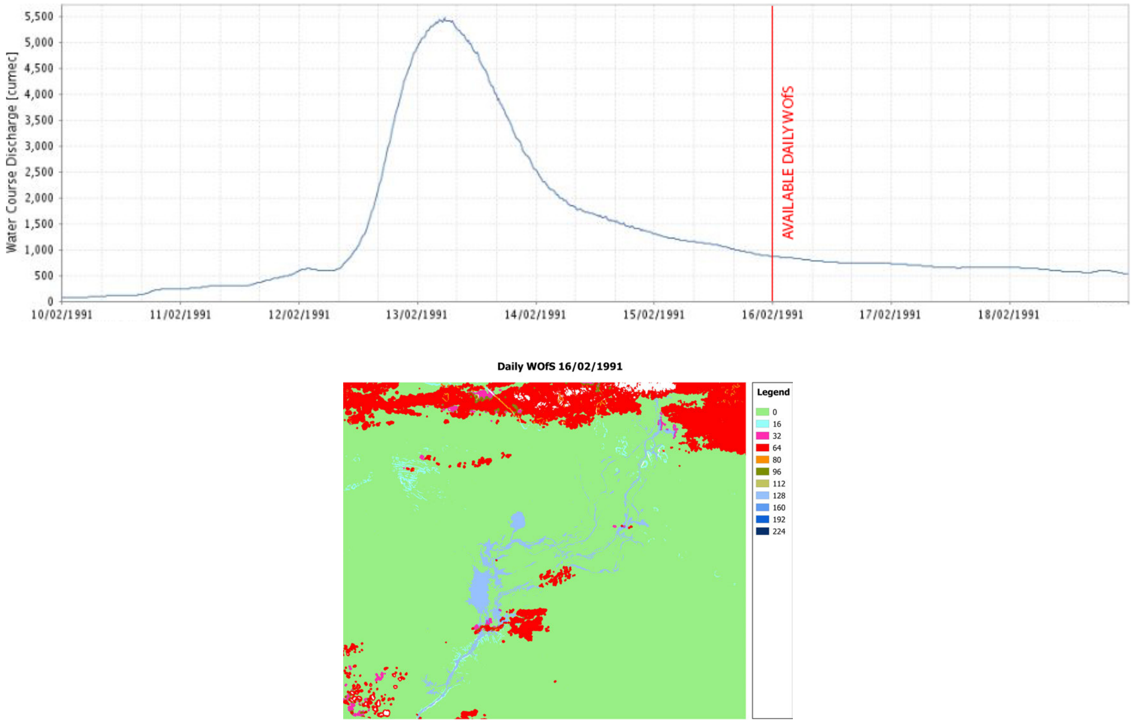

Figure 6.3. *1991 event: hydrograph and available daily WOfS image.*

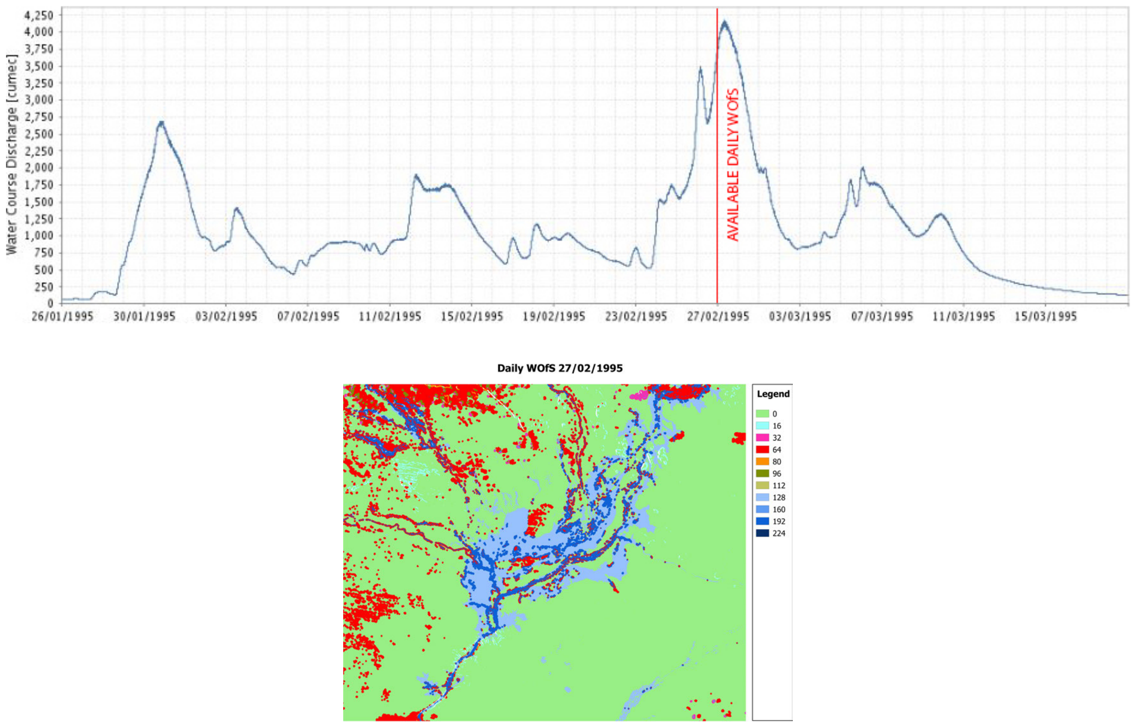

Figure 6.4. *1995 event: hydrograph and available daily WOfS image.*

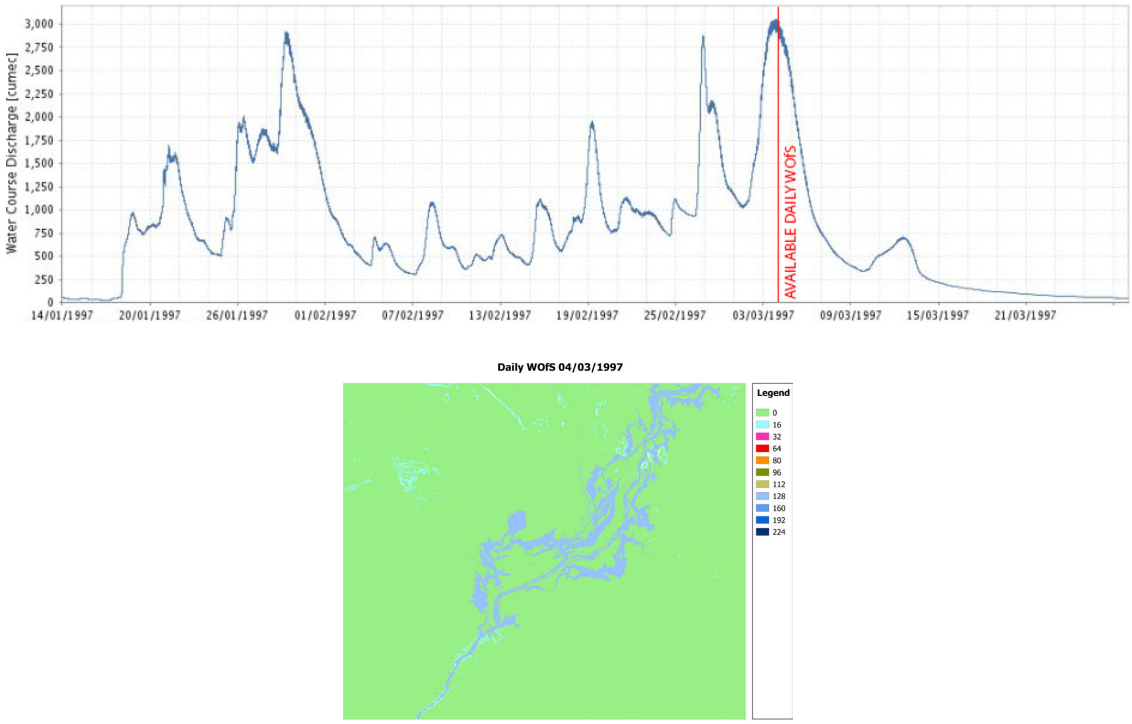

Figure 6.5. *1997 event: hydrograph and available daily WOfS image.*

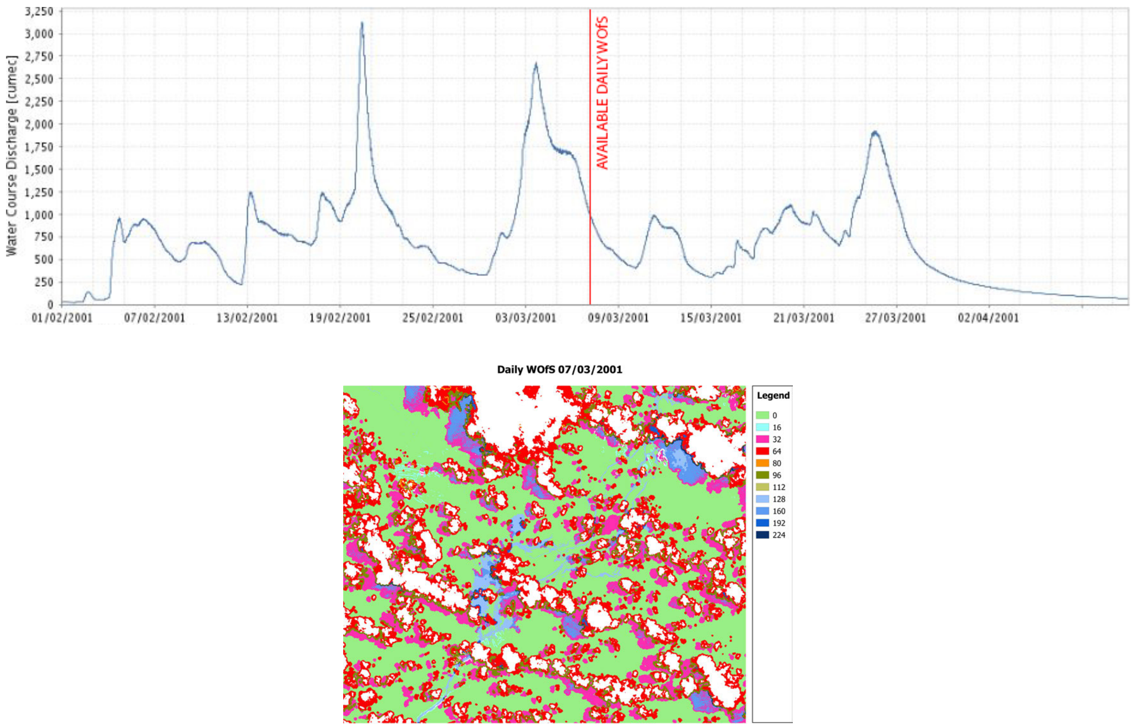

Figure 6.6. *2001 event: hydrograph and available daily WOfS image.*

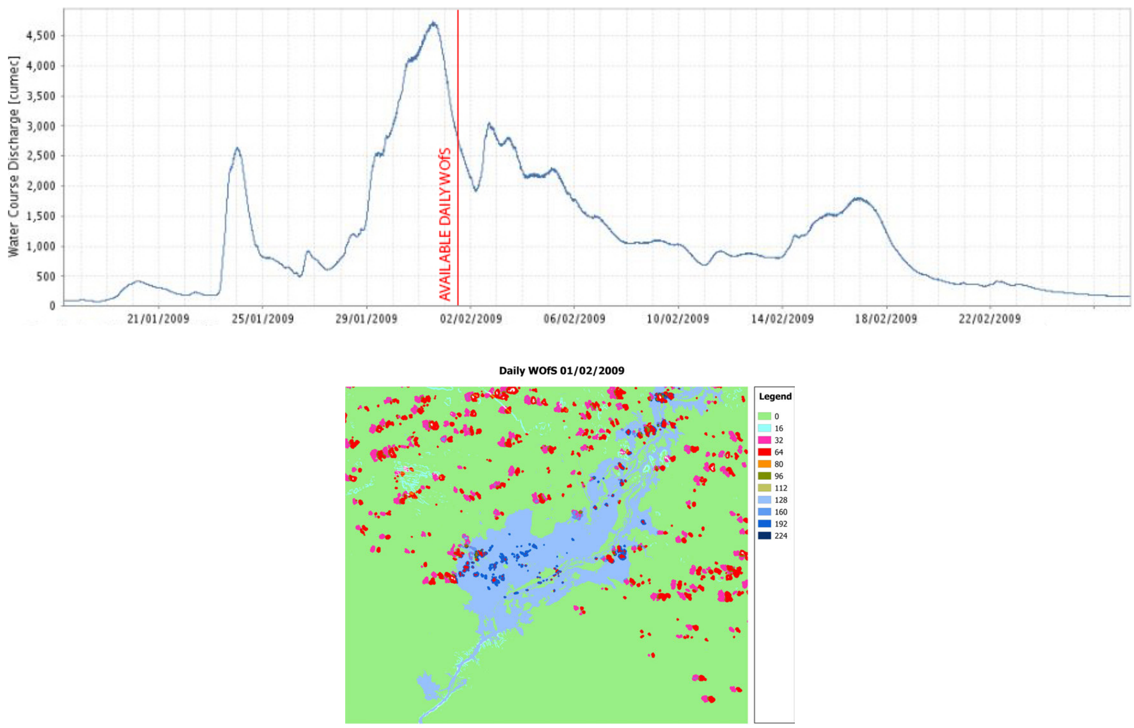

Figure 6.7. *2009 event: hydrograph and available daily WOfS image.*

6.2 Model of the 2009 historical event

In order to verify the model behaviour previously implemented for the 2016-2017 event, we decided to model one of the historical events described above. The most recent one of 2009 was chosen since it has the best acquisition of the flood extent compared to the other available WOfS images of 1995 and 1997. Indeed the 2009 WOfS is cloud-free and it was captured at a time close to the peak of the hydrograph, able thus to represent the maximum flood. The simulations were performed using the LISFLOOD-FP model and implementing the input data in the same way it has be done for the study case. In particular, four cases have been simulated, *Dem0_n0.025*, *Dem0_n0.018*, *Dem3_extended_n0.025* and *Dem3_extended_n0.018*, in order to analyse the results before and after the DEM correction and understand if the behaviour reflects the one obtained for the 2016-2017. The 2009 event took place between the end of January and the end of February. A time window of 30 days has been chosen to study the event, in particular the days between 13/01/2009 and 12/02/2009. Figures 6.8 and 6.9 report the plots of the data measured at gauge stations selected, used as input for simulation. Fitzroy Crossing and Noonkanbah stations data will be used as comparisons for hydrometric measurements comparisons in a similar way done for the study case. The daily WOfS of Figure 6.7 has to be treated in the same way done previously with the daily WOfS of the 2016-2017 event in order to obtain a post image processed with the HAND index. Then it will be used as comparison for simulation results. Next paragraphs shows the results of the comparison based on the use of gauged and RS data.

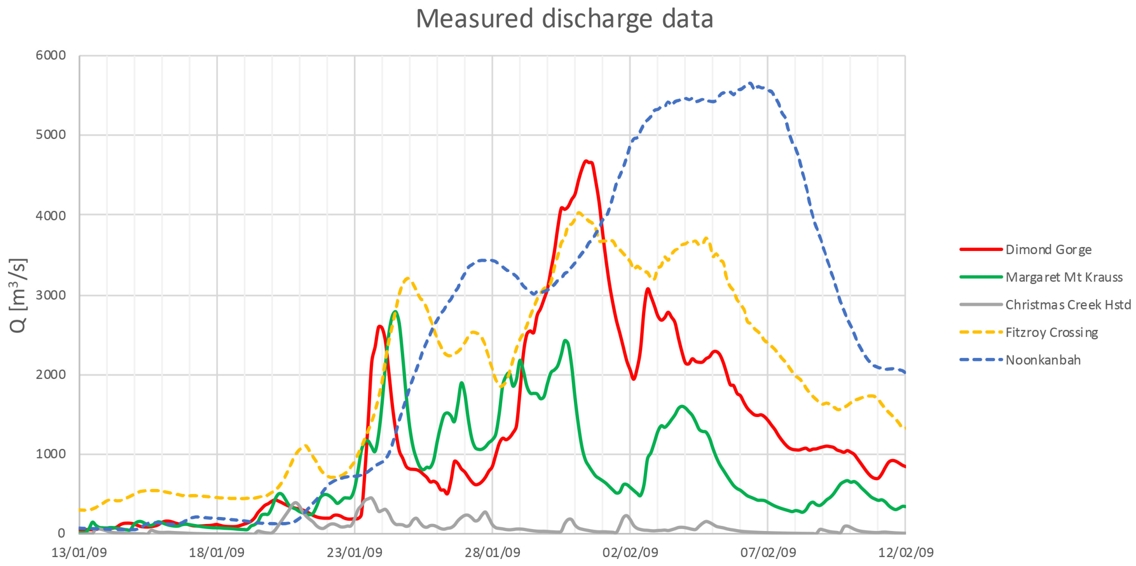

Figure 6.8. *Plot of gauged discharges of the 2009 event.*

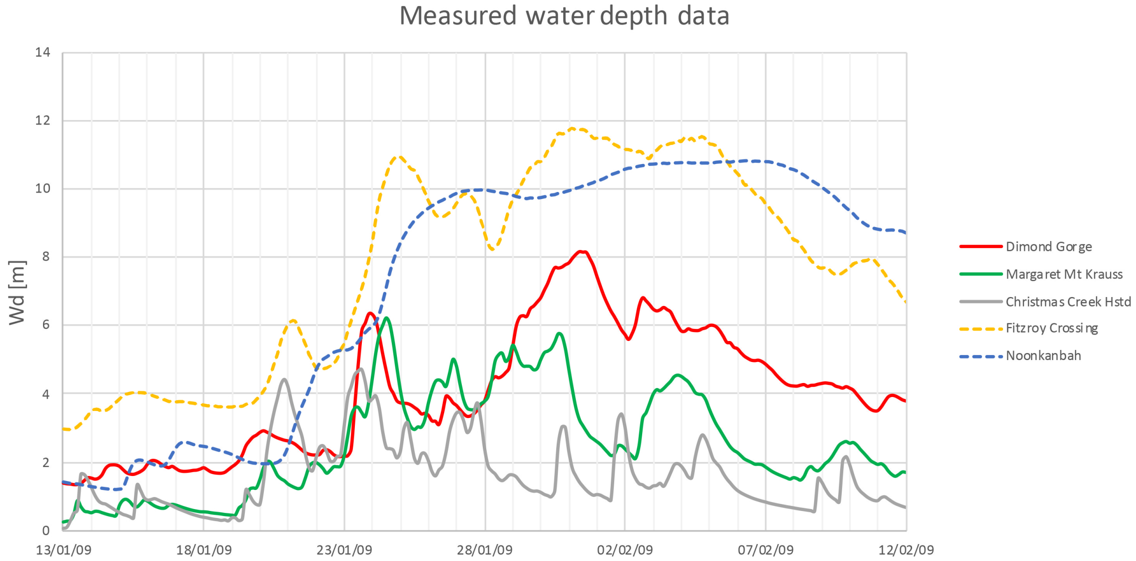

Figure 6.9. *Plot of gauged water depths of the 2009 event.*

6.2.1 Hydrometric measurements comparisons

Figures 6.10 and 6.11 and Tables 6.1, 6.2, 6.3 and 6.4 show the discharge and water depth time series comparisons at Fitzroy Crsossing and Noonkanbah stations and the related performance metrics computed for the cases selected. They confirm, both visually and quantitatively, how the cases with DEM corrected improve the behaviour of the model.

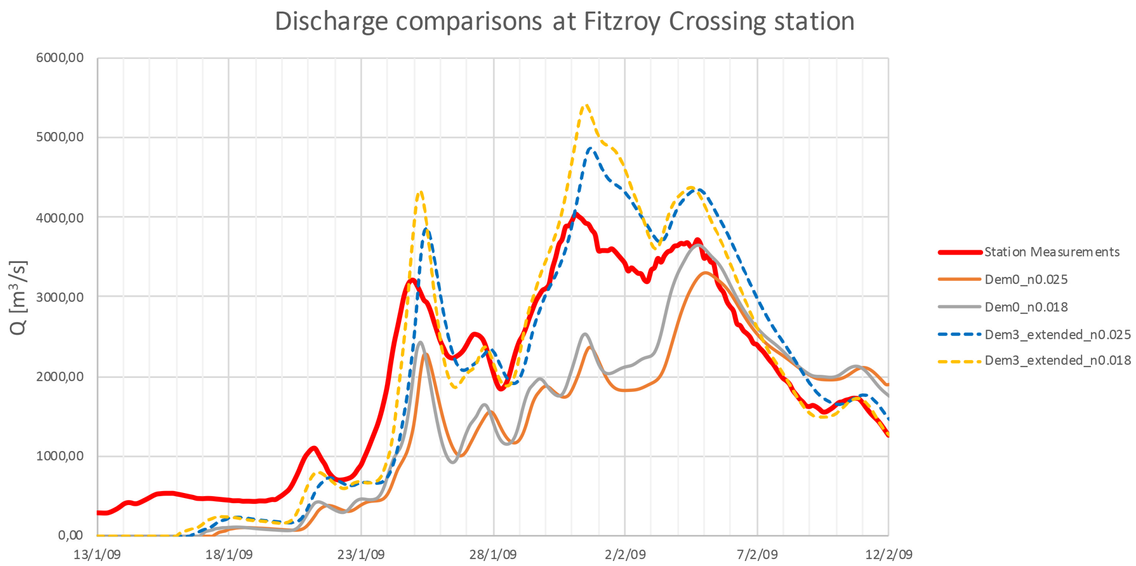

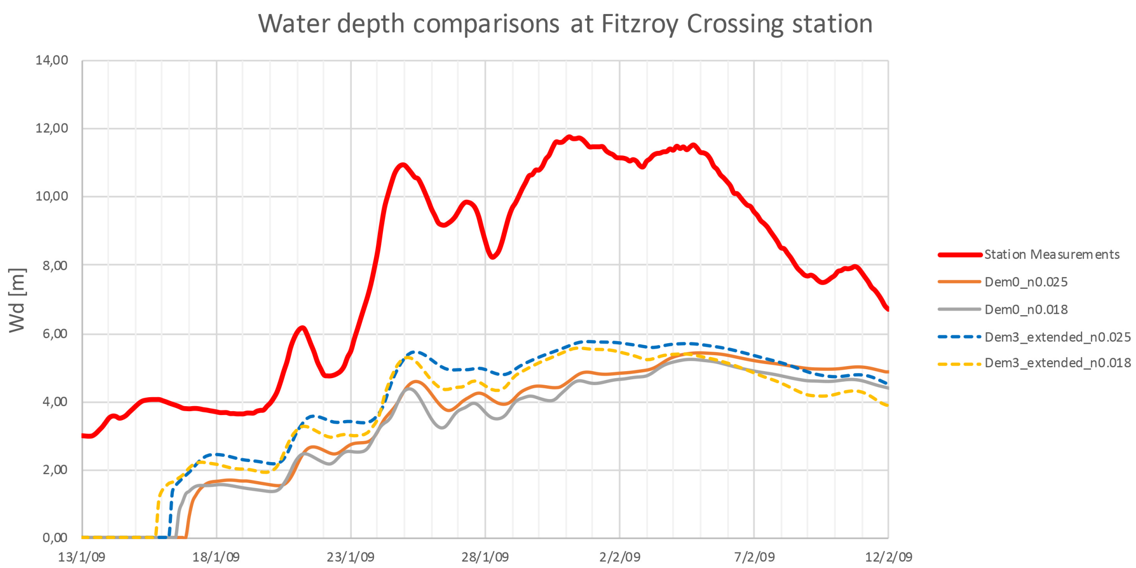

Figure 6.10. *2009 event: comparisons between observed and simulated data for all cases at Fizroy Crossing station.*

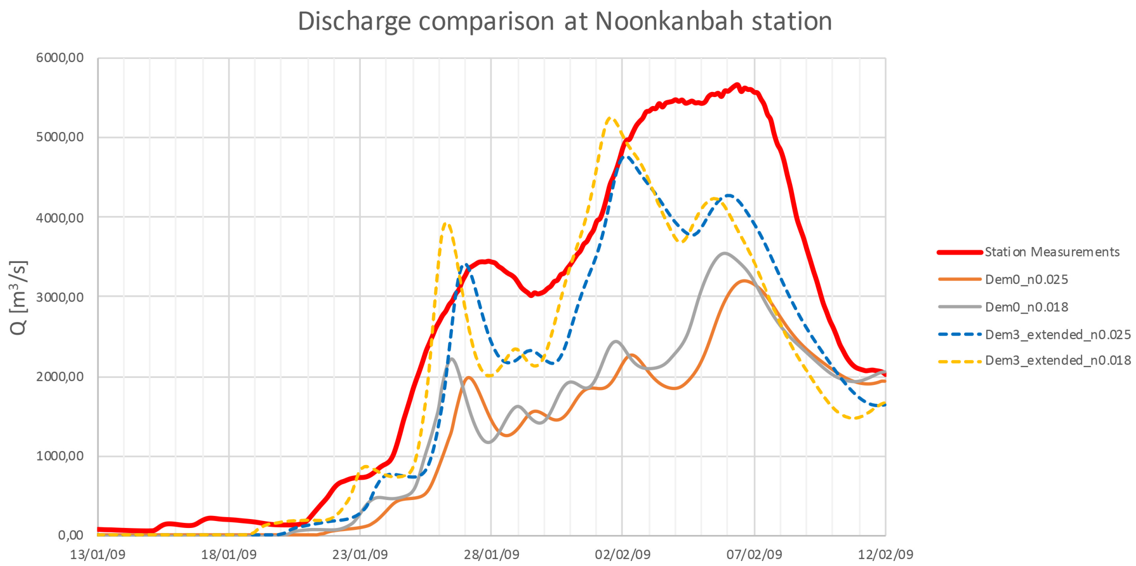

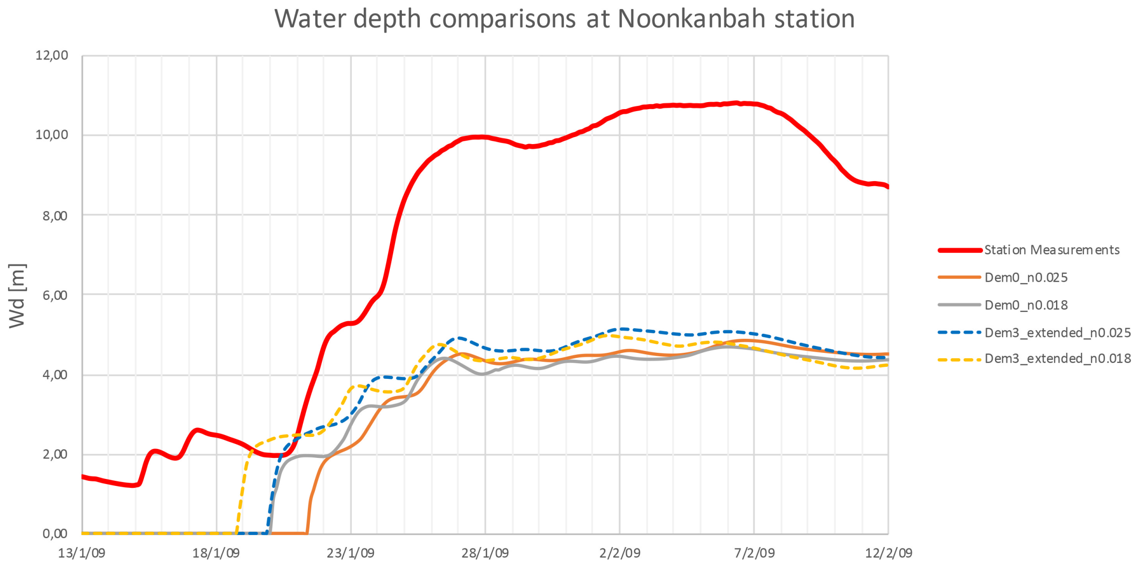

Figure 6.11. *2009 event: comparisons between observed and simulated data for all cases at Noonkanbah station.*

Case	NSE	PBIAS	RMSE	RSR
Dem0_n0.025	0.388	0.322	925.819	0.783
Dem0_n0.018	0.522	0.272	817.699	0.691
Dem3_extended_n0.025	0.788	-0.009	545.205	0.461
Dem3_extended_n0.018	0.794	-0.032	536.567	0.454

Table 6.1. *Performance metrics of comparisons between gauged and simulated discharge at Fitzroy Crossing station for the 2009 event.*

Case	NSE	PBIAS	RMSE	RSR
Dem0_n0.025	-1.493	0.560	4.684	1.579
Dem0_n0.018	-1.713	0.585	4.886	1.647
Dem3_extended_n0.025	-0.947	0.491	4.139	1.395
Dem3_extended_n0.018	-1.177	0.524	4.377	1.476

Table 6.2. *Performance metrics of comparisons between gauged and simulated water depth at Fitzroy Crossing station for the 2009 event.*

Case	NSE	PBIAS	RMSE	RSR
Dem0_n0.025	0.281	0.518	1686.794	0.848
Dem0_n0.018	0.407	0.468	1531.720	0.770
Dem3_extended_n0.025	0.827	0.256	828.551	0.416
Dem3_extended_n0.018	0.775	0.232	942.735	0.474

Table 6.3. *Performance metrics of comparisons between gauged and simulated discharge at Noonkanbah station for the 2009 event.*

Case	NSE	PBIAS	RMSE	RSR
Dem0_n0.025	-0.599	0.591	4.608	1.265
Dem0_n0.018	-0.619	0.584	4.637	1.273
Dem3_extended_n0.025	-0.379	0.537	4.280	1.174
Dem3_extended_n0.018	-0.470	0.541	4.418	1.212

Table 6.4. *Performance metrics of comparisons between gauged and simulated water depth at Noonkanbah station for the 2009 event.*

6.2.2 Remote sensing comparisons

The daily WOfS image of the 2009 historical event was captured on 01/02/2009 at 11:22. The simulations start on 13/01/2009 with saving time interval of three hours. Therefore the *wd* result file to plot is the one computed by the model after 1 684 800 seconds from the beginning of the simulation, or in other words, after 19.5 days.

It is interesting to note in figures and tables comparisons reported below that the historical data confirm that the initial simulations *Dem0* are not able to represent the real behavior of the river. It should be recalled for 2016-2017 event these models underestimated the observations for the area around Noonkanbah station. Now instead, considering the area between Dimond Gorge and Fitzroy Crossing stations, the comparison indicates they overestimate the flooded area. This fact further confirms the obstruction hypothesis that generates a backwater effect causing a huge flooding in this part of the catchment. On the other side the simulations with the DEM corrected clearly show an improvement of the model behaviour. Therefore, despite the historical data analysis cannot be considered a direct comparison to the event of 2016-2017, it is valid approach to evaluate the interested model and to confirm the methodology used is correct.

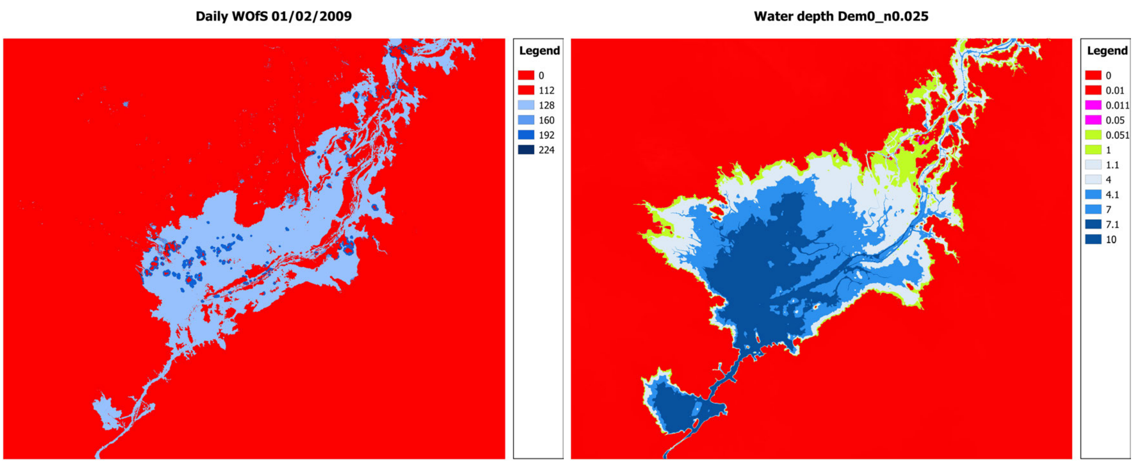

Figure 6.12. *Case Dem0_n0.025: visual comparison between 2009 daily WOfS image and correspondent water depth plot.*

	Present in observation	Absent in observation
Present in model	198 508	167 657
Absent in model	9704	1 211 812

BIAS	PC	CSI	$F^{<3>}$	$F^{<4>}$	H	F
1.759	0.888	0.528	0.502	0.082	0.953	0.122

Table 6.5. *Case Dem0_n0.025: quantitative comparison (contingency table and performance metrics) between 2009 daily WOfS image and correspondent water depth plot.*

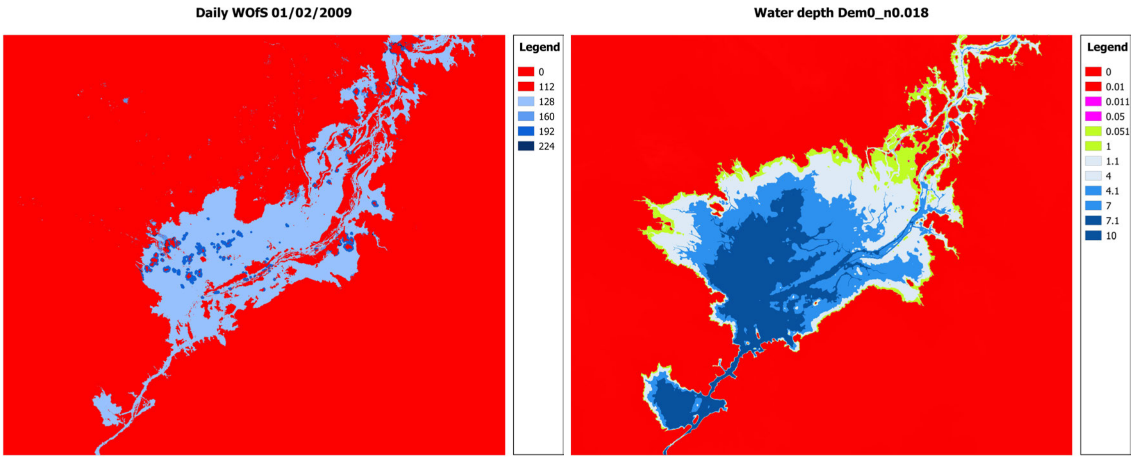

Figure 6.13. *Case Dem0_n0.018: visual comparison between 2009 daily WOfS image and correspondent water depth plot.*

	Present in observation	Absent in observation
Present in model	194 512	163 607
Absent in model	13 700	1 215 862

BIAS	PC	CSI	$F^{<3>}$	$F^{<4>}$	H	F
1.720	0.888	0.523	0.486	0.083	0.934	0.119

Table 6.6. *Case Dem0_n0.018: quantitative comparison (contingency table and performance metrics) between 2009 daily WOfS image and correspondent water depth plot.*

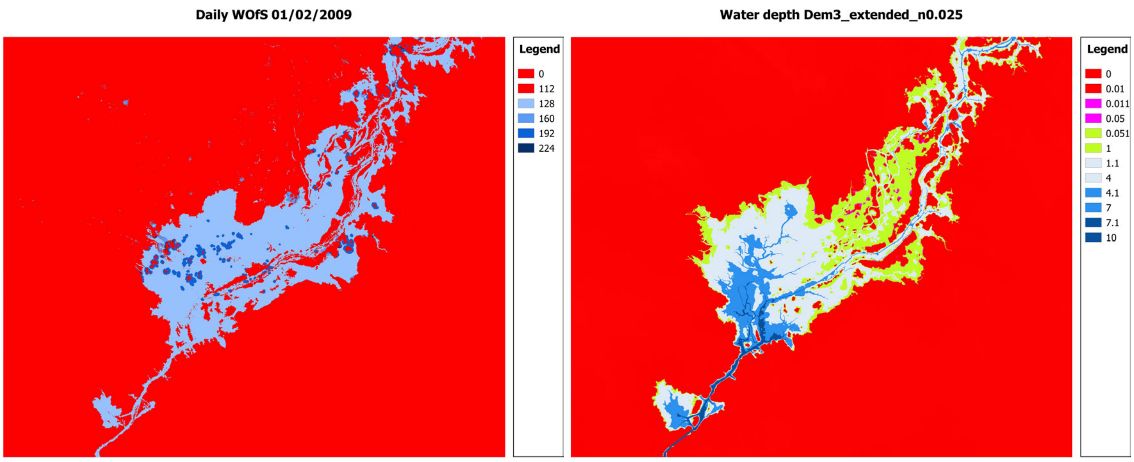

Figure 6.14. *Case Dem3_extended_n0.025: visual comparison between 2009 daily WOfS image and correspondent water depth plot.*

	Present in observation	Absent in observation
Present in model	186 668	63 400
Absent in model	21 544	1 316 069

BIAS	PC	CSI	$F^{<3>}$	$F^{<4>}$	H	F
1.201	0.946	0.687	0.608	0.454	0.897	0.046

Table 6.7. *Case Dem3_extended_n0.025: quantitative comparison (contingency table and performance metrics) between 2009 daily WOfS image and correspondent water depth plot.*

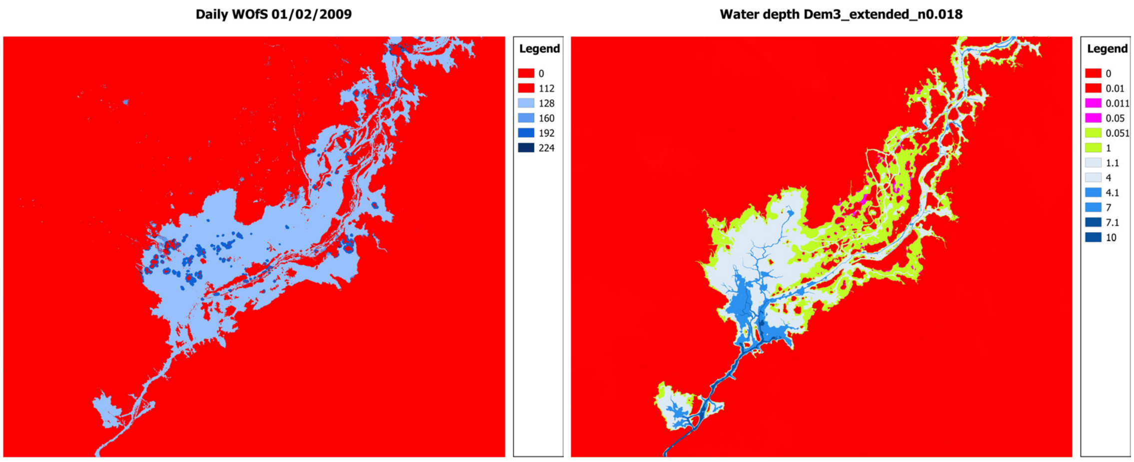

Figure 6.15. *Case Dem3_extended_n0.018: visual comparison between 2009 daily WOfS image and correspondent water depth plot.*

	Present in observation	Absent in observation
Present in model	171 830	42 123
Absent in model	36 382	1 337 346

BIAS	PC	CSI	$F^{<3>}$	$F^{<4>}$	H	F
1.028	0.951	0.686	0.541	0.518	0.825	0.031

Table 6.8. *Case Dem3_extended_n0.018: quantitative comparison (contingency table and performance metrics) between 2009 daily WOfS image and correspondent water depth plot.*

Chapter 7

Conclusions and future developments

The study of this thesis applied a multi-objective methodology for the evaluation of the predictive performances of a two-dimensional hydraulic model. We started from the study of the open source model LISFLOOD-FP and from the implementation of the case study according to best practice through the use of online available data. A multi-objective analysis, based on comparisons with the gauged data and the WOfS images, allowed to evaluate the results of the initial simulation. Comparisons provided information on flow propagation and flooded areas of the model, suggesting the hypothesis of errors in the DEM. A sensitivity analysis was then carried out in order to understand the influence of implementation structure and roughness parameter on the model behaviour. Thanks to the visual and quantitative comparisons it was possible to define the best conditions to represent the study event. The evaluation of the model was finally supported by a further comparison studying the behaviour of the 2009 historical event.

The semi-qualitative methodology developed, allowed thus to study an event of exceptional intensity such as the Fitzroy River of 2016-2017 and define a model for flood forecasting. The Australian territory is characterized by the presence of numerous water courses whose behaviour has not yet been studied in detail or for which a forecast model is not still available. The increasingly frequent flood events and the related disastrous effects are pushing the government policy attention on being focussed on quantifying the inundation dynamics and creating tools of flood forecasting. For these reasons the proposed approach developed during this work is an interesting tool for applications similar to the Fitzroy River case in which the object of study does not have accurate data and detailed surveys.

Although the results obtained demonstrated the usefulness of the proposed methodology, the study case model and more generally the methodology itself still require improvements and future developments. A starting point could be the parallel use of different types of satellite observations for model calibration and validation. Particularly interesting could be the analysis of Sentinel-1 images, a constellation of radar satellites launched on April 2014 by the European Space Agency (ESA) [38]. Or for future events, the using of the medium-resolution images (6-30 m) of the new NovaSAR-1 satellite, launched on 16 September 2018 by the Surrey Satellite Technology Ltd [39].

Appendix A

MATLAB Codes

A.1 Script to modify DEM pixels values

```
clear all
close all
clc

% Step 1: open and read raster file DEM original.
dem=fopen('file name.asc');
lab=fscanf(dem,'%s',1);
ncols=fscanf(dem,'%u/n',1);
lab=fscanf(dem,'%s',1);
nrows=fscanf(dem,'%u/n',1);
lab=fscanf(dem,'%s',1);
cellSize=fscanf(dem,'%f/n',1);
lab=fscanf(dem,'%s',1);
nodata=fscanf(dem,'%f/n',1);
lab=fscanf(dem,'%s',1);
minX=fscanf(dem,'%f/n',1);
lab=fscanf(dem,'%s',1);
minY=fscanf(dem,'%f/n',1);
RASTER_dem=fscanf(dem,'%f',[ncols nrows]);
RASTER_dem=RASTER_dem';
close all;

% Step 2: open and read file containing pixels to modify list.
pixels=load('file name.asc');
close all;

% Step 3: modify values of interested cells in the original DEM file.
a=0;
for j=1:1:length(pixels)
```

```
    a=a+2.0696*(10^(-4));
    x_cell=pixels(j,1);
    x_origin_distance=x_cell-minX;
    x_cell_distance=ceil(x_origin_distance/30);
    y_cell=pixels(j,2);
    y_origin_distance=y_cell-minY;
    y_cell_distance=nrows-ceil(y_origin_distance/30)+1;
    RASTER_dem(y_cell_distance,x_cell_distance)=111.6-a;
end

% Step 4: write and save the new DEM.
fclose all;
COLUMNS=size(RASTER_dem,2);
clear format1
clear format0
format1 = {'%f';' %f';'\r\n'};
format0=[format1{[1 2*ones(1,(COLUMNS-1)) 3]}];
fid1=fopen('file name.asc','w');
RASTER_dem=RASTER_dem';
fprintf(fid1,'%s','ncols ');
fprintf(fid1,'%u\n',size(RASTER_dem,1));
fprintf(fid1,'%s %u\n','nrows ',size(RASTER_dem,2));
fprintf(fid1,'%s %f\n','cellsize ', cellSize);
fprintf(fid1,'%s %u\n','nodata_value ', nodata);
fprintf(fid1,'%s %f\n','xllcorner ', minX);
fprintf(fid1,'%s %f\n','yllcorner ',minY);
fprintf(fid1,format0,RASTER_dem);
fclose all;
```

A.2 Script to create the roughness input file

```
clear all
close all
clc

% Step 1: open and read a raster file with same.
% characteristics of studied DEM.
dem=fopen('file name.asc');
lab=fscanf(dem,'%s',1);
ncols=fscanf(dem,'%u/n',1);
lab=fscanf(dem,'%s',1);
nrows=fscanf(dem,'%u/n',1);
lab=fscanf(dem,'%s',1);
cellsize=fscanf(dem,'%f/n',1);
lab=fscanf(dem,'%s',1);
nodata=fscanf(dem,'%f/n',1);
lab=fscanf(dem,'%s',1);
minX=fscanf(dem,'%f/n',1);
lab=fscanf(dem,'%s',1);
minY=fscanf(dem,'%f/n',1);
RASTER_dem=fscanf(dem,'%f',[ncols nrows]);
RASTER_dem=RASTER_dem';
close all;

% Step 2: assign a Manning's value for each cell.
for i=1:1:nrows
    for j=1:1:ncols
    RASTER_dem(i,j)=0.025;
    end
end

% Step 3: write and save the roughness file.
fclose all;
COLUMNS=size(RASTER_dem,2);
clear format1
clear format0
format1 = {'%f';' %f';'\r\n'};
format0=[format1{[1 2*ones(1,(COLUMNS-1)) 3]}];
fid1=fopen('file name.asc','w');
RASTER_dem=RASTER_dem';
fprintf(fid1,'%s','ncols ');
fprintf(fid1,'%u\n',size(RASTER_dem,1));
fprintf(fid1,'%s %u\n','nrows ',size(RASTER_dem,2));
fprintf(fid1,'%s %f\n','cellsize ', CellSize);
```

```
fprintf(fid1,'%s %u\n','nodata_value ', nodata);
fprintf(fid1,'%s %f\n','xllcorner ', minX);
fprintf(fid1,'%s %f\n','yllcorner ',minY);
fprintf(fid1,format0,RASTER_dem);
fclose all;
```

A.3 Script to compute discharge values

```
clear all
close all
clc

for j=10800:10800:3715200;
    i=j/10800;

% Step 1: open and read raster files qy.
    clear number
    path=['\qy_'];
    file_type=['.asc'];
    number=num2str(j);
    file_name=[path number file_type];
    fid=fopen(file_name);

    lab=fscanf(fid,'%s',1);
    ncols=fscanf(fid,'%u/n',1);
    lab=fscanf(fid,'%s',1);
    nrows=fscanf(fid,'%u/n',1);
    lab=fscanf(fid,'%s',1);
    cellsize=fscanf(fid,'%f/n',1);
    lab=fscanf(fid,'%s',1);
    nodata=fscanf(fid,'%f/n',1);
    lab=fscanf(fid,'%s',1);
    minX=fscanf(fid,'%f/n',1);
    lab=fscanf(fid,'%s',1);
    minY=fscanf(fid,'%f/n',1);
    RASTER=fscanf(fid,'%f',[ncols nrows]);
    RASTER=RASTER';
    close all

% Step 2: read qy values in the cells of the cross section.
    for k=1:1:1600
        x_section_qy=745225;
        x_origindistance_qy=x_section_qy-minX;
        x_celldistance_qy=ceil(x_origindistance_qy/30)+k-1;
        y_section_qy=7976943;
        y_origindistance_qy=y_section_qy-minY;
        y_celldistance_qy=nrows-ceil(y_origindistance_qy/30);
        qy(i,k)=RASTER(y_celldistance_qy,x_celldistance_qy);
    end

% Step 3: calculate the sum of qy values in the cross section.
```

```
    a=0;
    for k=1:1:1600
        qysum(i,1)=a+abs(qy(i,k));
        a=qysum(i,1);
    end

% Step 4: print and save gauged qy values.
    t(i,1)=i*3*3600;
    tab=[t,qysum];
    save('\Gauge_qy.ascii','tab','-ascii');

% Step 5: open and read raster files qx.
    clear number
    path=['\qx_'];
    file_type=['.asc'];
    number=num2str(j);
    file_name=[path number file_type];
    fid=fopen(file_name);

    lab=fscanf(fid,'%s',1);
    ncols=fscanf(fid,'%u/n',1);
    lab=fscanf(fid,'%s',1);
    nrows=fscanf(fid,'%u/n',1);
    lab=fscanf(fid,'%s',1);
    cellsize=fscanf(fid,'%f/n',1);
    lab=fscanf(fid,'%s',1);
    nodata=fscanf(fid,'%f/n',1);
    lab=fscanf(fid,'%s',1);
    minX=fscanf(fid,'%f/n',1);
    lab=fscanf(fid,'%s',1);
    minY=fscanf(fid,'%f/n',1);
    RASTER=fscanf(fid,'%f',[ncols nrows]);
    RASTER=RASTER';
    close all

% Step 6: read qx values in the cells of the cross section.
    for k=1:1:700
        x_section_qx=694344;
        x_origindistance_qx=x_section_qx-minX;
        x_celldistance_qx=ceil(x_origindistance_qx/30);
        y_section_qx=7964408;
        y_origindistance_qx=y_section_qx-minY;
        y_celldistance_qx=nrows-ceil(y_origindistance_qx/30)+k-1;
        qx(i,k)=RASTER(y_celldistance_qx,x_celldistance_qx);
    end
```

```
% Step 7: calculate the sum of qx values in the cross section.
    a=0;
    for k=1:1:700
        qxsum(i,1)=a+abs(qx(i,k));
        a=qxsum(i,1);
    end

% Step 8: print and save gauged qx values.
    t(i,1)=i*3*3600;
    tab=[t,qxsum];
    save('\Gauge_qx.ascii','tab','-ascii');

end
```

A.4 Script to compute water depth values

```
clear all
close all
clc

for j=10800:10800:3715200;
    i=j/10800;

% Step 1: open and read raster files wd.
    clear number
    path=['\water_depth_'];
    file_type=['.asc'];
    number=num2str(j);
    file_name=[path number file_type];
    fid=fopen(file_name);

    lab=fscanf(fid,'%s',1);
    ncols=fscanf(fid,'%u/n',1);
    lab=fscanf(fid,'%s',1);
    nrows=fscanf(fid,'%u/n',1);
    lab=fscanf(fid,'%s',1);
    cellsize=fscanf(fid,'%f/n',1);
    lab=fscanf(fid,'%s',1);
    nodata=fscanf(fid,'%f/n',1);
    lab=fscanf(fid,'%s',1);
    minX=fscanf(fid,'%f/n',1);
    lab=fscanf(fid,'%s',1);
    minY=fscanf(fid,'%f/n',1);
    RASTER=fscanf(fid,'%f',[ncols nrows]);
    RASTER=RASTER';
    close all

% Step 2: read wd values at Fitzroy Crossing station.
    x_fitz_wd=772875;
    x_origindistance_fitz_wd=x_fitz_wd-minX;
    x_celldistance_fitz_wd=ceil(x_origindistance_fitz_wd/30);
    y_fitz_wd=7984659;
    y_origindistance_fitz_wd=y_fitz_wd-minY;
    y_celldistance_fitz_wd=nrows-ceil(y_origindistance_fitz_wd/30)+1;
    wd_fitz(i,1)=RASTER(y_celldistance_fitz_wd,x_celldistance_fitz_wd);
    t(i,1)=i*3*3600;

% Step 3: print and save wd values gauged at fitz Crossing station.
    tab=[t,wd_fitz];
```

```
    save('\Gauge_wd_FitzroyCrossing.ascii','tab','-ascii');

% Step 4: read wd values at Noonkanbah station.
    x_noonk_wd=694246;
    x_origindistance_noonk_wd=x_noonk_wd-minX;
    x_celldistance_noonk_wd=ceil(x_origindistance_noonk_wd/30);
    y_noonk_wd=7953463;
    y_origindistance_noonk_wd=y_noonk_wd-minY;
    y_celldistance_noonk_wd=nrows-ceil(y_origindistance_noonk_wd/30)+1;
    wd_noonk(i,1)=RASTER(y_celldistance_noonk_wd,x_celldistance_noonk_wd);
    t(i,1)=i*3*3600;

% Step 5: print and save wd values gauged at noonk station.
    tab=[t,wd_noonk];
    save('\Gauge_wd_Noonkanbah.ascii','tab','-ascii');

end
```

A.5 Script to apply the HAND index to the DEM

```
clear all
close all
clc

% Step 1: open and read raster file WOfS processed.
raster_WOfS=fopen('\file name.asc');
lab=fscanf(raster_WOfS,'%s',1);
ncols=fscanf(raster_WOfS,'%u/n',1);
lab=fscanf(raster_WOfS,'%s',1);
nrows=fscanf(raster_WOfS,'%u/n',1);
lab=fscanf(raster_WOfS,'%s',1);
minX=fscanf(raster_WOfS,'%f/n',1);
lab=fscanf(raster_WOfS,'%s',1);
minY=fscanf(raster_WOfS,'%f/n',1);
lab=fscanf(raster_WOfS,'%s',1);
cellSize=fscanf(raster_WOfS,'%f/n',1);
lab=fscanf(raster_WOfS,'%s',1);
nodata=fscanf(raster_WOfS,'%f/n',1);
RASTER_WOfS=fscanf(raster_WOfS,'%f',[ncols nrows]);
RASTER_WOfS=RASTER_WOfS';
close all;

% Step 2: open and read raster file DEM processed with HAND index.
raster_DemHAND=fopen('\file name.asc');
lab=fscanf(raster_DemHAND,'%s',1);
ncols=fscanf(raster_DemHAND,'%u/n',1);
lab=fscanf(raster_DemHAND,'%s',1);
nrows=fscanf(raster_DemHAND,'%u/n',1);
lab=fscanf(raster_DemHAND,'%s',1);
minX=fscanf(raster_DemHAND,'%f/n',1);
lab=fscanf(raster_DemHAND,'%s',1);
minY=fscanf(raster_DemHAND,'%f/n',1);
lab=fscanf(raster_DemHAND,'%s',1);
cellSize=fscanf(raster_DemHAND,'%f/n',1);
lab=fscanf(raster_DemHAND,'%s',1);
nodata=fscanf(raster_DemHAND,'%f/n',1);
RASTER_DemHAND=fscanf(raster_DemHAND,'%f',[ncols nrows]);
RASTER_DemHAND=RASTER_DemHAND';
close all;

% Step 3: "clearing" process.
clear r;
clear c;
```

```
for r=1:1:1943
    for c=1:1:2559
    if (RASTER_DemHAND(r,c)>20)
    RASTER_WOfS(r,c)=0;
    end
    end
end

% Step 4: write and save new raster file WOfS
fclose all;
COLUMNS=size(RASTER_WOfS,2);
clear format1
clear format0
format1 = {'%f';' %f';'\r\n'};
format0=[format1{[1 2*ones(1,(COLUMNS-1)) 3]}];
fid1=fopen('\new file name.asc','w');
RASTER_WOfS=RASTER_WOfS';
fprintf(fid1,'%s','ncols ');
fprintf(fid1,'%u\n',size(RASTER_WOfS,1));
fprintf(fid1,'%s %u\n','nrows ',size(RASTER_WOfS,2));
fprintf(fid1,'%s %f\n','xllcorner ', minX);
fprintf(fid1,'%s %f\n','yllcorner ',minY);
fprintf(fid1,'%s %f\n','cellsize ', cellSize);
fprintf(fid1,'%s %u\n','nodata_value ', nodata);
fprintf(fid1,format0,RASTER_WOfS);
fclose all;
```

A.6 Script to plot simulated water depth results

```
clear all;
close all
clc

path=['\water_depth_'];
path_save=['\folder directory'];
name_save='wd_';
file_type=['.asc'];

% Step 1: open and read raster files wd.
for j=86400:86400:3715200
    clear n1
    clear number
    number=num2str(j);
    file_name=[path number file_type];

    fid=fopen(file_name);
    lab=fscanf(fid,'%s',1);
    ncols=fscanf(fid,'%u/n',1)
    lab=fscanf(fid,'%s',1);
    nrows=fscanf(fid,'%u/n',1)
    lab=fscanf(fid,'%s',1);
    cellSize=fscanf(fid,'%f/n',1)
    lab=fscanf(fid,'%s',1);
    nodata=fscanf(fid,'%f/n',1)
    lab=fscanf(fid,'%s',1);
    minX=fscanf(fid,'%f/n',1)
    lab=fscanf(fid,'%s',1);
    minY=fscanf(fid,'%f/n',1)
    RASTER=fscanf(fid,'%f',[ncols nrows]);
    RASTER=RASTER';
    close all

% Step 2: plot each raster file read and save the image.
    imagesc(RASTER)
    xlabel('')
    ylabel('')
    day=j/86400;
    dayplot=num2str(day);
    title({'\fontsize{10} Name of file';['\fontsize{8} Day ' dayplot]})
    c = colorbar;
    c.Label.String = 'Water depth [m]';
    load '\myCustomColormap'
```

```
    colormap(myCustomColormap);
    caxis([0 15])
    xlim([0 5640])
    ylim([0 4702])

    name_fig_save=[path_save name_save number '.jpeg'];
    print(name_fig_save,'-djpeg', '-r300')
end
```

A.7 Script to count wet cells in simulated data

```
clear all
close all
clc

a=0;
b=0;

for j=10800:10800:3715200;
    i=j/10800;

% Step 1: open and read raster files wd.
    clear number
    path=['\water_depth_'];
    file_type=['.asc'];
    number=num2str(j);
    file_name=[path number file_type];
    fid=fopen(file_name);

    lab=fscanf(fid,'%s',1);
    ncols=fscanf(fid,'%u/n',1);
    lab=fscanf(fid,'%s',1);
    nrows=fscanf(fid,'%u/n',1);
    lab=fscanf(fid,'%s',1);
    cellSize=fscanf(fid,'%f/n',1);
    lab=fscanf(fid,'%s',1);
    nodata=fscanf(fid,'%f/n',1);
    lab=fscanf(fid,'%s',1);
    minX=fscanf(fid,'%f/n',1);
    lab=fscanf(fid,'%s',1);
    minY=fscanf(fid,'%f/n',1);
    RASTER1=fscanf(fid,'%f',[ncols nrows]);
    RASTER1=RASTER1';
    close all

% Step 2: count wet cells.
    n_wet_cells=0;
    clear r;
    clear c;
    for r=1:1:1943
        for c=1:1:2559
        if (RASTER1(r,c)>0.01)
        n_wet_cells=n_wet_cells+1;
        end
```

```
        end
    end
    total_wet_cells(i+1,1)=n_wet_cells;

% Step 3: calculate total inunded area.
    total_flooded_area(i+1,1)=n_wet_cells*30*30/(1000^2);

% Step 4: print and save information obtained in time.
    t(i+1,1)=i*3*3600;
    tab=[t,total_wet_cells,total_flooded_area];
    save('\file name.ascii','tab','-ascii');

% Step 5: find the solution with maximum flooded area.
    if a<n_wet_cells
    a=n_wet_cells;
    b=i*3*3600;
    end

    fid1=fopen('\file name.asc','w');
    fprintf(fid1,'%s%f%s%f%s','The solution with maximum
    flooded area is at time ',b,' seconds and its flooded
    area is ',(a*30*30)/(1000^2),' [km^2].');

end
```

A.8 Script to count wet cells in observed data

```
clear all
close all
clc

% Step 1: open and read raster file daily WOfS.
daily_WOfS=fopen('\file name.asc');
lab=fscanf(daily_WOfS,'%s',1);
ncols=fscanf(daily_WOfS,'%u/n',1);
lab=fscanf(daily_WOfS,'%s',1);
nrows=fscanf(daily_WOfS,'%u/n',1);
lab=fscanf(daily_WOfS,'%s',1);
minX=fscanf(daily_WOfS,'%f/n',1);
lab=fscanf(daily_WOfS,'%s',1);
minY=fscanf(daily_WOfS,'%f/n',1);
lab=fscanf(daily_WOfS,'%s',1);
CellSize=fscanf(daily_WOfS,'%f/n',1);
lab=fscanf(daily_WOfS,'%s',1);
nodata=fscanf(daily_WOfS,'%f/n',1);
RASTER_daily_WOfS=fscanf(daily_WOfS,'%f',[ncols nrows]);
RASTER_daily_WOfS=RASTER_daily_WOfS';
close all;

% Step 2: count wet cells.
n_wet_cells=0;
clear r;
clear c;
    for r=1:1:1943
        for c=1:1:2559
        if (RASTER_daily_WOfS(p,o)>=128)
        n_wet_cells=n_wet_cells+1;
        end
        end
    end
total_wet_cells=n_wet_cells;

% Step 3: calculate total inunded area.
total_flooded_area=n_wet_cells*30*30/(1000^2);

% Step 4: print and save information obtained.
fid1=fopen('\file name.asc','w');
fprintf(fid1,'%s%u\n','Num of wet cells= ',total_wet_cells);
fprintf(fid1,'%s%f %s','Tot flooded area= ',total_flooded_area,'[km^2]');
```

A.9 Script to calculate performance metrics indexes

```
clear all
close all
clc

% Step 1: open and read raster file wd.
model=fopen('\file name.asc');
lab=fscanf(model,'%s',1);
ncols=fscanf(model,'%u/n',1);
lab=fscanf(model,'%s',1);
nrows=fscanf(model,'%u/n',1);
minX=fscanf(model,'%f/n',1);
lab=fscanf(model,'%s',1);
minY=fscanf(model,'%f/n',1);
lab=fscanf(model,'%s',1);
CellSize=fscanf(model,'%f/n',1);
lab=fscanf(model,'%s',1);
nodata=fscanf(model,'%f/n',1);
lab=fscanf(model,'%s',1);
RASTER_model=fscanf(model,'%f',[ncols nrows]);
RASTER_model=RASTER_model';
close all;

% Step 2: open and read raster file daily WOfS.
observation=fopen('\file name.asc');
lab=fscanf(observation,'%s',1);
ncols=fscanf(observation,'%u/n',1);
lab=fscanf(observation,'%s',1);
nrows=fscanf(observation,'%u/n',1);
lab=fscanf(observation,'%s',1);
minX=fscanf(observation,'%f/n',1);
lab=fscanf(observation,'%s',1);
minY=fscanf(observation,'%f/n',1);
lab=fscanf(observation,'%s',1);
CellSize=fscanf(observation,'%f/n',1);
lab=fscanf(observation,'%s',1);
nodata=fscanf(observation,'%f/n',1);
RASTER_observation=fscanf(observation,'%f',[ncols nrows]);
RASTER_observation=RASTER_observation';
close all;

% Step 3: calculate contingency table values.
a=0;
b=0;
```

```
c=0;
d=0;
clear i;
clear j;

for i=1:1:1943
    for j=1:1:2559
        if (RASTER_model(i,j)>0.01)&&(RASTER_observation(i,j)>128)
        a=a+1;
        else if (RASTER_model(i,j)>0.01)&&(RASTER_observation(i,j)<=128)
        b=b+1;
        else if (RASTER_model(i,j)<=0.01)&&(RASTER_observation(i,j)>128)
        c=c+1;
        else if (RASTER_model(i,j)<=0.01)&&(RASTER_observation(i,j)<=128)
        d=d+1;
        end
        end
        end
        end
    end
end

% Step 4: calculate performance metrics indexes.
BIAS=(a+b)/(a+c);
PC=(a+d)/(a+b+c+d);
CSI=(a/(a+b+c));
F3=((a-c)/(a+b+c));
F4=((a-b)/(a+b+c));
H=a/(a+c);
F=b/(b+d);

% Step 5: print and save values calculated.
fid1=fopen('\name.asc','w');
fprintf(fid1,'%s %u\n','a=', a);
fprintf(fid1,'%s %u\n','b=', b);
fprintf(fid1,'%s %u\n','c=', c);
fprintf(fid1,'%s %u\n\n','d=', d);
fprintf(fid1,'%s %f\n','BIAS=', BIAS);
fprintf(fid1,'%s %f\n','PROPORTION CORRECT=', PC);
fprintf(fid1,'%s %f\n','CRITICAL SUCCESS INDEX=', CSI);
fprintf(fid1,'%s %f\n','F<3>=', F3);
fprintf(fid1,'%s %f\n','F<4>=', F4);
fprintf(fid1,'%s %f\n','HIT RATE=', H);
fprintf(fid1,'%s %f\n','FALSE ALARM RATE=', F);
```

A.10 Script to write the envelope raster file of simulated data

```
clear all
close all
clc

% Step 1: open and read headers from a raster file
% with characteristics of the studied one.
raster_initial=fopen('file name.asc');
lab=fscanf(raster_initial,'%s',1);
ncols=fscanf(raster_initial,'%u/n',1);
lab=fscanf(raster_initial,'%s',1);
nrows=fscanf(raster_initial,'%u/n',1);
lab=fscanf(raster_initial,'%s',1);
minX=fscanf(raster_initial,'%f/n',1);
lab=fscanf(raster_initial,'%s',1);
minY=fscanf(raster_initial,'%f/n',1);
lab=fscanf(raster_initial,'%s',1);
cellSize=fscanf(raster_initial,'%f/n',1);
lab=fscanf(raster_initial,'%s',1);
nodata=fscanf(raster_initial,'%f/n',1);
RASTER_initial=fscanf(raster_initial,'%f',[ncols nrows]);
RASTER_initial=RASTER_initial';
close all;

for j=10800:10800:3715200;
    i=j/10800;

% Step 2: open and read raster files wd.
    clear number
    path=['\water_depth_'];
    file_type=['.asc'];
    number=num2str(j);
    file_name=[path number file_type];
    fid=fopen(file_name);

    lab=fscanf(fid,'%s',1);
    ncols=fscanf(fid,'%u/n',1);
    lab=fscanf(fid,'%s',1);
    nrows=fscanf(fid,'%u/n',1);
    lab=fscanf(fid,'%s',1);
    cellSize=fscanf(fid,'%f/n',1);
    lab=fscanf(fid,'%s',1);
    nodata=fscanf(fid,'%f/n',1);
```

```
    lab=fscanf(fid,'%s',1);
    minX=fscanf(fid,'%f/n',1);
    lab=fscanf(fid,'%s',1);
    minY=fscanf(fid,'%f/n',1);
    RASTER=fscanf(fid,'%f',[ncols nrows]);
    RASTER=RASTER';
    close all

% Step 3: read wet cells and assign a binary value.
    clear r;
    clear c;
    for r=1:1:nrows
        for c=1:1:ncols
        if (RASTER(r,c)>0.01)
        RASTER_initial(r,c)=1;
        end
        end
    end

end

% Step 4: write and save the envelope raster file.
fclose all;
COLUMNS=size(RASTER_initial,2);
clear format1
clear format0
format1 = {'%f'; ' %f'; '\r\n'};
format0=[format1{[1 2*ones(1,(COLUMNS-1)) 3]}];
fid1=fopen('\name.asc','w');
RASTER_initial=RASTER_initial';
fprintf(fid1,'%s','ncols ');
fprintf(fid1,'%u\n',size(RASTER_initial,1));
fprintf(fid1,'%s %u\n','nrows ',size(RASTER_initial,2));
fprintf(fid1,'%s %f\n','xllcorner ', minX);
fprintf(fid1,'%s %f\n','yllcorner ',minY);
fprintf(fid1,'%s %f\n','cellsize ', cellSize);
fprintf(fid1,'%s %u\n','nodata_value ', nodata);
fprintf(fid1,format0,RASTER_initial);
fclose all;
```

Bibliography

[1] *Financial Management of Flood Risk*, OECD, 2016.

[2] Katharine Haynes, Lucinda Coates, Rob van den Honert, Andrew Gissing, Deanne Bird, Felipe Dimer de Oliveira, Rebecca D'Arcy, Chloe Smith, Deirdre Radford. *Exploring the circumstances surrounding flood fatalities in Australia 1900 – 2015 and the implications for policy and practice*, Environmental Science and Policy 76:165–176, 2017.

[3] Gerry FitzGerald, Weiwei Du, Aziz Jamal, Michele Clark and Xiang-Yu Hou. *Flood fatalities in contemporary Australia (1997–2008)*, Emergency Medicine Australasia 22:180–186, 2010.

[4] *Food, Fibre & Forestry Facts - A summary of Australian agriculture sector*, National Farmers' Federation (NFF), 2017.

[5] Tom Jackson, Kirk Zammit and Steve Hatfield-Dodds. *Snapshot of Australian Agriculture*, Department of Agriculture and Water Resources, 2018.

[6] Bill Binks, Nyree Stenekes, Heleen Kruger, Robert Kancans. *Snapshot of Australia's Agricultural Workforce*, Department of Agriculture and Water Resources, 2018.

[7] Fazlul Karim, Jorge Peña-Arancibia, Catherine Ticehurst, Steve Marvanek, John Gallant, Justin Hughes, Dushmanta Dutta, Jai Vaze, Cuan Petheram, Lynn Seo and Simon Kitson. *Floodplain inundation mapping and modelling for the Fitzroy, Darwin and Mitchell catchments*, Csiro land and water, 2018.

[8] Department of Fire and Emergency Services. *Western Australia Post Flood Social Research*, 2017.

[9] *WA floods: Homes evacuated in Fitzroy Crossing as aerial food drops made to isolated communities*, ABC News (Australian Broadcasting Corporation), 2017, https://www.abc.net.au/news/2017-02-17/wa-floods-fitzroy-crossing-homes-evacuated/8279744.

[10] J. Teng, A.J. Jakeman, J. Vaze, B.F.W. Croke, D. Dutta , S. Kim. *Flood inundation modelling: A review of methods, recent advances and uncertainty analysis*, Environmental Modelling & Software 90: 201-216, 2017.

[11] N. Nomeritae, E. Daly, S. Grimaldi, H. Bui. *Explicit incompressible SPH algorithm for free-surface flow modelling: a comparison with weakly compressible schemes*, Adv. Water Resour, 2016.

[12] Paul D. Bates, Matthew S. Horritt, Timothy J. Fewtrell. *A simple inertial formulation of the shallow water equations for efficient two-dimensional flood inundation modelling*, Journal of Hydrology 387(1-2):33-45, 2010.

[13] Paul Bates, Mark Trigg, Jeff Neal and Amy Dabrowa. *LISFLOOD-FP User manual*

Code release 5.9.6, School of Geographical Sciences, University of Bristol, University Road, Bristol, BS8 1SS, UK, 2013.

[14] Stefania Grimaldi, Yuan Li, Valentijn R. N. Pauwels, Jeffrey P. Walker. *Remote Sensing-Derived Water Extent and Level to Constrain Hydraulic Flood Forecasting Models: Opportunities and Challenges*, Surveys in Geophysics 37:977-1034, 2016.

[15] D. N. Moriasi, J. G. Arnold, M. W. Van Liew, R. L. Bingner, R. D. Harmel, T. L. Veith. *Model evaluation guidelines for systematic quantification of accuracy in watershed simulations*, American Society of Agricultural and Biological Engineers ISSN 0001-2351, 2007.

[16] World Meteorological Organization. *Manual on Stream Gauging, Volume I – Fieldwork*, WMO-No. 1044, 2010.

[17] Robert Sanderson. *An introduction to remote sensing*, GeoJournal 6(3):251-260, 1982.

[18] Qiuhong Tang, Huilin Gao, Hui Lu and Dennis P. Lettenmaier. *Remote sensing: hydrology*, Progress in Physical Geography 33(4):490-509, 2009.

[19] *Historic Landsat 5 Mission Ends*, NASA, 2013.

[20] *LANDSAT 7 Satellite details 1999-020A NORAD 25682*, N2YO, 2015.

[21] *LANDSAT 8 Satellite details 2013-008A NORAD 39084*, N2YO, 2015.

[22] N.Mueller, A. Lewis, D. Roberts, S. Ring, R.Melrose, J. Sixsmitha, L. Lymburner, A.McIntyre, P. Tan, S. Curnow, A. Ipa. *Water observations from space: Mapping surface water from 25 years of Landsat imagery across Australia*, Remote Sensing of Environment 174:341–352, 2016.

[23] *Landsat Overview*, NASA's Goddard Space Flight Center, 2019, https://www.nasa.gov/mission_pages/landsat/overview/index.html.

[24] Elisabeth Stephens, Guy Schumann, Paul Bates. *Problems with binary pattern measures for flood model evaluation*, Wiley, 2013.

[25] Antara Dasgupta, Stefania Grimaldi, RAAJ Ramsankaran, Valentijn R.N. Pauwels, Jeffrey P. Walker. *Use of Crowd-sourced Data to Assess the Skill of Hydraulic Flood Forecast Models*, 2017.

[26] *ELVIS - Elevation and Depth - Foundation Spatial Data*, Intergovernmental Committee on Surveying and Mapping (ICSM), 2019, https://elevation.fsdf.org.au.

[27] Gary W. Brunner. *Calibration of Unsteady Flow Models*, 2008.

[28] *Water Data Online*, Australian Government Bureau of Meteorology, 2019, http://www.bom.gov.au/waterdata.

[29] *Water Observations from Space*, Australian Government Geoscience Australia, 2019, https://www.ga.gov.au/scientific-topics/community-safety/flood/wofs.

[30] A.D. Nobre, L.A. Cuartas, M. Hodnett, C.D. Rennó, G. Rodrigues, A. Silveira, M. Waterloo, S. Saleska. *Height Above the Nearest Drainage – a hydrologically relevant new terrain model*, Journal of Hydrology 404 (2011) 13–29, 2010.

[31] *Australia in flood Fitzroy River in Western Australia rises 11 metres in 5 days!*, YouTube video, 4:01, posted by "Oz Outback Family", 2016, https://www.youtube.com/watch?v=CXIyfcB-4d4.

[32] *Kimberley residents braced for flooding and possible evacuation*, Australian Associated Press, 2016, https://www.theguardian.com/australia-news/2016/dec/26/kimberley-residents-braced-for-flooding-and-possible-evacuation.

[33] Andrew R Taylor, Glenn A Harrington, Steven Clohessy, Warrick R Dawes, Russell S Crosbie, Rebecca C Doble, Daniel L Wohling, Jordi Batlle-Aguilar, Phil J Davies,

Mark Thomas and Axel Suckow. *Hydrogeological assessment of the Grant Group and Poole Sandstone – Fitzroy catchment, Western Australia*, Csiro land and water, 2018.

[34] Bradley J. Pusey and Jarrod Kath. *Environmental Water Management in the Fitzroy River Valley Information availability, knowledge gaps and research needs*, Western Australian Department of Water, 2015.

[35] S.A. Islam, A.H.M.F. Anwar, G. Ezzy and M. Bari. *LUCICAT Model as a river flow forecasting tool: an experiment with Fitzroy River catchment of Western Australia*, 2013.

[36] Bureau of Meteorology. *Monthly Weather Review Australia December 2016*, 2016.

[37] Bureau of Meteorology. *Special Climate Statement 59—humidity, heavy rain and heat in central and southern Australia*, 2017.

[38] Evert Attema, Malcolm Davidson, Paul Snoeij, Björn Rommen, Nicolas Floury. *Sentinel-1 mission overview*, European Space Agency, 2010.

[39] *NovaSAR-1 A low cost S-band SAR mission on a Minisatellite*, Earth Observation portal, 2019, `https://directory.eoportal.org/web/eoportal/satellite-missions/n/novasar-1`.

Acknowledgements

Al termine di questo percorso è doveroso ringraziare tutte le persone che mi hanno accompagnato in questi anni ed aiutato a giungere al traguardo.
Ringrazio innanzitutto il mio relatore, il Prof. Francesco Laio, per avermi coinvolto in questo lavoro e permesso di realizzare l'avventura australiana. I suoi preziosi consigli e la sua disponibilità mi hanno consentito di svolgere al meglio questa ricerca. Un gigantesco grazie va alla mia correlatrice Stefania Grimaldi. La sua passione per la ricerca e il suo meraviglioso carattere mi hanno insegnato e guidato lungo questi ultimi mesi. Mi ha supportato (e sopportato) quotidianamente con una dedizione ed una pazienza che vanno ben oltre il ruolo accademico.
Ed ora a voi, Cinzia e Sergio, i miei due archi. Non bastano i grazie per voi due. Mi avete sostenuto ed aiutato in ogni scelta, sopportato i miei umori durante le sessioni d'esame e consentito di studiare e vivere questi anni nelle migliori condizioni possibili. Non ho dubbi, senza di voi sarebbe stato impossibile portare a termine questo viaggio. Vi voglio bene garsunetti! Un grazie di cuore alla mia sorellona Greta per tutte le scampagnate post esame e per avermi sempre tranquillizzato con un "vabbè al massimo lo dai la prossima volta". Un bacio alle mie nonne Lilla e Mina per non smettere mai di coccolarmi e illudermi, stando a quel che dicono, che sto ancora crescendo. Un abbraccio ai miei zii Franca e Gustin per essersi sempre informati sui miei studi con dolcezza e interesse. Maledizione quanto vorrei poter portarvi a vedere questo papiro nel vostro nido dei Crovi.
Un grazie ed un brindisi agli amici genovesi, quelli di vecchia data e i nuovi, i liceali, i ragazzi della festa della birra di Mele, quelli del cineporto ed il mio gruppo della saletta 57, per tutte le serate, i concerti e le risate che mi hanno riempito l'anima (ma c'è ancora spazio). Grazie agli amici di Torino, a partire dalla piccola Ludovip con cui tutto è iniziato, passando per i compagni di università fino ai dolci ragazzi di Peano con cui ho vissuto le ultime fatiche. Un grazie agli amici di viaggio, i barcellonesi e gli australiani, con cui ho condiviso momenti indelebili e che mi hanno confermato che di cuccioli ne è pieno il mondo. Infine un bacio a voi che mi avete divertito, emozionato, a volte intristito, ma sempre insegnato.
Insomma bella gente, vi abbraccio tutti.